nagra.

ARBEITSBERICHT NAB 24-07 Rev. 1

Treatment of ^{14}C in the Post-Closure Safety Assessments

October 2024

Nagra | National Cooperative for the Disposal of Radioactive Waste
Hardstrasse 73 | 5430 Wettingen | Switzerland
+41 56 437 11 11 | info@nagra.ch | nagra.ch

nagra.

ARBEITSBERICHT NAB 24-07 Rev. 1

Treatment of ^{14}C in the Post-Closure Safety Assessments

October 2024

KEYWORDS
C-14 source term; C-14 transport; biosphere; safety assessments; safety case

Nagra | National Cooperative for the Disposal of Radioactive Waste
Hardstrasse 73 | 5430 Wettingen | Switzerland
+41 56 437 11 11 | info@nagra.ch | nagra.ch

Nagra Arbeitsberichte ("Working Reports") present the results of work in progress that have not necessarily been subject to a comprehensive review. They are intended to provide rapid dissemination of current information. In this case, a comprehensive review has been performed by Andra (Stephan Schumacher, Guillaume Pépin, Christelle Martin, Benjamin Frasca, Jean-Charles Robinet, Jacques Wendling, Achim Albrecht and Yves Thiry) in 2023. The authors would like to thank them for their valuable contributions.

This report has been revised due to findings made during the course of the project development. As a result, certain formulations have been adjusted to reflect updated information and ensure consistency across the reports.

The report "Treatment of ^{14}C in the Post-Closure Safety Assessments" has been elaborated by a project team consisting of T. Guillemot[1], P. Hunkeler[1], A. Poller[2], S. Diem[2], R. Walke[3], S. Watson[3], S. Pudollek[1], A. Papafotiou[1], H. Javanmard[1].

[1] Nagra
[2] CSD, Switzerland
[3] Quintessa, UK

Abstract

The potential radiological consequences of ^{14}C being released from the deep geological repository need to be assessed in support of the post-closure safety case for the general licence application. The present report provides an overview of the ^{14}C treatment in the post-closure safety assessments. This radionuclide is of importance in post-closure safety assessments because: (i) it can be released both as dissolved and gaseous species in the repository system; (ii) ^{14}C organics readily migrate in the near-field due to weak interaction with mineral surfaces in alkaline to near-neutral conditions; and (iii) ^{14}C could be subject to substantial accumulation in the biosphere, if it does not decay in the host rock or overlying strata.

This report includes the description of:

- the ^{14}C source term (inventory, speciation and release rate from the individual waste materials);
- the potential migration of ^{14}C within the engineered structures of the repository, the host rock and confining geological units, and the deep groundwater systems;
- and its potential migration and accumulation within the biosphere, including the exposure of potentially exposed groups to ^{14}C.

The overall structure of the report therefore reflects the potential ^{14}C release into spatial domains with distinct characteristics and the potential exposure pathways. For each spatial domain (i.e., waste, repository structures, containment-providing rock zone, deep groundwater systems and biosphere), a clear separation is made between the state of knowledge (including various sources of uncertainty), and the adopted approaches to safety assessment (including treatment of uncertainty).

^{14}C is present in different types of radioactive waste and in various chemical states. The total inventory at repository closure is ~ 2.4×10^{14} Bq. A quarter of this inventory (i.e., ~ 24.5%) is present in low- and intermediate-level waste, mainly activated steel, contaminated materials, ion-exchange resins and graphite. The majority of the initial ^{14}C inventory (i.e., ~ 75.5%) is associated with high-level waste, mainly activated Zircaloy, spent fuel pellets and activated steel. While the period of complete containment of high-level waste ensures an important decay of ^{14}C within the disposal canister, no containment is assumed for low- and intermediate-level waste after repository closure. Therefore, in terms of potential releases, ^{14}C present in low- and intermediate-level waste is more safety-relevant than in high-level waste. The mechanisms of ^{14}C release from these materials and the speciation of the released compounds have been experimentally investigated in detail or, where experimental evidence was lacking, assessed by experts. For the purpose of safety assessment, the ^{14}C-containing materials are assigned to so-called release classes, for which the expected release is modelled by means of an instant and a congruent release fraction of the respective ^{14}C content. In addition, the various compounds to be released are classified either as organic (i.e., reduced chemical form) or inorganic (i.e., oxidised chemical form) ^{14}C compounds. Once released from the waste forms, the individual ^{14}C compounds will either dissolve in porewater, migrating through the containment-providing rock zone primarily by means of molecular diffusion, or enter the gas phase and migrate along unsaturated repository structures.

The migration of ^{14}C is modelled numerically with two complementary modelling approaches: one for the migration of dissolved ^{14}C-bearing species, and the other for the migration of ^{14}C-bearing volatiles. The former approach is identical to that for the migration of all other relevant radionuclides and assumes fully saturated and stationary hydraulic conditions, whereas the latter approach explicitly accounts for the generation and migration of gas within the deep geological repository. The release of ^{14}C to the wider geological environment of the repository system may

be both local at the position of underground access structures (shafts and/or ramp) and widespread at the interfaces of the confining geological units with the adjacent major aquifers above and below the deep geological repository. Depending on whether the released ^{14}C compounds are dissolved or present in a gas phase, they may migrate further along deep aquifers to the respective discharge areas or upwards to the near-surface environment, respectively. The exact transport routes are very specific with respect to the geology, exact waste emplacements, and design of underground access structures. For the general licence application, where such information is not yet available, no credit for potential delay and dispersion of ^{14}C during transport to the near-surface environment is therefore taken for post-closure safety assessments.

Upon entering the biosphere (near-surface environment), the ^{14}C compounds would be subject to various transfer and conversion processes, leading to the accumulation of ^{14}C in different environmental media, such as the soil, local groundwater or crops. Humans, who use these media as natural resources, would then be exposed to ^{14}C, mostly by ingestion of contaminated food and water. The modelling approach consists of representing the most important environmental media as compartments, which are linked by transfers of stable carbon within solids, liquids and gases. The calculated equilibrium state is then used as a proxy for the equilibrium state of radioactive ^{14}C that enters the biosphere over a prolonged period. Potential human exposure is calculated from the ^{14}C concentrations determined in the different compartments.

Based on recent scientific knowledge from experiments and models, the treatment of ^{14}C in post-closure safety assessments for the general licence application is more detailed, less conservative in view of the ^{14}C inventory and source term, and more realistic regarding ^{14}C migration in the repository near-field and biosphere than the previous Stage of the project. Moreover, Nagra's approach is generally in line with those of other international waste disposal programmes. Differences are related primarily to waste inventories, repository concepts, stages of the disposal programmes and purposes of the respective post-closure safety assessments.

Table of Contents

List of Tables

List of Figures

List of Acronyms

AGT	Waste package type (*Abfallgebindetyp*)
ATW	Alpha-toxic waste
BDCF	Biosphere dose conversion factor
BWR	Boiling water reactor
CANDU	Canada deuterium uranium (reactor)
CAST	Carbon source term (project)
CRF	Congruent release fraction
CRR	Congruent release rate
CRZ	Containment-providing rock zone
EDZ	Excavation-damaged zone
HC	Hydrocarbon
HCP	Hardened cement paste
HLW	High-level waste (spent fuel assemblies and high-level waste from reprocessing)
ICRP	International Commission on Radiological Protection
IER	Ion-exchange resin
IRF	Instantaneous release fraction
LB	Lower bound
L/ILW	Low- and intermediate-level waste
LMW	Low molecular weight
LWR	Light water reactor
MIR	(Radioactive waste from) medicine, industry and research
MIRAM	Model inventory for radioactive materials
NPP	Nuclear power plant
PWR	Pressurised water reactor
RBG	General licence application (*Rahmenbewilligungsgesuch*)
RP-HLW	(Vitrified) reprocessing high-level waste
RPO	Swiss radiological protection ordinance
RWM	Radioactive waste management
SF	Spent fuel
SFAs	Spent fuel assemblies

SGT	Sectoral plan for deep geological repositories (*Sachplan geologische Tiefenlager*)
SKB	Swedish nuclear fuel and waste management company (*Svensk Kärnbränslehantering Aktiebolag*)
UB	Upper bound
WMO	Waste management organisation
ZWILAG	Zwischenlager Würenlingen AG (interim storage facility)

1 Introduction

1.1 Context

In Switzerland, legal regulations (Nuclear Energy Act (KEG 2003) and Nuclear Energy Ordinance (KEV 2004)) and guidelines are in place for the management of radioactive waste. The Nuclear Energy Ordinance (KEV) classifies Switzerland's radioactive waste into low- and intermediate-level waste (L/ILW), alpha-toxic waste[1] (ATW) and high-level waste (HLW), the latter comprising spent fuel (SF) and vitrified HLW from reprocessing (RP-HLW). The Nuclear Energy Act (KEG) requires the disposal of all these types of radioactive waste in deep geological repositories. The feasibility of this disposal solution has been demonstrated for L/ILW in Nagra (1985) and for long-lived intermediate-level waste and HLW in Nagra (2002b).

The Sectoral Plan for Deep Geological Repositories (SGT) regulates the search for suitable siting regions for deep geological repositories in Switzerland. This site selection process is conducted in three stages (BFE 2008). Stages 1 and 2 have already been completed and Nagra is currently in Stage 3 (SGT-E3). Clarifications on the safety-related specifications for this stage are provided in ENSI 33/649 (ENSI 2018), while ENSI Guideline G03 and the corresponding explanatory report (ENSI 2020b, ENSI 2020a) specify the protection objective, protection criteria and design principles for deep geological repositories.

In SGT-E3, three siting regions located in Northern Switzerland have been considered – Jura Ost (JO), Nördlich Lägern (NL) and Zürich Nordost (ZNO) – with the objective of selecting one siting region for an HLW repository, one for an L/ILW repository, or one for a combined repository for all waste types.

Following a comparison of these siting regions, Nagra concluded that NL is the safest and most flexible siting region. Therefore, it is applying for a general licence for a repository for both HLW and L/ILW, with surface facilities at the Haberstal site (municipality of Stadel, ZH).

The justification for this selection and the safety demonstration for a repository at the site are submitted as part of the general licence application (RBG[2]). The reports relating to post-closure safety, shown in Fig. 1-1, are structured as follows:

- The overall safety-related argumentation, including post-closure and operational safety, is summarised in an overarching safety report ("*Sicherheitsbericht*") NTB 24-01 (Nagra 2025b) shown at the top of Fig. 1-1.
- The upper left side of Fig. 1-1 shows the reports supporting Nagra's site comparison. The available options are compared with respect to safety and technical feasibility and the results are synthesised in NTB 24-03 (Nagra 2025a) ("*Bericht zur Begründung der Standortwahl*").
- The upper right side of Fig. 1-1 shows the reports documenting the post-closure safety case for the combined repository at the site, including its synthesis in the post-closure safety report NTB 24-10 (Nagra 2024h).
- The lower part of Fig. 1-1 shows a report that presents the safety and repository concept, including the provisional design, and reports providing the assessment basis.

---

[1] According to Nagra (2024a), ATW can coexist with L/ILW within the same emplacement caverns. As a result, for the sake of simplicity, the term L/ILW encompasses ATW without explicit mention.

[2] From the German *Rahmenbewilligungsgesuch*.

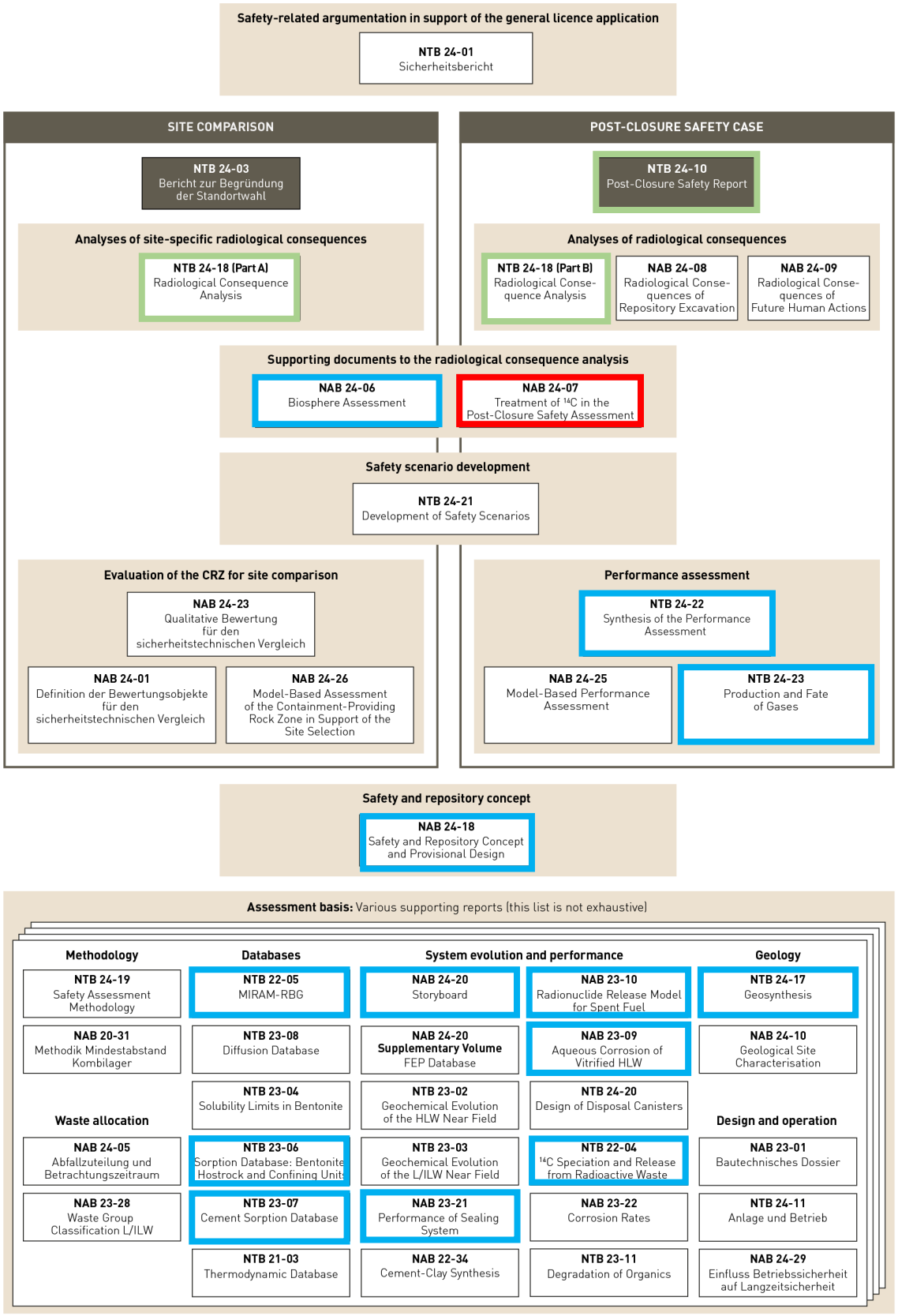

Fig. 1-1: Structure of reports covering post-closure safety aspects of the site comparison and the post-closure safety case

The current study is indicated with a red box and based on various reports highlighted in blue. It supports the radiological consequence analysis (Nagra 2024j) for the site selection and the post-closure safety report (Nagra 2024h) for a combined repository at the site (green boxes).

Nagra (2024j) involves the estimation of radiological dose or risk to potentially exposed individuals based on the estimated release of key radionuclides from the deep geological repository to the surface environment in the distant future. To this end, assumptions must be made with regard to the content of such radionuclides in individual waste package types, on the processes by which they are released from the waste and on transfer processes in both the containment-providing rock zone (CRZ) and the biosphere. Such assumptions must reflect the state of knowledge at the time of the analysis, including the associated uncertainty. In the post-closure safety report (Nagra 2024h), post-closure safety assessments for a deep geological repository are defined. They consist of four main processes:

- **performance assessment**, in which the thermal, hydraulic, mechanical, and chemical evolution of the repository system is analysed;
- **safety scenario development**, which entails the identification and description of a set of safety scenarios that capture uncertainty in initial state and subsequent evolution of the repository system over time;
- **analysis of radiological consequences**, which consists of an evaluation of radionuclide release rates to the surface environment as a function of time; and
- **demonstration of post-closure safety**, in which evidence, arguments and results from the three previous steps are brought together in the post-closure safety report.

1.2 Aims and purpose

The radionuclide ^{14}C has been identified as one of the predominant radionuclides in post-closure safety assessments for future deep geological repositories in Switzerland and abroad (cf. Wieland et al. 2023 and references therein). This is because ^{14}C can be released from the waste as dissolved and gaseous species. ^{14}C-bearing organic compounds readily migrate in the near-field and the geosphere due to weak interaction with mineral surfaces in alkaline to near-neutral conditions. The chemical form of the ^{14}C-bearing carbon species dictates the routes of ^{14}C migration in the engineered barrier system of a deep geological repository and the surrounding host rock and therefore determines the long-term contribution of ^{14}C to the dose potentially released from a repository for radioactive waste. Furthermore, ^{14}C released from a deep geological repository could be subject to substantial accumulation in the biosphere, given the key role of carbon as the main building block of any life form on earth. ^{14}C hence deserves particular attention in post-closure safety assessments carried out in the context of the RBG.

The present report contributes to the specific requirement for the demonstration of safety that the long-term behaviour of the repository barrier system must be understood (KEV 2004). The objective of this report is to provide: (i) an overview of the current scientific understanding about the inventory of ^{14}C in individual waste package types; (ii) the processes by which ^{14}C is released from these waste types; (iii) the behaviour of ^{14}C-bearing compounds in the deep geological repository and its environment; and (iv) the dynamics of ^{14}C-bearing compounds in the biosphere, including the potential exposure of humans to ^{14}C. The report also outlines how this understanding leads to a set of assumptions for post-closure safety assessments and how remaining sources of uncertainty in the current understanding are handled in these assessments.

For better readability, the content of this report is tailored to the provisional concept of a combined repository (Nagra 2021a), but any information reported is, in principle, also applicable to single L/ILW and HLW repositories, respectively. Only ^{14}C-specific data and concepts in post-closure safety assessments are given in this report. ^{14}C-related calculations are documented in the consequence analysis report (Nagra 2024j).

Historical outline

The last formal safety case for a repository for L/ILW in Switzerland was made in the context of the general licence application for a deep geological repository at the Wellenberg site in 1994 (Nagra 1994). The overall repository concept envisaged the emplacement of L/ILW within cement-backfilled caverns that would be constructed in an alpine marlstone host rock. Potential ^{14}C-bearing compounds in the near-field and the geosphere were broadly classified into organic and inorganic species, the latter being released from activated metals[3]. Dissolved ^{14}C inorganics were in most cases assumed to weakly sorb in the near-field and the geosphere, whereas dissolved ^{14}C organics were conservatively treated as non-sorbing in the reference case. Two safety scenarios were considered for the ^{14}C release to the biosphere: i) release with flowing groundwater and ii) release via continuous gas pathways along distinct faults in the geosphere. No distinction of different ^{14}C compounds was made for the biosphere; all were assumed to weakly sorb in different environmental media. For the gas pathway, it was assumed that organic waste would be fully degraded microbially, thereby releasing ^{14}C in the form of $^{14}CO_2$ or $^{14}CH_4$. $^{14}CO_2$ was considered to precipitate as calcite, whereas $^{14}CH_4$ would be present in the gas phase. $^{14}CH_4$ was further assumed to be released at a constant rate between 100 years and 200 years after closure of the repository. In the biosphere, it was assumed that shallow groundwater would be saturated with CH_4. Therefore, a complete degassing of $^{14}CH_4$ into the atmosphere was assumed and no dose contribution from volatile ^{14}C compounds would occur. The estimated maximum dose rate for ^{14}C from the so-called waste group 2 (medium content of complexing agents) in the groundwater scenario and with reference assumptions was about 2×10^{-3} mSv/a.

The last formal safety case for a deep geological repository for SF, RP-HLW and ILW in Switzerland was compiled as part of the "Opalinus Clay" project in 2002 (Nagra 2002a, Nagra 2002b). The overall repository concept envisaged the emplacement of SF and RP-HLW within drifts backfilled with granular bentonite, constructed in clay rock in the Zürcher Weinland in Northern Switzerland. ILW would be emplaced in cement-backfilled caverns in the same clay rock at some distance from the SF/RP-HLW drifts. Again, potential ^{14}C-bearing compounds in the near-field and the geosphere were broadly classified into organic and inorganic species. ^{14}C within the SF matrix and within the RP-HLW glass matrix was assumed to be released in inorganic form and mainly congruently with the slow dissolution of the respective matrices. In contrast, ^{14}C present either in structural materials of intact spent fuel assemblies (SFAs) or in compacted cladding and end pieces from SF reprocessing in certain ILW types was considered to be released in organic form. This reflects a marked shift in the understanding of carbon speciation and release from activated metals since the Wellenberg safety assessment. Once water came into contact with these waste forms, 20% of these ^{14}C organics were assumed to be instantly mobile; the remainder was assumed to be released congruently with metal corrosion. ^{14}C inorganics were assumed to be solubility-controlled and weakly sorbing in the bentonite near-field as well as in the clay rock, whereas no retention was assumed for ^{14}C organics. In the cementitious ILW near-field, similar assumptions were made (i.e., ^{14}C inorganics were weakly sorbing, while no retention was assumed for ^{14}C organics). Assumptions for the biosphere were similar to those in the earlier assessment

[3] The term "activated" is used for materials that contain relevant amounts of activation (and associated decay) products in their bulk structure.

for an L/ILW repository at the Wellenberg site, except that complete degassing into the atmosphere for volatile ^{14}C species was not assumed, which resulted in a dose contribution from these compounds. In summary, ^{14}C organics released from activated metals were assumed to be highly mobile in the barrier system of the repository for SF, RP-HLW and ILW and to contribute to radiation exposure in the biosphere. With regard to the release of ^{14}C into the biosphere, two assessment scenarios were distinguished: i) release through clay rock porewater to adjacent aquifers; and ii) release via gas accumulations in the repository and an overlying porous rock formation, the so-called Wedelsandstein, to adjacent aquifers. The pathway from the aquifers to the biosphere was not explicitly considered. The estimated maximum dose rates from ^{14}C organics in the groundwater scenario with reference assumptions were about 7×10^{-7} mSv/a from SF and 3×10^{-7} mSv/a from ILW. The model for the gas release scenario consisted of two parts: i) a simplified semi-analytical model for gas migration and accumulation in the repository and its geological environment; and ii) a semi-analytical model for transport of volatile ^{14}C organics based on gas transfer results obtained with the former gas model. The consumption of ^{14}C-contaminated drinking water was considered the sole radiation exposure pathway in this case. The estimated maximum dose rates based on the reference assumptions were about 6×10^{-7} mSv/a from SF and 1×10^{-7} mSv/a from ILW, largely comparable with the results for the groundwater pathway. The assumption of dysfunctional seals along the access structures as part of an alternative conceptualisation of the gas assessment scenario resulted in estimated maximum dose rates of about 4×10^{-5} mSv/a from SF and 7×10^{-6} mSv/a from ILW.

In SGT Stage 1, post-closure safety assessments were carried out based on generic repository concepts suitable to different types of host rock and different geological settings (Nagra 2008b). Given that the release of volatile ^{14}C organics along gas pathways would be rather specific to a certain repository configuration, which itself would be tailored to the geological conditions at a given site, this aspect was not looked at in the same level of detail as in the preceding site-specific safety cases described above. In SGT Stage 2, the modelling was based on the realistically expected evolution of the repository systems at that time (i.e., the radionuclide release from the deep geological repository systems as dissolved species along the groundwater pathway) (Nagra 2014a). The release via the gas phase was outside the reference scenario and therefore beyond the scope of SGT Stage 2. Consequently, no quantitative dose estimates for ^{14}C release via gas pathways were calculated in SGT Stage 1 and Stage 2. This approach in the context of the site selection process for a deep geological repository was later approved in the respective regulatory reviews (ENSI 2010, ENSI 2017). Despite the generic geological settings, the repository concepts considered in SGT Stage 1 resembled those developed in the preceding projects in many aspects. The approach to the ^{14}C-related safety assessment in SGT Stage 2 was also very similar to that of Stage 1 but included some amendments (Nagra 2014b). The first modification was the conceptualisation of ^{14}C speciation and release. Instead of two groups of ^{14}C compounds in the near-field and the geosphere, three were considered: i) ^{14}C inorganics with an assumed instant release from the waste forms; ii) ^{14}C organics with an assumed instant release from the waste forms; and iii) ^{14}C organics released from activated metals at a constant rate for 10,000 years[4]. Subsequently, a detailed analysis was carried out to derive the best estimate or conservative values for the ^{14}C content of each waste sort, based on the source of the waste (i.e., operational, decommissioning, reprocessing, reactor waste and SF) (Cloet et al. 2014). The second modification was to make the conservative assumption that ^{14}C incorporated in the SF matrix would be released in organic form due to prevailing reducing conditions. Finally, a weak sorption behaviour was attributed to ^{14}C organics in cement-backfilled caverns for ILW and L/ILW. Major progress was made with respect to the modelling of ^{14}C in the biosphere, mainly initiated through progress in international collaborations, such as the BIOPROTA forum and the Environmental Modelling for Radiation Safety (EMRAS) programmes (EMRAS 2012) of the International Atomic Energy

[4] This release rate clearly overestimated metal corrosion rates.

Agency (IAEA), in which Nagra actively took part. This resulted in an updated biosphere model that took the cycling of carbon between the soil, the crops and the canopy air explicitly into account (Nagra 2008a). Furthermore, the canopy air was subdivided into a diffusion-dominated layer and a turbulence-dominated layer. Plant uptake of ^{14}C was assumed to occur from both layers as $^{14}CO_2$, as well from the soil solution in the form of ^{14}C bicarbonate. In addition, a free atmosphere layer was added, which acted both as a source of carbon not originating from the repository and as a sink for ^{14}C originating from the repository (Walke et al. 2013). It was also suggested that low-molecular weight (LMW) organic species in soils and sediments (e.g., carboxylic acids) might also be oxidised to CO_2 and hence $^{14}CO_2$ would be available for plant uptake. If not oxidised in the soil or in the near-surface aquifer, CH_4, however, was still considered to not enter the food chain, thus limiting the exposure contributions of $^{14}CH_4$ to the inhalation pathway. In SGT Stage 2, the so-called provisional safety analyses were carried out for the geological siting regions that had been identified in SGT Stage 1 (Nagra 2014b). Maximum dose rates in the reference case were significantly lower than in earlier programme milestones, but ^{14}C was still identified to be one of the dominating dose-relevant radionuclides for the future L/ILW repository and a key radionuclide for the future HLW repository, especially for alternative calculation cases with unfavourable parameter values for diffusion in the host rock.

In summary, in the course of the Swiss radioactive waste disposal programme, Nagra has continuously monitored the international state of knowledge regarding the origin of ^{14}C in different radioactive waste materials and its fate during the post-closure phase of a deep geological repository. Nagra has also actively participated in international programmes and/or initiated its own research on ^{14}C-related issues (Nagra 2009, Nagra 2016, Nagra 2021b). This has led to new insights and a progressively reduced level of uncertainty. The evolving state of knowledge has gradually been integrated into Nagra's safety assessment approaches as was deemed appropriate for the respective programme stages and broadly confirmed in the respective regulatory reviews (ENSI 2017, ENSI 2010, HSK 2000, HSK 2005).

^{14}C-related assessments for the RBG

As previously laid out, several safety-related comparisons of potential siting regions for a deep geological repository are being carried out and involve site-specific dose calculations. The calculations are based on the most likely evolution (i.e., the reference scenario) of the respective potential repository sites (Nagra 2024c) and address the subsurface transport of both dissolved and gaseous ^{14}C-bearing compounds. With respect to the post-closure safety case for the proposed repository at the Haberstal site, dose calculations are performed within the framework of the RBG (Nagra 2024c). All these results are not evaluated and documented here but in the consequence analysis report (Nagra 2024j).

1.3 Uncertainty management

On the ^{14}C source term

General provisions are adopted for the ^{14}C source term based on Nagra (2024l):

- Where information is not available or publicly available scientific literature shows highly variable results, conservative[5] assumptions are made.

[5] The term "conservative" applies to simplifications, assumptions, parameter values, etc., that are confidently expected to lead to calculated consequences that are less favourable than those anticipated under real conditions, taking uncertainty into account. Conservative choices can lie outside the range of what is physically possible (e.g., hypothetical assumptions).

- In case of sparse information in the publicly available scientific literature, cautious, i.e., pessimistic[6] assumptions are made.
- In case of relatively mature and highly confident information in the literature, realistic assumptions are made based on scientific expectations and provisional repository design.
- For aspects that are not deemed to have a strong impact on the behaviour of ^{14}C in any of the domains, simplifications of the previous assumptions can be made in the workflow of the ^{14}C source term.
- In general, probabilistic and deterministic uncertainty and sensitivity analyses include the sampling of the parameters related to the ^{14}C source term within their ranges of uncertainty (i.e., assumed parameter distributions and/or bandwidths) (cf. Nagra 2024j).

On the migration of ^{14}C in the repository system and geological environment

- Experimentally observed ^{14}C species are assigned to simplified release species corresponding to stylised model components in the modelling approach for the migration of ^{14}C within the geological environment (i.e., repository system, CRZ and the deep groundwater systems).
- Uncertainties related to model abstractions and simplifications are documented in Nagra (2024j).
- In general, probabilistic and deterministic uncertainty and sensitivity analyses include the sampling of the parameters related to the transport processes within their ranges of uncertainty (i.e., assumed parameter distributions and/or bandwidths) (cf. Nagra 2024j).

On the migration of ^{14}C in the biosphere

There is significant uncertainty about the nature of the surface environment into which radionuclide releases might occur in the distant future. Given these uncertainties, the biosphere modelling aims to deliver an overall pessimistic assessment to help ensure that potential dose consequences to humans who could be exposed are not underestimated (cf. Nagra 2024g). To ensure this, a wide range of potential exposure pathways are evaluated in the biosphere, with humans making maximum but reasonable usage of the local environment. To help avoid overly pessimistic assessments, pessimism about the range of potential exposure pathways is balanced by seeking to be realistic in modelling the behaviour of ^{14}C in the biosphere (Walke & Thorne 2023) and in adopting plausible, internally consistent assumptions about individual lifestyles (Nagra 2024g).

To quantify the significance of individual parameter uncertainties on long-term safety, a global sensitivity analysis using the Monte Carlo approach will be performed in the context of consequence analysis for the reference safety scenario (Nagra 2024j).

[6] The term "pessimistic" is used in this report to refer to assumptions or parameter values which are possible, but lead to results less favourable than the reality or the most likely outcome.

1.4 Organisation of this report

After this first introductory chapter followed by a general overview of the repository system (Chapter 2), the overall organisation of this report reflects the potential fate of ^{14}C in the post-closure phase of a deep geological repository, starting from:

- Chapter 3: its release from the individual waste materials in the near-field of the L/ILW (Section 3.2) and HLW (Section 3.3) repository sections;
- Chapter 4: to its potential migration within the geological environment, including the repository system (Section 4.1), CRZ (Section 4.2), and the deep groundwater systems (Section 4.3);
- Chapter 5: and its migration within the biosphere (Section 5.1), including the ^{14}C exposure of potentially exposed groups (Section 5.2).

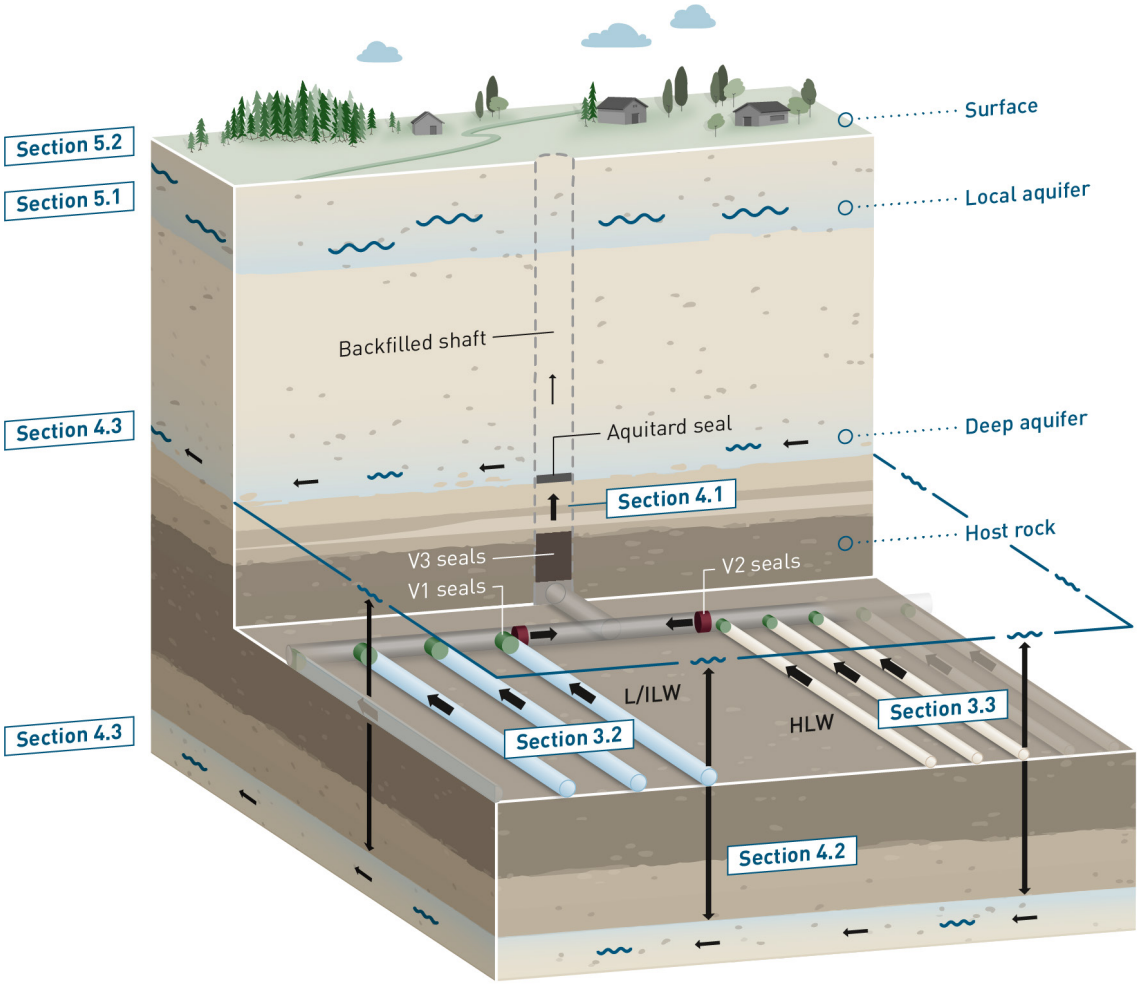

Fig. 1-2: Illustration of the organisation of this report by means of a schematic disposal situation with potential ^{14}C release, transfer and exposure pathways shown with the black arrows

The overall structure therefore adheres to different spatial domains and the processes that occur in these domains (Fig. 1-2). Note that the delimitation of the domains goes hand in hand with an increasing level of uncertainty, or a correspondingly decreasing predictability of the processes in the respective domains over the assessment period, which requires the adoption of progressively stylised approaches to post-closure safety assessment.

The further subdivision of the individual chapters reflects the different environmental conditions in the L/ILW and HLW near-fields (alkaline vs. neutral environments) (Chapter 3), the different types of media within and outside the repository system (engineered vs. natural media) (Chapter 4), or the transfer and exposure processes in the biosphere (Chapter 5) (Fig. 1-2).

Throughout the report, it is endeavoured to provide a clear separation between the state of knowledge (including various of uncertainty) and the approaches to post-closure safety assessments (including treatment of uncertainty) adopted by Nagra. Remarks about major similarities and differences between Nagra's assessment approaches and those of other waste management organisations (WMOs) and links to regulatory or international guidelines are made where appropriate. It should be mentioned, however, that relatively few reports about the treatment of ^{14}C in other WMOs are publicly available.

2 Overview of the provisional repository system

The provisional repository system in its configuration after closure comprises the entirety of the emplaced waste, the backfilled and sealed underground structures and the installed engineered barriers, along with the part of the geological environment that provides high-level safety functions at a given site (called geological barriers). The current reference repository concept for L/ILW and HLW in a combined repository is described in Nagra (2021a). Fig. 2-1 presents a schematic view of the provisional combined repository which will be constructed in the Opalinus Clay formation at a depth of several hundred metres below the surface. It features two spatially separated repository sections, one for SF and RP-HLW (called HLW repository section), and one for L/ILW and ATW (called L/ILW repository section).

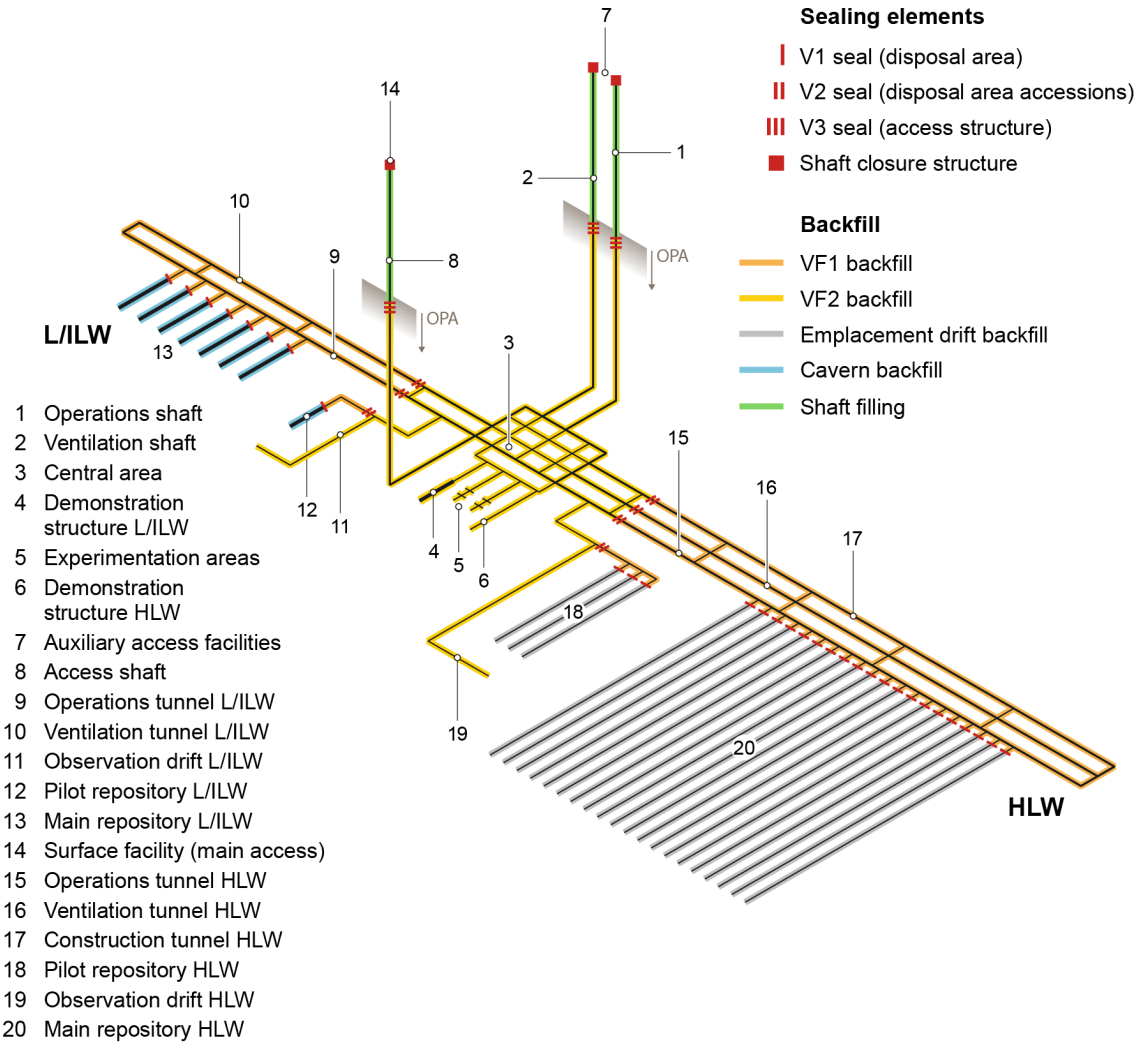

Fig. 2-1: Schematic view of the provisional combined repository and its main components after closure

From Nagra (2021c). Note that the current design may be refined and modified in the future Stages of the project.

The provisional concept for the closure of a deep geological repository is reported in Nagra (2021c). It involves the complete backfilling of all underground structures and the construction of seals at the entrance to emplacement drifts and caverns (V1 seals), within the underground access structures to the two repository sections (V2 seals) and within the underground access structures (shafts or possibly a ramp) in the upper part of the clay host rock (V3 seals). The main tasks of these seals are to segregate the individual repository parts and to limit water flow and gas pressure. The distance between the two repository sections and the design of the seals are such that no substantial interactions between the two repository sections are expected to occur (Nagra 2024m, Nagra 2024i). The closure concept also foresees the construction of seals at the location of aquitards outside the repository system to keep individual major aquifers hydraulically separated.

3 ^{14}C source term

The approach of the ^{14}C source term is illustrated Fig. 3-1 and specifically includes: (i) the inventory of the ^{14}C-bearing materials and their associated activity (characterised in Section 3.2), (ii) the ^{14}C speciation and rate of release from these materials (defined in Section 3.3), and (iii) the integration of this information to the ^{14}C source term (detailed in Section 3.4), which will serve as input for the ^{14}C transport model described in Chapter 4.

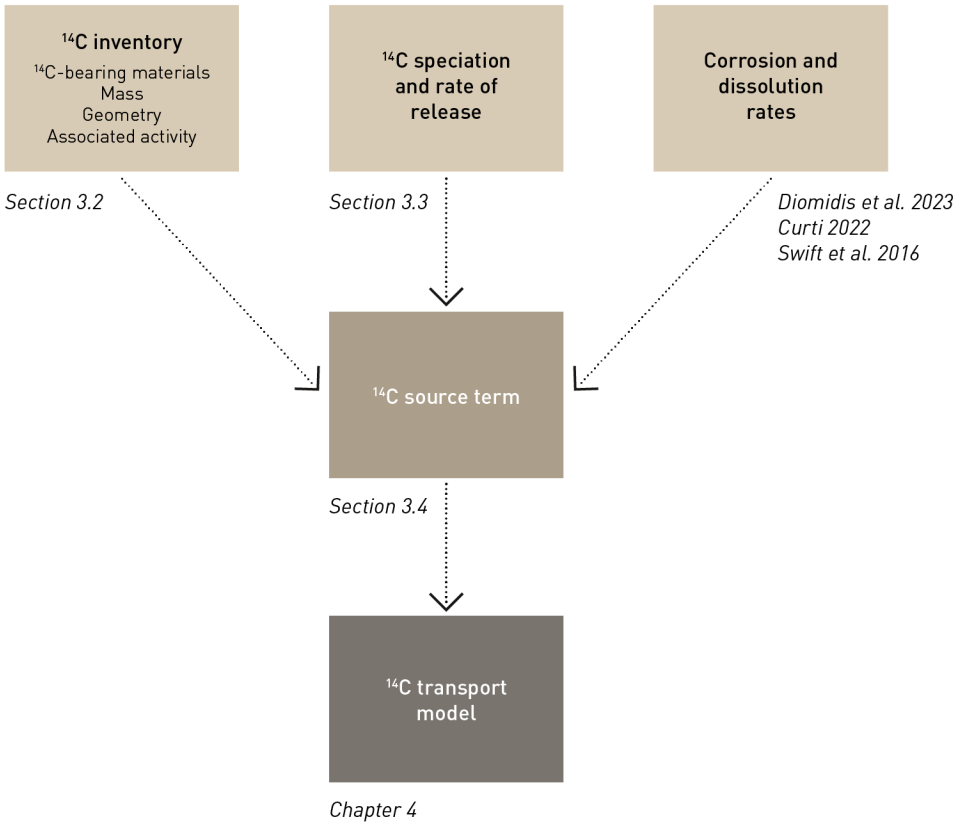

Fig. 3-1: Illustration of the ^{14}C source term approach

3.1 ^{14}C origin

In nuclear power plants (NPPs), ^{14}C is produced in SFAs, reactor core structural materials and reactor system coolants by the interaction of thermal neutrons with the (stable) precursor isotopes ^{14}N, ^{17}O and ^{13}C. These isotopes are present as major components or impurities in the different media (Yim & Caron 2006). They are involved in three major reactions to produce ^{14}C, as described in Tab. 3-1.

Tab. 3-1: ^{14}C production mechanisms and thermal neutron cross-sections

Precursor isotope	Nuclear reaction	Isotopic abundance of precursor (%)	Thermal neutron cross-section (barns)
^{14}N	$^{14}N(n,p)^{14}C$	99.632	1.82
^{17}O	$^{17}O(n,\alpha)^{14}C$	0.038	0.235
^{13}C	$^{13}C(n,\gamma)^{14}C$	1.07	0.0014

In structural materials of SFAs and reactor core structural materials from light-water reactors (LWRs), the production of ^{14}C is mostly associated with the presence of ^{14}N impurities in stainless steel, Zircaloy cladding and nickel alloys (Yim & Caron 2006, Gras 2014). In the oxide layer of the cladding, ^{17}O originally present in the uranium dioxide (UO_2; UOX) or mixed oxide (U-PuO_2; MOX) fuels and the water coolant is also a significant precursor of ^{14}C (Necib et al. 2018b, Gras 2014). The nuclear reaction of thermal neutrons with ^{13}C may also contribute to the ^{14}C production in activated steel and Zircaloy, but at a negligible level due to its very low effective cross-section for thermal neutrons and its small natural isotopic abundance (Tab. 3-1).

In nuclear fuel from LWRs, the formation of ^{14}C is related to the activation of ^{14}N and ^{13}C, both introduced during sintering of UO_2 pellets, as impurity in the case of ^{14}N and due to the use and decomposition of binder in the case of ^{13}C (Ferrari 1963). Generation of ^{14}C from ^{17}O may also occur to some extent in spite of the lower cross-section for neutron capture, due to the higher ^{17}O content of UOX and MOX fuels (Yim & Caron 2006, Gras 2014, Johnson & Schwyn 2008).

In activated graphite, the main part of ^{14}C after operation arises from the activation of ^{13}C, as most of the ^{14}C originating from ^{13}N has been released during operation (Poncet & Petit 2009, Marsden et al. 2002). It has also been attested that some ^{14}C could also originate from the activation of ^{14}N or ^{17}O, due to gas (air or nitrogen) entrapped in the pores during graphite manufacture or coolant gas absorbed on the pore surface (Swift et al. 2016, RWM 2016a, Toulhoat et al. 2018, Wareing et al. 2013).

No information is available about the generation of ^{14}C in activated concrete. A preliminary assessment of the importance of the various activation processes can be made based on the nitrogen, oxygen, and carbon contents in hardened cement paste (HCP) and in view of the nuclear reactions leading to ^{14}C formation (Tab. 3-1). The formation of ^{14}C by ^{14}N activation is considered to be negligibly small due to the low amount of air entrapped in saturated HCP as pores are expected to be mainly filled with water. As carbon is present as calcium carbonate in HCP and oxygen is an important structure-forming element of all cement phases, activation of ^{13}C and ^{17}O could also contribute to ^{14}C formation in concrete. The amount of carbon is estimated to be 0.227 mol/kg HCP in a hydrated CEM I cement, while the amount of oxygen in HCP is expected to reach 22.9 mol/kg (Wieland & Kosakowski 2020, Kosakowski et al. 2023). Thus, the amount of oxygen is about a factor of 100 higher than the amount of carbon in HCP. With a view to the

isotopic abundance of ^{13}C and ^{17}O and their cross-sections for thermal neutrons (Tab. 3-1), it could be anticipated that ^{17}O activation is the main contributor to ^{14}C formation in concrete.

In the reactor coolant, ^{14}C is mostly produced by activation of ^{17}O present in water molecules. ^{14}C is also formed from ^{14}N present in water, but to a smaller degree, as it is considerably less abundant than ^{17}O. Generation of ^{14}C from ^{13}C in reactor coolant is several orders of magnitude lower than from the former two ^{14}C precursor isotopes, due to both its small cross-section and the low concentration of bicarbonates and organic compounds present in water coolant (Yim & Caron 2006).

Apart from the operation of NPPs, ^{14}C is also produced for various applications in medicine, industry and research (MIR), for example fluorescent pigments and labelled molecules. The primary source for such applications is ^{14}C barium carbonate ($Ba^{14}CO_3$). It is formed by the irradiation of aluminium nitride (AlN) with neutrons according to the $^{14}N(n,p)^{14}C$ reaction. Under oxidising conditions, $^{14}CO_2$ is released from activated AlN and carried by Ar to several wash bottles containing basic solution with barium ions. $^{14}CO_2$ therefore precipitates into $Ba^{14}CO_3$. $Ba^{14}CO_3$ can be directly used as fluorescent pigments or converted to $^{14}CO_2$ to generate a variety of ^{14}C-labelled molecules. A recent technique also allows the direct absorption of the $^{14}CO_2$ in stainless steel traps after irradiation of AlN.

3.2 ^{14}C inventory

3.2.1 Total ^{14}C inventory

The amounts (i.e., mass, volume) and the radionuclide inventories of the individual waste to be disposed of in the deep geological repository have been compiled in the MIRAM-RBG database (Nagra 2023). According to the activity measurements, calculations and prognoses that underpin MIRAM-RBG, the total ^{14}C inventory will reach ~ 2.4×10^{14} Bq (Nagra 2023).

Within MIRAM-RBG, the individual waste is grouped by waste package types (AGTs from the German term *"Abfallgebindetyp"*) with similar characteristics and/or similar origin. ^{14}C is not homogeneously distributed over the individual waste types but rather clusters within a few waste types (10 AGTs regroup ~ 87% of the total ^{14}C inventory and the ~ 13% left is non-homogeneously distributed within the other 591 AGTs containing ^{14}C). Moreover, ^{14}C is predominantly present in several material groups: i) activated materials, such as metals and concrete, which contain relevant amounts of activation (and associated decay) products in their bulk structure; ii) ^{14}C-containing materials, such as ion-exchange resins (IERs) and $Ba^{14}CO_3$, where ^{14}C is integrated within the structure of the material but is not the result of an activation in the reactor of NPPs; and iii) contaminated materials (including metal, organic and inorganic substances), having ^{14}C present only on their surfaces.

3.2.2 L/ILW ^{14}C inventory

3.2.2.1 State of knowledge

In the Swiss L/ILW inventory (including ATW), ^{14}C represents ~ 24.5% of the total ^{14}C inventory with an estimated total activity of ~ 5.7×10^{13} Bq (Nagra 2023). In L/ILW, ~ 61% of the ^{14}C inventory is in decommissioning waste (~ 3.5×10^{13} Bq), ~ 30% is in operational waste (~ 1.7×10^{13} Bq), ~ 7% is in reactor waste (~ 0.4×10^{13} Bq) and ~ 2% is in reprocessing waste (~ 0.1×10^{13} Bq). In decommissioning waste, ^{14}C is mostly found in activated metals and contaminated materials. In operational waste, it is mainly associated with contaminated materials, IERs and incineration products. In reactor waste, ^{14}C is only contains activated metals and in

reprocessing waste, it is inventoried in both vitrified waste and activated metals. Within L/ILW, ~ 67% of the total ^{14}C inventory is present in activated metals (~ 3.9×10^{13} Bq), ~ 26% in contaminated materials (~ 1.5×10^{13} Bq), ~ 5% in IERs (~ 0.2×10^{13} Bq) and ~ 2% in graphite (~ 0.1×10^{13} Bq) (Fig. 3-2a). Activated concrete (~ 2.7×10^{10} Bq), vitrified reprocessing waste (~ 1.5×10^{9} Bq), incineration products (~ 1.0×10^{8} Bq) and heavy elements (~ 1.3×10^{7} Bq) contain negligeable amounts of ^{14}C (Nagra 2023), which are not visible in Fig. 3-2a. A total of 21 AGTs contain more than ~ 75% of the ^{14}C inventory from L/ILW, the rest being distributed across the other 570 ^{14}C-containing L/ILW AGTs (Nagra 2023).

^{14}C contaminated waste is mainly operational waste, including waste from MIR (Nagra 2023). They contained a wide variety of materials from various origins. Hence, the material with which the ^{14}C is associated with is usually not precisely known. Based on expert judgements, the materials with which ^{14}C is associated in contaminated waste for the AGTs contributing > 1% of the L/ILW total ^{14}C inventory (i.e., 7 in total) were characterised. These AGTs contain more than ~ 14% of the total ^{14}C inventory in the L/ILW. In terms of mass, metals (~ 38%) (i.e., Pb, Al, Fe, Cu) comprise the largest fraction of the ^{14}C present in contaminated waste (Fig. 3-2b). Inorganic (i.e., cement, glass), organic (i.e., cellulose, plastics) and $Ba^{14}CO_3$ were also identified in the ^{14}C contaminated waste at ~ 29%, ~ 20% and ~ 10%, respectively (Fig. 3-2b). The rest (~ 3%) are unknown materials.

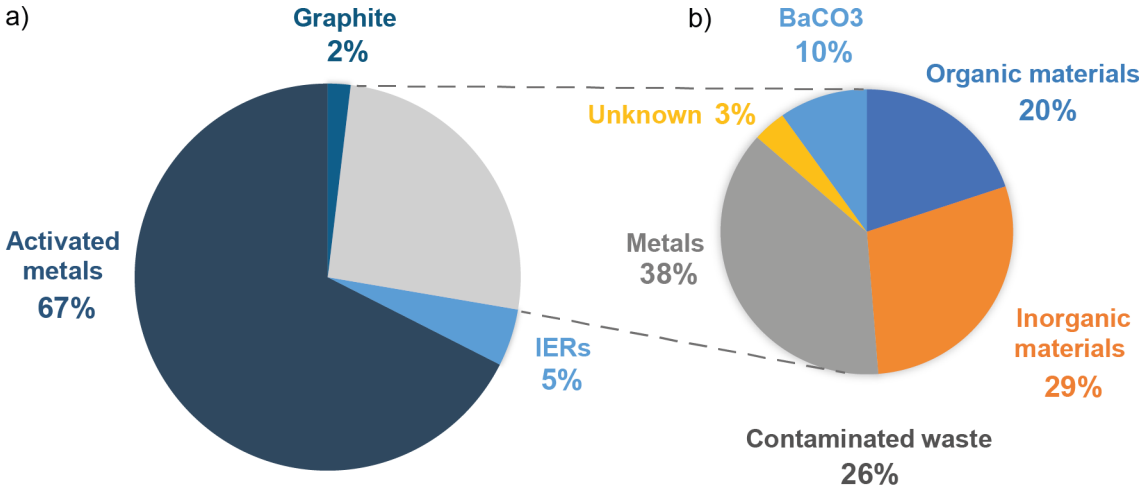

Fig. 3-2: a) Distribution of the ^{14}C inventory within the materials present in the 591 L/ILW AGTs containing ^{14}C. b) Mass distribution of the ^{14}C contaminated materials present in the L/ILW AGTs contributing > 1% of the L/ILW total ^{14}C inventory

Based on Nagra (2023).

In MIRAM-RBG, the basic unit is the reference waste package – this is a theoretical and model waste package with mean properties representing all actual waste packages of a given AGT (Nagra 2023). For the AGTs with already existing waste packages, their mean properties are based on data from the actual waste packages. For proposed AGTs, their mean properties are based on prior knowledge, comparable existing waste, investigations and assessments from producers and users regarding future applications and expert judgments.

According to the type of waste considered (i.e., already existing *vs.* prognosed waste and operational *vs.* decommissioning *vs.* reactor waste), ^{14}C activity has been either measured, calculated or estimated (Nagra 2023). For operational waste from NPPs, representative samples for each waste stream from the different waste producers are radiochemically analysed every 10-15 years. ^{60}Co activity in waste packages is usually measured by γ-detectors. Using scaling factors, the ^{14}C activity can be determined within waste packages. Different sets of scaling factors exist and are used for expected operational waste streams as well. For the expected and prognosed contaminated decommissioning waste from NPPs, the interim storage facility (Zwilag, *"Zwischenlager"*) and the packaging facilities of the repository, one representative nuclide vector (i.e., set of scaling factors) has been determined, based on the known scaling factor sets of operational NPP waste. For MIR waste, the radionuclide inventory is based on the declared inventory of individual existing waste packages. For some AGTs with very high ^{14}C content, the declared activities have been verified by Nagra. The ^{14}C content in reprocessing waste is based either on declaration by the facility or (for the majority of AGTs) on calculations and rough assumptions regarding activities within the waste. For decommissioning waste, nuclide vectors and ultimately the ^{14}C activity are based on activation calculations. For a given component, the ^{14}C activity is determined by the N impurity content in the activated materials (steel, concrete, etc). For some materials, measurements of N impurity content are available (Tab. 3-2), but for most of them, no information is available. In these cases, impurity content is determined based on literature data, ideally for the same materials, albeit from different material sources, or for similar materials as well as expert judgments. For reactor waste, ^{14}C activity is ultimately either determined or assumed based on N impurities (in the case of activation calculations used for determining activities) (Tab. 3-2) or by setting scaling factors based on radiochemical analyses of respective samples (in the case that dose measurements are linked to ^{60}Co activities).

Tab. 3-2: Assumed N impurities for all NPPs and different L/ILW materials

Based on Nagra (2023).

Swiss NPPs	Component	Reference (ppm)	Maximum (ppm)	Source
Gösgen	reactor internals (stainless steel)	452	980	Evans et al. (1984)
	reactor pressure vessel (carbon steel)	89	n.a.	samples
	reactor pressure vessel liner (stainless steel)	452	n.a.	Evans et al. (1984)
Mühleberg	reactor internals (stainless steel)	452	570	Evans et al. (1984)
	reactor pressure vessel (carbon steel)	89	n.a.	samples
	reactor pressure vessel liner (stainless steel)	452	n.a.	Evans et al. (1984)
Leibstadt	reactor internals (stainless steel)	452	570	Evans et al. (1984)
	reactor pressure vessel (carbon steel)	89	n.a.	Evans et al. (1984)
	reactor pressure vessel liner (stainless steel)	452	n.a.	Evans et al. (1984)
Beznau	reactor internals (stainless steel)	452	570	Evans et al. (1984)
	reactor pressure vessel (carbon steel)	100	n.a.	samples
	reactor pressure vessel liner (stainless steel)	452	n.a.	Evans et al. (1984)

n.a.: not applicable

3.2.2.2 Approach to post-closure safety assessments

The section summarises how the state of knowledge regarding the L/ILW ^{14}C inventory is used for safety assessment.

The mean ^{14}C activities and associated uncertainty are determined for one representative package (e.g., drum) (called the reference waste package) and apply to all waste packages present in this AGT. Hence, the “mean activity” of this reference waste package multiplied by the number of packages in the AGT represents the best estimate inventory for this AGT. The term “maximum activity” within MIRAM-RBG is to be understood as an upper bandwidth, always referring to the uncertainty of the full inventory within the AGT and not to single waste packages.

The uncertainties, including in the “maximum activity”, take into account the uncertainty of sources of activity measurement/estimation (Nagra 2023). For operational waste, the uncertainty

considers measurement uncertainties (i.e., from the scaling factor of ^{14}C to ^{60}Co), taking into account waste heterogeneity and the small number of samples. For MIR waste, the uncertainty is differentiated between waste streams and based on expert judgments regarding the reliability of known properties. For contaminated decommissioning waste, the uncertainty is estimated based on expert judgement, taking into account measurement uncertainties, waste heterogeneity and the small number of samples. For activated decommissioning waste, the uncertainty contribution of the N impurity content is taken into account as well as uncertainty from calculations. Hence, considering the "maximum activity" as a strict upper bound would be over-pessimistic and is therefore omitted for dose calculations (Nagra 2024j).

All ^{14}C-containing L/ILW AGTs, together with their mean ^{14}C activity predicted in 2075, are listed in App. A.

3.2.3 HLW ^{14}C inventory

3.2.3.1 State of knowledge

^{14}C in the HLW inventory, with an estimated total activity of ~ 1.8×10^{14} Bq, represents ~ 75.5% of the total ^{14}C inventory. In HLW, ~ 56% of the ^{14}C is associated with activated Zircaloy from the SF cladding (Fig. 3-3), with a total activity of ~ 9.9×10^{13} Bq. Around 37% is present in SF pellets made of UO_2 or MOX, with a total ^{14}C activity of ~ 6.5×10^{13} Bq, and ~ 7% is in activated steel, used in spacers and plates of SFAs (Fig. 3-3). Less than 1% of the total ^{14}C in HLW is inventoried in RP-HLW. RP-HLW is the product of the calcination of highly radioactive liquids from reprocessing operations, mixed at high temperatures with borosilicate glass and poured into steel flasks (Bradbury et al. 2014). A negligeable amount of ^{14}C (~ 0.004%) is also present in operational mixed waste including contaminated inorganic and metallic materials (Nagra 2023).

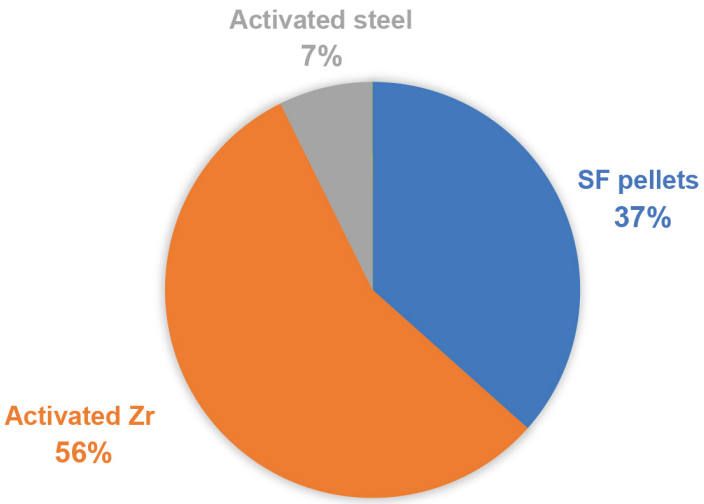

Fig. 3-3: Repartition of the ^{14}C inventory within the materials present in the 10 HLW AGTs containing ^{14}C

SFAs are grouped into 6 different AGTs, according to their origin (i.e., NPP) and fuel type (i.e., UO_2 or MOX) (Nagra 2023). The radiological inventory in each AGT is based on the arithmetic average considering the calculated individual assembly-wise total inventory and the number of SFAs. Before the averaging process, the inventory of each single SFA is determined with numerical simulations (i.e., depletion and decay calculations as well as activation calculations), taking into account its individual material, fuel design and irradiation history (Nagra 2023).

Three individual components are accounted for in each SFA: the fuel pellets, the cladding and the structural materials in the "active" part, and the structural materials in the top/bottom part of the assembly to which a specific ^{14}C activity is associated as they are subjected to significantly different neutron fluxes (Nagra 2023).

Impurities in the fresh fuel are essential for calculating the radionuclide's activity primarily produced by activation and fission processes, such as ^{14}C. In reactor materials, ^{14}C is mainly related to the activation of ^{14}N (Tab. 3-1), present in the form of impurities in the fuel matrix (cf. Section 3.1). Even though an average value of 25 ppm N was cited in publicly available data for fuel pellets, a maximum value of 75 ppm was retained based on ASTM specifications (Tab. 3-3). The N impurities determined for cladding (i.e., Zircaloy) and structural materials (i.e., stainless steel and Inconel) reach 0.008 wt.%, 0.04 wt.% and 0.03 wt.% for Zircaloy, stainless steel and Inconel, respectively (Tab. 3-3). They are used for the calculations of both the best estimate as well as the maximum activities as they are rather conservative. For RP-HLW, ^{14}C is measured in samples, declared by the producer and scaled to the mean ^{14}C activity of the reference AGT, based on the existing individual package properties. ^{14}C in RP-HLW can also be determined based on assumptions from the producers. If no information is available, ^{14}C is calculated based on the N impurities of SF. For the AGT with operational mixed waste, the ^{14}C calculation is based on those from SF as it contains debris of fuel rods. It should be noted that the values of the N impurities used for the calculations of the ^{14}C activity of HLW calculations are in agreement with the assumptions of other WMOs.

Tab. 3-3: Assumed N impurities for all NPPs and different HLW materials

Component	Best estimate	Maximum	Source
SF (pellets)	25 ppm	75 ppm	ASTM specifications (for the maximum value) and expert judgements.
Cladding (Zircaloy)	80 ppm		Expert judgements.
Cladding (stainless steel)	4 ppm		
Cladding (Inconel)	3 ppm		
Vitrified reprocessing waste	25 ppm	75 ppm	Producer assumptions or SF assessments (if no information is available from the producers).

The calculations of radionuclide inventory are performed using the SCALE nuclear modelling and simulation code system (Version 6.2.3) (Nagra 2023), which is widely used for nuclear system analysis and design. The nuclear data are based on the ENDF/B-VII.1 nuclear data library and the ORIGEN code is applied for SFAs-wise depletion and decay calculations (Nagra 2023). This code sequence is also used in international benchmarking activities.

3.2.3.2 Approach to post-closure safety assessments

Similar to L/ILW, the mean activities given for each HLW AGT are considered as best estimate. For the calculation of the ^{14}C mean activity, conservative values for N impurities are selected and uncertainties result from nuclear data, fuel design data, irradiation history and respective assumptions. In general, the uncertainty considered is different for each AGT and can be found in the respective AGT reports within Nagra (2023).

The term "maximum activity" is an upper bandwidth, taking into account the uncertainties of activity estimation and referring to a 95% confidence interval, based on a detailed uncertainty propagation calculation. The "maximum activity" as a strict upper bound would be overly pessimistic and is therefore omitted for dose calculations (Nagra 2024j).

All ^{14}C-containing HLW AGTs, together with their mean ^{14}C activity predicted in 2075, are listed in App. B.

3.3 ^{14}C speciation and rate of release

3.3.1 L/ILW ^{14}C speciation and rate of release

3.3.1.1 State of knowledge

Even though the ^{14}C inventory in L/ILW is small in comparison to HLW (~ 24.5%; cf. Section 3.2.2), it is expected to contribute most to the dose release as no period of complete containment is assumed in L/ILW. On the contrary, complete containment of HLW is ensured for a certain period of time (Nagra 2024b), allowing an important decay of ^{14}C within the HLW disposal canister.

The expected speciation and release of ^{14}C is closely linked to the expected phenomenological evolution of the L/ILW section of the repository, which is summarised in Kosakowski et al. (2023) and in Nagra (2024f). The following sections provide information on the ^{14}C speciation and release from the L/ILW materials with which the majority of the ^{14}C is associated.

Activated steel

In L/ILW, the majority of the ^{14}C is associated with activated metals (~ 67%) (Fig. 3-2), and especially steel (at ~ 95%) (Nagra 2023). Stainless steel is one of the main components of NPP reactor internals, while carbon steel is part of the reactor pressure vessel, reactor building reinforcements and liners. Even though the carbon steel components are less exposed to high neutron fluxes during reactor operation, both steel types can become activated and arise as reactor and decommissioning L/ILW.

In both stainless and carbon steel, ^{14}C is mainly formed due to the activation of ^{14}N impurities that are initially present in the bulk matrix (Yim & Caron 2006, Gras 2014). The chemical form of ^{14}C might predominantly be elemental C(0), retained in the interstices of the crystal structure, and/or, to some degree, accommodated by carbide (Wieland et al. 2023). According to Swanton et al. (2015), it is conceivable that ^{14}C produced by activation in steel is not in the same chemical form as stable carbon at the time of steel production. However, the nature of stable carbon compounds released from activated steel during corrosion might still be identical to that of ^{14}C compounds.

Early studies on the ^{14}C release during corrosion of activated steel were conducted in the framework of the Japanese waste management programme. In these studies, Kaneko et al. (2002)

identified ^{14}C-bearing organic carbon species, such as formic acid, acetic acid, formaldehyde, methanol and ethanol, in the leaching solutions during corrosion of activated carbon steel at both pH 8 and 12.5. Similar compounds were observed in solutions during the leaching of iron carbide powder (Fe_3C).

The study of Sasoh (2008) showed similar results to the study of Kaneko et al. (2002) for activated stainless steel, but the authors additionally mentioned the existence of gaseous carbon compounds such as CH_4 or C_2H_6, although the concentrations measured were found to be very low. Later, Miyauchi et al. (2011) characterised the speciation of ^{14}C-bearing compounds released during long-term corrosion (i.e., 42 months) of activated stainless steel in alkaline solution. In this study, summarised in Mibus et al. (2018), 25% of the ^{14}C inventory was released to the gas phase. In solution, organic species were identified to be predominantly in anionic forms (i.e., carboxylates) rather than neutral (i.e., alcohols, aldehydes), with a ratio of organic to inorganic compounds nearly equal to one.

More recently, several studies on the speciation of ^{14}C compounds released from activated steel in conditions relevant to a deep geological repository were performed in the framework of the EU project "Carbon Source Term (CAST)" (Visser-Týnová et al. 2018a, Visser-Týnová et al. 2018b, Druyts et al. 2018, Cvetković et al. 2018b). In the study of Druyts et al. (2018) using carbon steel, a predominance of $^{14}CH_4$ was observed in the gas phase after 231 days of leaching. $^{14}C_2H_6$, $^{14}C_2H_4$ and $^{14}CO_2$ were also detected, but at lower concentrations. ^{14}C compounds released to solution were unfortunately not identified. In Visser-Týnová et al. (2018a) and Visser-Týnová et al. (2018b), activated stainless steel was immersed in NaOH solution (at pH 13) under anoxic conditions for 1.13 years. The main part of the ^{14}C activity (> 94%) released was primarily present in the dissolved form, whereas the ^{14}C fraction released to the gas phase was rather small (1 to 6% over the first year). In solution, between ~ 20% and ~ 50% of ^{14}C released was present in the organic form. However, no information was available on the individual aqueous ^{14}C compounds. The rest, i.e., between ~ 80% and ~ 50% of the dissolved ^{14}C species, was inorganic in the chemical form of ^{14}C carbonates (Visser-Týnová et al. 2018a, Visser-Týnová et al. 2018b). In the gas phase, $^{14}CH_4$ was the main gaseous species released, amounting to ~ 90% of the total ^{14}C in the gas phase. ^{14}CO only reached ~ 10%, while the contribution of $^{14}CO_2$ was negligible.

In the study of Cvetković et al. (2018b), which was pursued after the CAST project by Guillemot et al. (2022), activated stainless steel was immersed in saturated portlandite ($Ca(OH)_2$) solution at pH 12.5 under an anoxic atmosphere for 4.48 years. Over this time, approximately equal fractions of ^{14}C were released to the liquid and gas phases (i.e., 47% ± 10% versus 53% ± 16%, respectively). It should, however, be kept in mind that, in this study, the fraction of ^{14}C in the gas phase was found to continuously increase with time (see below in this section). In solution, ~ 75% of the released ^{14}C was in the form of organics and ~ 25% was present as carbonate. Five ^{14}C carboxylates were identified (i.e., formate, acetate, lactate, malonate and oxalate) but they only represented ~ 50% of the ^{14}C-bearing organics present in solution. The other half is not yet identified and could contain additional carboxylic acids, alcohols, or aldehydes (Cvetković et al. 2018b; Guillemot et al. 2021).

Because of the small difference in molecular weight between ^{14}C and the lighter, stable ^{12}C, difference in behaviour, due to isotopic fractionation/discrimination, is sufficiently small that ^{14}C can reasonably be expected to behave in the same way as stable carbon. Hence, Guillemot et al. (2021) postulated, based on comparative studies with non-activated iron carbide powders (Cvetković et al. 2018a; Guillemot et al. 2020), that oxygenated dissolved ^{14}C compounds could most likely be formed during exposure of the activated metal to oxic conditions (i.e., in the reactor core of a NPP, during material transfer and storage in air, etc.) and were accommodated in the oxidised surface layer. The authors also did not exclude that such oxidised carbon species might alternatively be produced due to the presence of O_2 or other oxidising agents in the leaching solution (residual and/or produced by radiolysis). It is further conceivable that the oxidation of

^{14}C proceeds over time into the bulk metal below the passivating oxide layer, thus implying diffusion of the oxidising agent, through the oxide layer, into the bulk matrix.

In the gas phase, three ^{14}C hydrocarbons (HCs) (i.e., CH_4, C_2H_6 and C_3H_8) and ^{14}C-bearing carbon monoxide were detected, with $^{14}CH_4$ as the main species (i.e., > 80% of the ^{14}C present in the gas phase). A small portion of ^{14}C in the gas phase has not yet been identified (i.e., up to 20%) (Guillemot et al. 2021). As the concentrations of HCs released to the gas phase tended to decrease with increasing number of carbon atoms per molecule, the formation of HCs was interpreted in terms of a Fischer-Tropsch type mechanism, based on the corrosion studies with non-activated iron powders (Cvetković et al. 2018a; Guillemot et al. 2020; Cvetković et al. 2018b). It should also be noted that small ^{14}C compounds may be able to preferentially diffuse through the passivating layer along with H_2.

Regardless of the very different designs of the two leaching experiments, carried out with activated steel under the highly alkaline conditions by Visser-Týnová et al. (2018a), Visser-Týnová et al. (2018b) and Guillemot et al. (2021), Guillemot et al. (2022), the results reported are relatively consistent in terms of the ^{14}C speciation in both the liquid and gas phases, in particular the predominance of $^{14}CH_4$ in the gas phase. The different proportions of the ^{14}C-bearing compounds released to solution versus those released to the gas phase, but also the different proportions of organics versus inorganics released to solution in the two studies, are probably due to various parameters, such as the conditions, to which the materials were exposed prior to use (i.e., oxic conditions), the different types of stainless steel used (e.g., N impurities, surface areas) and the surface dose rate of the materials (Wieland et al. 2023, Mibus et al. 2018).

Regarding the surface dose rate, it should be noted that in the study of Visser-Týnová et al. (2018a) and Visser-Týnová et al. (2018b), the surface dose rate of the activated steel nuts investigated was about two orders of magnitude higher than that of the ones used by Guillemot et al. (2021) and Guillemot et al. (2022) (i.e., 10 – 20 Gy/h versus ~ 0.12 Gy/h). This is probably the reason why higher concentrations of oxygenated ^{14}C compounds were measured by Visser-Týnová et al. (2018a) and Visser-Týnová et al. (2018b). γ-radiation emitted from ^{60}Co (the main activation product in activated steels) gives rise to water radiolysis, thereby producing radicals and oxidants, such as $HO^{\bullet}$, $HO_2^{\bullet}$ and H_2O_2, which may in turn affect the ^{14}C speciation by increasing the proportion of oxidised ^{14}C compounds. Due to the short half-life of ^{60}Co ($t_{1/2}$ = 5.27 years), the radiation intensity rapidly decreases over time, and it is therefore not expected that γ-radiation will have a long-term effect on the chemical nature of the ^{14}C compounds released. Consequently, reduced ^{14}C compounds, such as HCs, should become predominant with time.

The long-term release of ^{14}C compounds was monitored in two corrosion studies with stainless steel (Guillemot et al. 2021, Guillemot et al. 2022, Visser-Týnová et al. 2018a, Visser-Týnová et al. 2018b). In the study of Guillemot et al. (2021) and Guillemot et al. (2022), the concentrations of individual ^{14}C species present in both the liquid and gas phases were quantified. The concentration of dissolved ^{14}C organics (mostly carboxylates) increased quite rapidly, corresponding to a release of 1.7×10^{-3}% of the total ^{14}C inventory after 0.08 years (30 days). After that, the concentrations of dissolved ^{14}C organics remained constant over time. In a similar way, ^{14}C inorganics showed stable concentrations in the long term. Guillemot et al. (2021) and Guillemot et al. (2022) suggested that oxidised ^{14}C species (both carboxylates and carbonates) were virtually instantaneously released by desorption from the oxide layer once the activated steel was in contact with alkaline solution. In the gas phase, the concentrations of ^{14}C compounds could only be determined in the period between 3 and 4.48 years of the experiment due to methodological issues. Good agreement was found between the ^{14}C release rate into the gas phase and the corrosion rate of activated stainless steel of ~ 1 nm/a (based on independent measurements of H_2 concentrations in the gas phase).

The other long-term study of Visser-Týnová et al. (2018a) and Visser-Týnová et al. (2018b) showed similar outcomes to that of Guillemot et al. (2021) and Guillemot et al. (2022). The authors registered an initial fast release of ^{14}C organics and ^{14}C inorganics both to the liquid and gas phases during the first week of leaching, followed by a drop and a stabilisation of the rate of release. During the first three experimental weeks, 1.0×10^{-3}% of the total ^{14}C inventory of the activated steel was released to solution. In the gas phase, the released fraction reached between 4×10^{-6} and 8.6×10^{-4}% of the total ^{14}C inventory. The initial release of ^{14}C seems therefore to be markedly higher to liquid phase than to the gas phase. For the long-term release, the total ^{14}C release measured in the experiment was converted to a corrosion rate of ~ 3 nm/a, which is comparable to the corrosion rate determined by Guillemot et al. (2021) and Guillemot et al. (2022) and within the range of the rates measured for stainless steel under highly alkaline conditions (Diomidis et al. 2023).

In summary, the release of ^{14}C from activated steel in alkaline anoxic conditions seems to occur in two distinct phases:

i) A fast release of ^{14}C (mainly in solution, both in organic and inorganic chemical forms) over a period of a few days to weeks, as a result of the release of ^{14}C from the oxide layer as soon as the metal comes in contact with alkaline solution. The released amount was estimated to be of the order of 10^{-3}% of the total ^{14}C inventory.

ii) The remaining (and largest fraction) of the total ^{14}C inventory (i.e., > 99.999%) is subject to a slow release of ^{14}C compounds (mainly in the form of $^{14}CH_4$) at a similar rate to that of corrosion.

Activated Zircaloy

In L/ILW, activated Zircaloy is one of the main components present in compacted metallic waste from the reprocessing of SF and accounts for ~ 3% of the activated metals in the L/ILW (Nagra 2023). As for activated steel, the production of ^{14}C is mostly associated with the presence of ^{14}N impurities (Yim & Caron 2006, Gras 2014). In the oxide layer of the Zircaloy cladding, ^{17}O is also a significant precursor of ^{14}C, due to the proximity of the uranium dioxide (or $(U\text{-}Pu)O_2$) fuel to the cladding and the exposure of the latter to the water coolant within reactor pools (Necib et al. 2018b, Gras 2014). Regarding the bulk of the Zircaloy cladding, it has been suggested that ^{14}C is present in the zirconium matrix or/and in carbide precipitates (Smith & Baldwin 1993, IAEA 1998, Aomi et al. 2008).

Activated Zircaloy from reprocessing was subject to various treatments during reprocessing, which are described at length in Gras (2014). To summarise, the SFAs are first sheared up into pieces with an average length of 35 mm and put in a dissolver (Bourgeois 2000). In there, boiling concentrated nitric acid solution is used to dissolve as fully as possible the fuel pellets contained in the pieces. The Zircaloy cladding is not supposed to be attacked. Following the fuel dissolution stage, the cladding is rinsed with acid and then with water at ~ 80 °C before being compacted and conditioned into steel flasks (Gras 2014).

The first experimental studies on the chemical form of ^{14}C released during the corrosion of activated Zircaloy in alkaline solution were carried out in the framework of the Japanese disposal programme (Yamaguchi et al. 1999, Kaneko et al. 2002, Tanabe et al. 2009, Sasoh 2008, Takahashi et al. 2014). So far, Yamashita et al. (2014) is the only study with activated Zircaloy (from boiling water reactor (BWR) cladding) pretreated in a similar way to during reprocessing (i.e., exposure to a nitric acid solution and removal of the oxide layers corresponding to freshly cut metallic surfaces). The pretreated activated Zircaloy was then immersed in a highly alkaline solution for a total of 2 years. Only the ratio between total gaseous ^{14}C compounds, totally dissolved ^{14}C inorganics and totally dissolved ^{14}C organics was monitored, and not the concentrations of single ^{14}C compounds. Over the two years of leaching, the distribution of the ^{14}C

speciation was constantly changing (i.e., an initial predominance of gaseous ^{14}C compounds was followed by a higher proportion of dissolved ^{14}C inorganics and dissolved ^{14}C organics), making any interpretation rather difficult.

In the framework of CAST, additional studies on activated Zircaloy exposed to alkaline conditions were conducted and individual ^{14}C species were identified (Bucur et al. 2018, Caes et al. 2018, Druyts et al. 2018, Sakuragi 2017, Necib et al. 2018a, Necib et al. 2018b). A common conclusion of these studies is that only small molecules were formed and released both to the liquid and gas phases. Examples of such molecules are carboxylates (i.e., formate, acetate, oxalate, propionate and glycolate), alcohols (i.e. methanol, ethanol), carbonates and HCs (i.e., CH_4, C_2H_6, C_2H_4). It should, however, be noted that the release of acetate and formate was still to be confirmed, as contamination from other sources could not be excluded (Necib et al. 2018a, Necib et al. 2018b).

The study of Yamashita et al. (2014) was pursued within the CAST framework (Sakuragi 2017) and is, until now, the only long-term experiment with activated Zircaloy with a total leaching time of ~ 6.5 years under alkaline anoxic conditions. After two years and until 5.5 years of corrosion, a predominance of dissolved ^{14}C organics was observed, compared to dissolved ^{14}C inorganics and gaseous ^{14}C compounds (Sakuragi 2017). The distribution of ^{14}C compounds was also quantified on activated Zircaloy with an external oxide layer after 6.5 years of corrosion and the results were similar (Sakuragi 2017). Hence, the reprocessing of used nuclear fuel does not seem to have a marked effect on the speciation of ^{14}C compounds being released from activated Zircaloy, as was also previously suggested by Necib et al. (2018b) and Smith & Baldwin (1993).

Large variations in the proportions of dissolved ^{14}C inorganics and organics were generally observed in the CAST studies, probably due to the different analytical techniques and Zircaloy types used in the experiments (Necib et al. 2018a, Necib et al. 2018b), making interpretations difficult. Hence, additional long-term experiments with similar types of Zircaloy and analytical techniques, including the identification of single ^{14}C species released, would be required to better constrain the ^{14}C speciation and rate of release from activated Zircaloy in conditions relevant for a deep geological repository.

The effect of redox conditions on the ^{14}C speciation during corrosion of activated Zircaloy has not been assessed to date. It can be assumed, based on the experimental data of activated (stainless) steel, that oxygenated ^{14}C species, such as carboxylates, are preferentially formed and retained in the oxidised surface layer when activated Zircaloy is exposed to oxic conditions (i.e., in the reactor core of a NPP, during material transfer and storage in air, etc.), noting that, in the long term, reducing conditions are supposed to prevail in a repository (Wieland et al. 2023).

The mechanisms and the rate of ^{14}C release from activated Zircaloy cladding are expected to be controlled in large part by the diffusion rate of ^{14}C through zirconia oxide layers, the dissolution rate of the oxide layer itself and the uniform corrosion rate of Zircaloy (Gras 2014).

In the preliminary Japanese and French safety cases (FEPC & JAEA 2007, Hélie 2004, Andra 2005), 20% of the total ^{14}C inventory of the Zircaloy cladding was expected to be present in the oxide layer of activated Zircaloy, based on scoping activation calculations. Later, Sakuragi et al. (2014) carried out more detailed calculations using the ORIGEN code and determined the abundance of ^{14}C in the oxide layer and the bulk Zircaloy to be at 3.5% and 96.5%, respectively. This ^{14}C distribution roughly corresponds to the results obtained within the framework of the CAST project, from which the respective percentages of 7.5% and 92.5% were obtained based on ^{14}C measurements on both base metal and oxide layer (thickness of 25.3 μm) from BWR cladding (Sakuragi 2017). In the long-term corrosion experiment with BWR cladding, the ^{14}C leaching ratio (i.e., the leached amount in both the liquid and gas phases divided by the initial ^{14}C inventory) only reached 3.8×10^{-3}% after 6.5 years of corrosion (Sakuragi 2017). In their shorter-term leaching tests with activated Zircaloy from a pressurised water reactor (PWR), Yamaguchi

et al. (1999) also measured small leaching ratios reaching ~ 0.03%. Similarly, a total leached ratio of less than 2×10^{-3}% was measured in the rapid leaching test of Sakuragi & Yamashita (2020) with activated Zircaloy from BWR without an oxide layer (pretreated with nitric acid). Finally, a leached ratio of 7.7×10^{-4}% was measured in the 18 months leaching test of Bucur et al. (2018) with Canada deuterium uranium reactor (CANDU) cladding, also pretreated with nitric acid. Based on both the activation calculations mentioned above and the leaching experiments on various types of activated Zircaloy (i.e., Zry-2; Zry-4) coming from different NPP types (i.e., BWR, PWR, CANDU), the initial assumption that all 20% of the total ^{14}C being present in the oxide layer is rapidly released once activated Zircaloy comes in contact with solution, is now judged to be overly pessimistic (Necib et al. 2018b).

Consisting of substoichiometric zirconia, the Zircaloy oxide layer features point defects. It is then conceivable that ^{14}C is trapped in these defects and not bound within the oxide matrix in the same way as the ^{14}C in the base metal (Aomi et al. 2008). Older experiments on thermally-activated ^{14}C release made by Smith & Baldwin (1993) suggest that there are at least two types of sites occupied by the ^{14}C atoms in the oxide layer of activated Zircaloy: ^{14}C adsorbed on the surface of the oxide, which is observed to desorb first; and ^{14}C occluded within the zirconium oxide layer, requiring more time for release as the solubility of zirconia is extremely low in alkaline media (i.e., around 10^{-6} M at pH 12.5) (Gras 2014). The slow diffusion of ^{14}C through zirconia can also not be excluded. Unfortunately, no information is available on zirconia dissolution and ^{14}C release. The only experimental study, in which the ^{14}C release was monitored both in the liquid and gas phases in the long term, was the study of Yamashita et al. (2014) and Sakuragi (2017). In the first year, a significant fraction of ^{14}C was released to the gas phase (53 to 55%). The proportion of dissolved ^{14}C compounds (both inorganics and organics) seemed to remain constant after three years of leaching.

Corrosion rates of non-activated and activated Zircaloy were also estimated in Sakuragi (2017), respectively using H_2 measurements for non-activated Zircaloy and ^{14}C concentrations released from activated Zircaloy. By comparing the corrosion rates for non-activated Zircaloy measured with H_2 with the rate for activated Zircaloy measured with ^{14}C concentrations, it was possible to check whether ^{14}C release can be linked to the process of corrosion. A lower corrosion rate was determined for the activated samples than for the non-activated ones. Since the difference could not be sufficiently explained by the differences in the test conditions (i.e., temperature was higher in the experiment with the non-activated samples), no direct link between ^{14}C leaching and corrosion could be confirmed and requires further research (Sakuragi 2017).

In summary, the following statements can be made regarding ^{14}C speciation and release from activated Zircaloy:

(i) After few years of leaching, the proportion of dissolved ^{14}C organics seems to be predominant, if compared with that of gaseous ^{14}C compounds and dissolved ^{14}C inorganics. Reprocessing treatment (i.e., exposure to nitric acid) does not seem to have a marked effect on the ^{14}C species distribution, but information on the distribution of single ^{14}C-bearing compounds is still missing. So far, single ^{14}C species such as carboxylates, alcohols, carbonates and HCs were identified but not quantified during long-term leaching experiments with activated Zircaloy.

(ii) The earlier assumption that 20% of the total ^{14}C inventory would be released rapidly from the oxide layer of activated Zircaloy is considered to be overly pessimistic. Latest experiments rather show rapid release fractions between 10^{-2} and 10^{-4}% of the total ^{14}C inventory (Sakuragi 2017, Sakuragi & Yamashita 2020, Bucur et al. 2018, Yamaguchi et al. 1999), even after few years of alkaline anoxic corrosion and regardless of whether the activated Zircaloy was exposed to reprocessing treatment (i.e., nitric acid) or not. This finding is independent from the different types and origins of the activated Zircaloy investigated.

(iii) Regarding the long-term release of ^{14}C from activated Zircaloy, it has so far not been possible to determine a clear link between the ^{14}C release and the corrosion of the bulk metal.

Other activated metals

The speciation and release of ^{14}C from activated metals other than steel or Zircaloy present in MIRAM-RBG (e.g., Al, Pb, Cu, Be) have so far not been investigated in dedicated experiments.

Activated graphite

In L/ILW, ~ 2% of the total ^{14}C inventory is present in activated graphite (Fig. 3-2). A part of the ^{14}C is bound covalently and distributed homogeneously throughout the graphite matrix, arising primarily from the activation of ^{13}C. The rest of ^{14}C is generated by the activation of ^{14}N or ^{17}O mainly present in hotspots and adsorbed on the graphite surface (Toulhoat et al. 2018, Swift et al. 2016, RWM 2016a, Wareing et al. 2013).

A great number of studies on the ^{14}C speciation and rate of release from activated graphite have been carried out in the framework of the earlier EU project CARBOWASTE and the recently concluded CAST project. The results from the latter project are summarised in Toulhoat et al. (2018), also including parts of the previous CARBOWASTE project. In the framework of the CAST project, acid stripping/wet oxidation tests were carried out by RATEN ICN on leachate solutions at pH 13 sampled at different intervals under anaerobic conditions. More organic than inorganic ^{14}C compounds were released (i.e., ~ 65% dissolved ^{14}C organics on average), while no ^{14}C volatiles were measured. It should be noted that any $^{14}CO_2$ released from the irradiated graphite would remain in solution as carbonates due to the high-pH conditions. After 364 days of leaching test, less than 2% of the initial ^{14}C inventory was released as dissolved species (Toulhoat et al. 2018).

The leaching experiments carried out by CEA at pH 13 under inert atmosphere showed that more than 95% of the released ^{14}C was found in the liquid phase mainly as inorganic species (i.e., carbonates), but ^{14}C organics could also be identified. After 100 to 200 days, the speciation of the released ^{14}C reached a quasi-steady state with around 70% inorganic / 30% organic species, with a maximum of 50% inorganics / 50% organics. In the gas phase, only a mixture of ^{14}C organics and/or ^{14}CO was measured. No $^{14}CO_2$ was observed due to the high pH of the solution (Toulhoat et al. 2018).

In the leaching experiment conducted by the Forschungszentrum Jülich in cementitious media (pH 13), ^{14}C was predominantly released to solution in the chemical form of carbonate. In the gas phase, $^{14}CO_2$, ^{14}CO or ^{14}C organics were detected in similar abundance, at two orders of magnitude lower than the dissolved ^{14}C compounds due to the highly alkaline leaching solution. Hence, most of ^{14}C compounds released are assumed to be considerably retarded if activated graphite is encapsulated in cementitious environment (Toulhoat et al. 2018). The average rate of ^{14}C release is equal to ~ 7×10^{-3}% a^{-1}, noting that it did not vary significantly with temperature (25 °C and 50 °C). Over the exposure time of ca. 140 days, the total release of ^{14}C only reached ~ 0.7% (Toulhoat et al. 2018).

In the leaching experiments of Radioactive Waste Management (RWM) under anoxic and highly alkaline conditions, the ratio of the dissolved to gaseous ^{14}C compounds was found to be typically of the order of 100, while it ranged from about 10 to a few hundred (RWM 2016a, Toulhoat et al. 2018). In solution, ^{14}C organics as well as ^{14}C inorganics (i.e., $^{14}CO_2$; carbonates) were measured with a predominance of ^{14}C organics. In the gas phase, both volatile ^{14}C organics (probably $^{14}CH_4$) and ^{14}C inorganics (i.e., ^{14}CO and $^{14}CO_2$ which was only removed from solution at near-neutral pH) were also detected. The form of gaseous ^{14}C compounds is affected by the redox conditions; lower redox conditions seem to promote the formation of ^{14}C organics, while the total ^{14}C release

to the gas phase was found to be similar. Moreover, the proportion of each gas phase species was found to be different between graphite samples from different sources (RWM 2016a, Toulhoat et al. 2018). The production of oxidised ^{14}C compounds quired a previous oxidation process, while reduced ^{14}C compounds could arise due to the presence of hydrogen at active carbon sites (Toulhoat et al. 2018). In the RWM leaching experiments (summarised in RWM 2016a and references therein), an initial fast ^{14}C release was observed (between 0 and 0.2% of the total ^{14}C inventory), followed by an approach to steady state with a very low incremental release rate (continuing for at least 4 years in some cases). From ~ 1% up to 30% of the total ^{14}C inventory was actually released to solution at a rate of 10^{-3} a^{-1} and 10^{-1} a^{-1} over a period of up to 4 years under highly alkaline and strongly acidic conditions, respectively. Hence, a significant fraction of ^{14}C in irradiated graphite appears to be bound as part of the graphite matrix and is inaccessible to leaching (RWM 2016a, Toulhoat et al. 2018).

The RWM studies also highlighted that the ^{14}C speciation and rates of release may depend on the type of graphite, its irradiation history and the reactor operational conditions.

In summary, ^{14}C can be released from activated graphite to both the liquid and gas phases as organic and inorganic species. However, it should be noted that a substantial fraction of the ^{14}C present in graphite seems to not be releasable. Part of the releasable fraction is initially released at a high rate, and the remaining fraction is subsequently released at a slower rate which continuously decreases with time.

Activated concrete

Structural elements of NPPs made of concrete and located close to the reactor core are exposed to neutron fluxes and therefore become activated. During demolition of the reactor at the end of its lifetime, the activated concrete elements arise as decommissioning L/ILW. Only ~ 0.1% of the total ^{14}C inventory in L/ILW is associated with activated concrete (Nagra 2023). Neither experimental studies nor theoretical considerations have previously been made about the ^{14}C speciation and release from activated concrete.

Activated heavy elements

In one AGT, activated heavy elements (e.g., thorium and uranium) are listed and correspond to only 2.3×10^{-5}% of the total ^{14}C inventory present in L/ILW (Nagra 2023). As in the case of activated concrete, neither experimental studies nor theoretical considerations have previously been made about the ^{14}C speciation and release from activated heavy elements.

Contaminated materials

Around 25% of the total ^{14}C inventory in L/ILW is associated with contaminated materials. This means that ^{14}C is expected to be predominantly attached to the surface of the materials and not actually bound to their chemical structure (Wieland et al. 2023). Contaminated materials include a wide variety of different materials, like metals (i.e., Pb, Al, Fe, Cu), inorganic (i.e., cement, glass, ashes) and organic (i.e., cellulose, plastics) substances (Fig. 3-2). They originate from NPPs, surface and research facilities, and are mainly present in operational and decommissioning waste.

There is currently very limited information on ^{14}C speciation and release from contaminated materials due to: (i) the heterogeneous origin of these types of waste (i.e., waste from NPPs, MIR), (ii) their different conditioning processes, and (iii) their different storage conditions.

In their study, Cloet et al. (2014) assumed a ratio of 70% ^{14}C inorganics / 30% ^{14}C organics for contaminated materials originating from PWRs and a ratio of 90% ^{14}C inorganics / 10% ^{14}C

organics for contaminated materials originating from BWRs, based on the only study available at that time on the speciation of ^{14}C compounds released from IERs (Magnusson & Stenström 2005) (see section "IERs" below). Concerning the waste from the Swiss pilot incineration facility and the plasma furnace at Zwilag (i.e., residues, ashes, slag), an entirely inorganic speciation is to be expected as they are exposed to high temperatures and oxic conditions during incineration.

In term of release, it can be assumed that as soon as the contaminated waste comes in contact with porewater, ^{14}C is quickly released to solution, as it is not bound to its structure but only adsorbed on its surface.

IERs

Around 5% of the total ^{14}C inventory are associated with IERs (Fig. 3-2), which are among the most abundant organic materials present in L/ILW (Nagra 2023, Guillemot et al. 2023). They are especially used in NPPs for the purification of the coolant system (primary, secondary circuits) and effluent treatment, removing corrosive ionic species and/or radionuclides that contribute to local dose rates (Rizzato et al. 2017). IERs are styrene-based polymers cross-linked with divinyl-benzene and functionalised with sulphonic groups (cationic IERs) or quaternary ammonium groups (anionic IERs), which selectively adsorb cations or anions and exchange them with others, thereby resulting in a selective sequestration of ionic components from the solution (Rizzo et al. 2018). Anionic IERs can act as a strong base, deprotonating ^{14}C anions such as $H^{14}CO_3^-$ (Abrahamsen et al. 2015).

Within the framework of the CAST project, leaching tests with IERs were mainly realised in alkaline solutions, as the ^{14}C release from IERs only occurs in highly basic media (Večerník et al. 2018). Unfortunately, neither similar IERs nor standard analytical procedures were applied among the organisations that participated in CAST. The samples came from various parts of the purification systems of NPPs and were also often mixed. Hence, the characterisation of the ^{14}C speciation and release from IERs was a rather difficult task (Večerník et al. 2018). Despite these shortcomings, it was still possible to draw some conclusions about the ^{14}C speciation from the CAST project. In leaching experiments with IERs collected in BWRs, more than 90% of the ^{14}C released was in the form of carbonate ions (Večerník et al. 2018, Rizzo et al. 2018). Formic acid was detected as organic species in some of the leachates, but only in small amounts (Večerník et al. 2018). It potentially originates from the reactor coolant and/or from the degradation of the IERs (Rizzato et al. 2017). In leaching experiments with IERs sampled from PWRs, it was difficult to define with certainty the percentage of ^{14}C inorganics and ^{14}C organics being released. The results from the individual experiments varied widely, ranging from 30% up to 99% for the inorganic fraction (Rizzo et al. 2018). It was however assumed by Večerník et al. (2018) that between 20 to 30% of the total ^{14}C was released in the form of organics. Similar percentages had previously been determined by Magnusson & Stenström (2005), who measured 70% ^{14}C inorganics / 30% ^{14}C organics and 90% ^{14}C inorganics / 10% ^{14}C organics in leaching experiments with IERs sampled from PWRs and BWRs, respectively. The difference of ^{14}C speciation between ^{14}C compounds released from PWR-IERs and BWR-IERs might be explained by the different chemistry of the water coolant. It should also be noted that experiments on solidified IERs showed no or only a negligible amount of ^{14}C leached (Večerník et al. 2018). Furthermore, the drying procedure of the leachate seems to affect the ^{14}C speciation (a predominance of ^{14}C organics is measured) (Rizzo et al. 2018, Večerník et al. 2018).

Several experiments on the degradation and leaching of IERs have shown that functional groups, including the quaternary ammonium groups that sorb ^{14}C-bearing anions, are the first component released from the polymer after exposure to radiation (Van Loon & Hummel 1995, Hall et al. 1970), at temperatures above 50 °C (Bucur et al. 2018, Rizzato et al. 2017) or upon aging (Rizzo et al. 2018). Hence, a fast release of ^{14}C from IERs might be expected, noting that it only occurs

in highly basic media (a concentration of at least 0.1 M alkaline hydroxide seems to be needed; cf. Večerník et al. 2018).

In summary, when adsorbed on the functional surface groups of IERs, ^{14}C is considered to be rapidly released, as these groups are easily degradable, predominantly in the form of ^{14}C carbonate. The ^{14}C speciation (i.e., inorganics/organics ratio) can however be influenced by the pre-operational treatment of the IERs, their position in the NPP cleaning circuits, their conditioning processes and their interim storage conditions.

$Ba^{14}CO_3$

Still used in the military sector today to produce fluorescent colour for assault rifle sights, compasses and other military objects, $Ba^{14}CO_3$ contributes to ~ 10% of the ^{14}C contaminated L/ILW (Nagra 2023). It is applied in the form of powder with zinc sulphide and covered by an acrylic lacquer on the parts of the equipment that need to be fluorescent. Only the pieces that contain $Ba^{14}CO_3$ are considered and disposed of as L/ILW. They are put into small boxes to avoid direct contact with other materials when conditioned into waste drums (200 L). When dissolved, ^{14}C is present in the chemical form of carbonate ions. As in the case for other carbonates, $Ba^{14}CO_3$ is virtually insoluble in highly alkaline solution. Although carbonate solubility is expected to increase with decreasing pH as a result of cement degradation, the solution pH is expected to be ~ 12.5 for at least the first 1,000 years after repository closure and to remain above 10, for the first 10,000 years (Nagra 2021b). It should also be noted that $Ba^{14}CO_3$ will not initially be in direct contact with solution as it will be protected by an acrylic lacquer and the above-mentioned small boxes (Nagra 2023).

In summary, ^{14}C from $Ba^{14}CO_3$ is released in the form of carbonate at a rate similar to its dissolution. The specific properties of $Ba^{14}CO_3$-containing waste types (i.e., presence of acrylic lacquer surface and storage in isolated compartments) and the initial highly alkaline conditions in the L/ILW near-field are expected to substantially delay and attenuate the release of ^{14}C.

Vitrified L/ILW

An extremely small amount of the ^{14}C inventory is associated with vitrified L/ILW (~ 0.03%) (Nagra 2023). Originating from reprocessing treatments, it is conditioned with borosilicate glass and packed into steel flasks. No experimental evidence about the ^{14}C speciation and release is currently available in the literature.

It is generally expected that ^{14}C is homogeneously distributed within the glass matrix because of intensive mixing prior to vitrification. Borosilicate glass corrosion rates under alkaline conditions have recently been reviewed in Cloet et al. (2019). The review shows that under alkaline conditions, borosilicate glass dissolves much faster in solution at pH ≥ 11.5 (90 °C) than in near-neutral conditions (i.e., pH ~ 9), as the amorphous surface layer (referred to as "gel layer" in the glass corrosion literature) no longer has a passivating effect. The experiments of Gin et al. (2015) indicate that this transition occurs between pH 9 and 11.5. The pH value of the porewater penetrating a breached steel flask is expected to be around 10.8 – 10.9 (at 54 °C) or between 10.1 and 10.5 (at 88 °C). Consequently, a loss of passivation cannot be ruled out and relatively high corrosion rates, as measured in experiments with pH ≥ 11.5, must be assumed. Current reference and conservative rates with a cement backfill used for the RBG are available in Curti (2022).

3.3.1.2 Approach to post-closure safety assessments

The way in which the current knowledge about ^{14}C speciation and release from L/ILW is implemented in safety assessments is linked to the knowledge about the migration of ^{14}C within the repository system and to the assumptions that are made about this (cf. Chapter 4). Of particular importance is the expected high mobility of organic compounds both in the liquid and gas phases compared with inorganic compounds. Assuming an organic speciation of released ^{14}C-bearing compounds when information is missing therefore overestimates ^{14}C release rates from the repository system and such an assumption is conservative.

The duration of the observed fast ^{14}C release from different materials is in the order of days to weeks, which is short compared with the expected residence times of ^{14}C in L/ILW near-field (cf. Chapter 4) and its half-life. Therefore, such rapid release is well approximated with the assumption of instant release, and the corresponding portion is termed instantaneous release fraction (IRF). In the long term, a slower ^{14}C release is expected, congruent to other processes like corrosion or matrix dissolution, and therefore named congruent release fraction (CRF). In contrast to the IRF, timescales for the CRF are expected to be much longer, thus markedly affecting ^{14}C migration in the deep geological repository. Hence, detailed release models are adopted for the remaining ^{14}C fraction for some of the materials, provided that the contribution of such materials to the total ^{14}C inventory in L/ILW and available additional information justifies such a detailed model. Where this is not the case, an entirely IRF is conservatively assumed. Note that various types of containment (e.g., metal boxes, steel flasks) may delay the release of ^{14}C from some waste forms or affect its speciation upon release (e.g., due to changing conditions during containment). These aspects are not taken into account for safety assessments but might occasionally influence the assumptions that are adopted regarding ^{14}C speciation and release from individual materials.

In the leaching experiments described in Section 3.3.1.1, three categories of radioactive and stable carbon compounds released from ^{14}C-bearing materials could be identified: dissolved organic species, dissolved inorganic species, and gaseous species (both organic and inorganic). Generally, the fractionation of carbon species between gas, liquid and solid phases depends on temperature, gas pressure, relative humidity, minerals present, as well as salinity, pH and the electrochemical potential of the liquid phase. The respective conditions in the deep geological repository and its surroundings during the period of interest are expected to be different from those in the experiments and to vary in space and time. Therefore, no a priori assignment of individual ^{14}C species to a specific phase (liquid or gaseous) can be made. Rather, a grouping of the various species identified in the experiments according to inorganic and organic species is adopted (cf. Fig. 3-4).

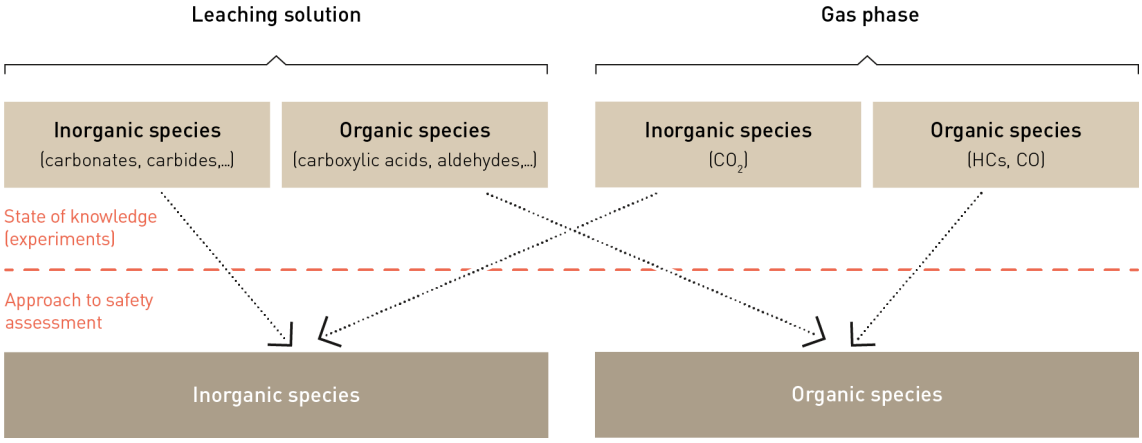

Fig. 3-4: Grouping of experimentally determined ^{14}C species (upper part) by inorganic and organic species (lower part)

Even though CO is an inorganic carbon compound, its chemical behaviour, which in terms of solubility is similar to the behaviour of HCs, justifies its classification as an "organic species" in safety assessments.

The following sections are structured as follows:

- First, the assumptions on ^{14}C speciation and release for the main ^{14}C-bearing materials in L/ILW (material classes) are reported based on the current state of knowledge.
- Afterwards, an aggregation of these material classes to so-called release classes is made (Tab. 3-4). In this table, the release model is shown (IRF *vs* CRF), together with the respective release fractions for three scenarios, e.g., lower bound (LB), best estimate and upper bound (UB), which will be used in the probabilistic sensitivity and uncertainty analyses in Nagra (2024j). When experimental data are available, the best estimate corresponds to the values reported in the literature with a small conservative margin, as not many experiments have been done so far. The LB and UB encompass the range of measured values reported in the literature by one order of magnitude difference with the best estimate. In the absence of data, the best estimate is chosen in the middle of the whole possible range of values, in order to minimise the potential error generated. The LB and UB correspond to the most optimistic and pessimistic case, respectively. The ^{14}C speciation will not be varied in the sensitivity analysis, as the variation of this parameter towards a more conservative assumption (especially when no scientific data are available as in the case for contaminated materials), negligibly impacts the dose release to the biosphere compared to other parameters. Therefore, just the best estimate value is given.
- In Section 3.4, the approach to derive the ^{14}C source term for L/ILW AGTs is described.

Activated steel

For activated (carbon and stainless) steel, a best estimate IRF of 0.01% is conservatively assumed, rounding up the fractions observed in (only) two long-term experiments conducted by Visser-Týnová et al. (2018a), Visser-Týnová et al. (2018b), Guillemot et al. (2021) and Guillemot et al. (2022). The selected UB value is 0.1% and the LB value reaches 0.001%, encompassing the best estimate by one order of magnitude. The speciation of the IRF is assumed to be 100% organic. This is a conservative assumption, since the respective fractions in the experiments also contained inorganic species, in proportions most likely linked to surface dose rates. The assumption that

100% of the ^{14}C compounds instantaneously released are organics is admitted to be the best option, due to the limited data available (i.e., only two experiments), and the negligeable contribution to the total ^{14}C released from activated steel.

The remainder of the ^{14}C inventory in activated steel is assumed to be congruently released with steel corrosion. This assumption reflects the outcome of some experiments, in which the corrosion rate was independently measured and compared to the ^{14}C release rate (e.g., Guillemot et al. 2022). Prevailing uncertainty in the CRF thus mainly reflects uncertainty in the corrosion rates, which is expressed as respective UB and LB values. The corrosion rates of steel, selected for RBG, can be found in Diomidis et al. (2023). The speciation of the CRF is assumed to be 100% organic. This assumption can be considered as realistic, given that $^{14}CH_4$ was the predominant species quantified in the two long-term experiments, and the potential for the generation of oxidising species by radiolysis declines with the gradual decrease in γ-radiation from activated steel (i.e., reducing conditions will prevail in the long term).

Activated Zircaloy

For activated Zircaloy from reprocessing a best estimate IRF of 0.01% is conservatively assumed. The selected UB value is 0.1% and the LB value reaches 0.001%, encompassing the best estimate by one order of magnitude and the range of measured values for activated Zircaloy from BWR and PWR fuel in the framework of the international CAST project. These assumptions are identical to those made for activated steel, given that the two materials are judged to be similar in terms of the oxide layer structure. The speciation of the IRF is conservatively assumed to be 100% organic. This choice reflects the difficulty in establishing consistent inorganic/organic ratios due to differences in analytical techniques and Zircaloy types between the various experiments. In any case, the bias introduced for the total ^{14}C released is negligeable because of the small value of the IRF.

The remainder of the ^{14}C in activated Zircaloy is assumed to be congruently released with bulk metal corrosion, albeit that no direct link between ^{14}C leaching and corrosion could yet be experimentally confirmed. Taking into account the similar ^{14}C speciation and two step release mode (i.e., initial fast release rate followed by a slower long-term one) observed in corrosion experiments with activated steel and Zircaloy, a similar congruent release mechanism can be expected for both activated metals. Prevailing uncertainty in the CRF thus mainly reflects uncertainty in the corrosion rates, which is expressed as respective UB and LB values. The corrosion rates of Zircaloy, selected for RBG, can be found in Diomidis et al. (2023). Likewise activated steel, an assumed 100% organic speciation for the CRF seems to be a realistic assumption.

Other activated metals

There is no experimental evidence for the release of ^{14}C from other activated metals such as Al, Cu, Pb and Be. For Al and Be, it is conservatively assumed that the total ^{14}C inventory is instantly released, as Al corrodes extremely fast under highly alkaline conditions, and no corrosion rates are available for Be (Diomidis et al. 2023). For Pb or other activated metals (e.g., Cu), 50% IRF and 50% congruent release with corrosion is the assumption with the least potential error as no experimental studies are available. The contribution of these materials to the total ^{14}C inventory in L/ILW is, however, negligeable (less than 1%) (Nagra 2023). The corrosion rates of Pb and Cu, selected for RBG, can be found in Diomidis et al. (2023). All the ^{14}C compounds released from activated Al, Cu, Pb and Be are expected to be in organic form, based on the information available for the steel and Zircaloy.

Activated graphite

For activated graphite, a best estimate IRF of 0.02% is assumed, based on the RWM approach (RWM 2016a). An LB of 0 is defined to reflect that a substantial fraction of the ^{14}C present in graphite might not be releasable and one order of magnitude higher than the best estimate is selected for the UB (RWM 2016a). The speciation of the IRF is conservatively assumed to be 50% / 50% organics/inorganics, based on the CAST experiments.

The CRF is based on the parametrisation especially selected in RWM (2016a), included within the CAST project. The best estimate considers that 5% of the total ^{14}C inventory is released from the activated graphite at a rate of 10^{-2} a^{-1}. The remaining ^{14}C inventory is irreversibly bound to the graphite matrix. The LB assumes that only 1% of the total ^{14}C inventory is released at a rate of 10^{-3} a^{-1}, while for the UB, 30% of the total ^{14}C inventory is expected to be released at a rate of 10^{-1} a^{-1}. Graphite is the only material for which the dissolution rate is linked to the CRF. However, the two parameters are varied independently in probabilistic uncertainty and sensitivity analyses for two main reasons: (i) this approach is used for all other materials and (ii) activated graphite represents only ~ 2% of the total L/ILW ^{14}C inventory. Hence, the effort to implement a separate approach for graphite is not proportionate to the low dose contribution. The speciation of the CRF is conservatively assumed to be a 50% / 50% ratio of organics/inorganics, based on the experiments performed within the CAST project.

Activated concrete

In absence of experimental evidence for the release of ^{14}C from activated concrete and its degradation rate, it is assumed that 50% of the total ^{14}C associated with activated concrete is instantly released. This best estimate is specifically selected in order to minimise potential error, in light of the fact that activated concrete has a negligeable contribution to the total ^{14}C inventory (less than 0.01%; Nagra 2023). The LB and UB are defined to 0 and 100%, respectively, in order to cover the whole possible range of values.

There is also a lack of dedicated experiments and possible analogues regarding the speciation of ^{14}C compounds released from activated concrete. A similar approach to the one taken for the ^{14}C release is selected in order to minimise potential error. Hence, an equal proportion of ^{14}C inorganics and ^{14}C organics is assumed to be released from activated concrete.

Activated heavy elements

In absence of experimental evidence and theoretical knowledge about the release of ^{14}C from activated heavy elements and taking into account their extremely negligeable contribution to the total ^{14}C activity in L/ILW (~ 2×10^{-5}%) (Nagra 2023), it is conservatively assumed that the total ^{14}C inventory is instantly released under the chemical form of ^{14}C organics. No UB or LB are considered.

Contaminated materials

Contaminated materials come from various origins (Nagra 2023) and therefore contain a wide variety of substances, such as metals, inorganic and organic ones (Fig. 3-2). Given that ^{14}C is predominantly present at the surface of these materials, it is assumed that the total ^{14}C inventory is instantly released. An IRF of 100% is hence selected. No UB or LB are considered.

Due to the absence of experimental knowledge, as well as the wide range of origins, conditioning process and storage condition of the contaminated materials, an equal proportion of ^{14}C inorganics and organics is assumed, to minimise potential error.

The AGTs with contaminated materials from the pilot incineration facility and plasma furnace at Zwilag, contain residues, ashes or slag. In such AGTs, an entirely inorganic speciation is assumed, as all organic materials present in the waste are expected to be fully oxidised after calcination.

IERs

For ^{14}C-containing IERs, an IRF of 100%[7] is defined. This assumption is based on the rapid degradation of the surface functional groups (Guillemot et al. 2023), which selectively adsorb ^{14}C. No UB or LB are considered.

The speciation of the released ^{14}C is set according to the origin of the AGT (i.e., type of NPP). When IERs are from BWRs, an inorganic/organic ratio of 90% / 10% has been defined experimentally, while it reaches 70% / 30% for IERs from PWRs.

$Ba^{14}CO_3$

^{14}C is expected to be congruently released with the dissolution of $BaCO_3$ in inorganic form (e.g., carbonates). However, the absence of geometric data for individual waste pieces does not allow a detailed congruent release model to be developed. Hence, an IRF of 100% has been adopted for post-closure safety assessments, without considering UB or LB. This value may be very conservative in view of the low solubility of carbonates at the initially high pH values expected within the cementitious L/ILW near-field, together with the protective function of the acrylic lacquer and the isolating boxes. However, it must be kept in mind that the contribution of such material to the total L/ILW ^{14}C inventory is negligeable (~ 0.05%) and the inorganic ^{14}C species released will anyway be effectively retained in the cementitious L/ILW near-field.

It should be noted that no AGT exclusively contains $Ba^{14}CO_3$ (App. A). It is present together with contaminated materials in only 4 AGTs originating from MIR (i.e., J-P-001113; J-P-001115; J-P-001251; J-P-001261), which were especially checked due to their high contribution to the total ^{14}C inventory in L/ILW (Nagra 2023).

Vitrified L/ILW

All ^{14}C present in vitrified L/ILW is assumed to be congruently released with the dissolution of the glass matrix, due to the intensive mixing during the vitrification process. Dissolution rates selected for RBG can be found in Curti (2022). No UB or LB are considered.

The speciation of the CRF is assumed to be 100% inorganic, given the high temperature and oxic conditions occurring during calcination of the radioactive solutions prior to vitrification.

Release classes

The above-mentioned ^{14}C-bearing materials with substantial contribution to the total L/ILW ^{14}C inventory are aggregated in Tab. 3-4 to so-called release classes, which specify the assumed release models (i.e., IRF *vs* CRF), release fractions (including LB, best estimate and UB) and speciation.

[7] This assumption is expected to be conservative for IERs solidified in bitumen (representing less than 1% of the total IERs inventoried in L/ILW; Nagra 2023). ^{14}C might be released congruently with the degradation rate of bitumen due to the intense mixing process during solidification and relative low porosity of bitumen compared to cement.

Tab. 3-4: ^{14}C speciation and rate of release for L/ILW

This table will be used for sensitivity calculations (Nagra 2024j).

Release class		Release model	Release fraction (% IRF / CRF)			Speciation (% organic / inorganic)	
			LB	Best estimate	UB	Organics (CH_4, CAs, CO)	Inorganics (CO_2, CO_3^{2-})
Activated materials	Steel	Instant	0.001	0.01	0.1	100	0
		Congruent*	99.999	99.99	99.9	100	0
	Zircaloy	Instant	0.001	0.01	0.1	100	0
		Congruent*	99.999	99.99	99.9	100	0
	Al, Be	Instant	/	100	/	100	0
		Congruent	/	0	/	/	/
	Pb and other activated metals	Instant	0	50	100	100	0
		Congruent*	100	50	0	100	0
	Concrete	Instant	0	50	100	50	50
		Congruent	/	0	/	/	/
	Graphite	Instant	0	0.02	0.2	50	50
		Congruent	1	5	30	50	50
	Heavy elements	Instant	/	100	/	100	0
		Congruent	/	0	/	/	/
Contaminated materials	Inorganic/organic materials and metals	Instant	/	100	/	50	50
		Congruent	/	0	/	0	0
	Products from incineration/ plasma furnace	Instant	/	100	/	0	100
		Congruent	/	0	/	0	0
^{14}C-containing materials	IERs from BWR	Instant	/	100	/	10	90
		Congruent	/	0	/	0	0
	IERs from PWR	Instant	/	100	/	30	70
		Congruent	/	0	/	0	0
	Vitrified L/ILW	Instant	/	0	/	0	0
		Congruent**	/	100	/	0	100
	$Ba^{14}CO_3$	Instant	/	100	/	0	100
		Congruent	/	0	/	0	0

* the associated corrosion rates of metals selected for RBG are available in Diomidis et al. (2023).

** the associated dissolution rates of vitrified glass selected for RBG are available in Curti (2022).

App. A lists the materials with which ^{14}C is expected to be associated, such as activated metals (i.e., steel, Zircaloy, Pb, Al, Be, Cu), activated graphite, activated concrete, contaminated (in-/organic/metallic) materials, IERs, products from incineration and vitrified reprocessing waste. Each of these "^{14}C-bearing materials" will be linked via Tab. 3-4 to a "release class" that specifies the type of release (i.e., IRF and CRF, given as best estimate, LB, UB) as well as the speciation of ^{14}C. When two material classes are listed in one single AGT (e.g., activated steel and activated concrete, or activated and contaminated steel), the assumptions regarding the ^{14}C speciation and rate of release from both respective release classes are considered equally. It should also be noted that for the 4 AGTs originating from MIR (i.e., J-P-001113; J-P-001115; J-P-001251; J-P-001261), the speciation assumption has been adjusted according to the respective proportions of contaminated materials containing ^{14}C and $Ba^{14}CO_3$. App. A, together with Tab. 3-4 is the basis for generating the ^{14}C source term (cf. Section 3.4) and dose calculations reported in the consequence analysis report (Nagra 2024j).

3.3.1.3 International approaches

Relatively few reports describing the treatment of ^{14}C by other waste management organisations (WMOs) are publicly available. Recent reports from NWS (including RWM), Swedish Nuclear Fuel and Waste Management Company "*Svensk Kärnbränslehantering Aktiebolag*" SKB and Posiva, together with relatively older information from the Ontario Power Generation's deep geological repository in Canada were especially reviewed.

For recent work, WMOs (including Nagra) underpin most of the modelling assumptions and parameters on the ^{14}C speciation and rate of release using outputs from the CAST project. Therefore, assumptions are generally similar as they are based on the same knowledge base. Differences relate primarily to: (i) the interpretation of some of the less well-constrained results from CAST; (ii) the site-/organisation-specific factors relating to the stage of the programme/purpose of the safety assessment; and (iii) the importance of particular waste streams.

All the reviewed L/ILW disposal concepts include cementitious backfill and/or grout, which dominates the geochemistry. Hence, assumptions regarding ^{14}C speciation and release could be compared.

In RWM's Integrated Project on Carbon-14 (Lever & Vines 2015), ^{14}C is concentrated in relatively few waste streams, notably reactor core graphite, activated steels and reactive metals such as Magnox and uranium, and to a smaller extent organic materials. The largest potential source of released ^{14}C is activated metals. In RWM's geological repository system safety case (RWM 2016b, RWM 2016c, RWM 2016d), the entire ^{14}C inventory is available to the groundwater pathway. No distinction is made between inorganic and organic forms (i.e., one single ^{14}C species is in the model) and the inventory is instantaneously released to the cementitious backfill when the containers fail. In the Simplified MOdel of Gas Generation (SMOGG), the entire ^{14}C inventory is available for release to the gas phase, using parameter values from the CAST project available at the time (Swift 2016). Releases due to corrosion of metals are assumed to be in the form of $^{14}CH_4$. Radiolysis and microbial degradation of organic materials result in the production of CH_4 and CO_2, which may contain ^{14}C, knowing that $^{14}CO_2$ is assumed to be removed immediately by reaction with cementitious phases.

In the safety assessments of SKB, ^{14}C was considered in three distinct forms: organic, inorganic and induced by activation of metals, allowing the release rates to be determined from the characteristics of the waste forms and potentially be treated differently in the safety assessment calculations. The slow release of ^{14}C through corrosion of activated metals substantially reduces the ^{14}C dose contribution.

In the previous post-closure safety assessment for the L/ILW repository in a crystalline host rock (SKB 2015a, SKB 2015b), degradation of organic material is assumed to generate equal quantities of CH_4 and CO_2. Any ^{14}C from the degradation of ^{14}C-containing organic waste would then be divided equally between these two species. It is however assumed that the pH is sufficiently high that microbial degradation is significantly inhibited. Hence, the release is dominantly via the groundwater pathway as organic and inorganic aqueous species, with CO_2 known to react with cementitious materials. In the most recent post-closure safety assumptions for the deep geological disposal of ILW in a crystalline host rock (SKB 2019a, SKB 2019b), the assessments are similar, but the pattern of releases is different due to the different mix of waste types.

In the L/ILW section of Posiva's repository, ^{14}C is omitted due to its low activity in the inventory.

For the Ontario Power Generation's deep geological repository at the Bruce site (Canada), ^{14}C is released from the waste forms in the same way as all other radionuclides and no distinction between ^{14}C organics and inorganics in the groundwater pathway is assumed (Quintessa et al. 2011). Release of gaseous ^{14}C arises mostly from the degradation of ILW moderator resins. The release rates used in the safety assessments are based on measured rates during resin storage. Both CH_4 and CO_2 are produced and some are ^{14}C-labelled. $^{14}CH_4$ and $^{14}CO_2$ gases are also assumed to be generated from ^{14}C present as carbides in metal waste, congruently released through corrosion under both saturated and unsaturated conditions.

3.3.2 HLW ^{14}C speciation and rate of release

3.3.2.1 State of knowledge

HLW (SF and RP-HLW) are emplaced in disposal canisters which ensure their complete containment for a certain period of time (Nagra 2024b). Thus, an important decay of ^{14}C occurs within the HLW disposal canisters and ^{14}C compounds are released only when the HLW disposal canisters are breached.

The expected speciation and release of ^{14}C is closely linked to the expected phenomenological evolution of the HLW section of the repository, which is summarised in Nagra (2024n) and in Nagra (2024f). In the following section, information about the expected ^{14}C speciation and release is given for those materials that contain a majority of ^{14}C in SF and RP-HLW.

Activated Zircaloy

In HLW, the majority of the ^{14}C is associated with activated Zircaloy (~ 56%; Fig. 3-3) (Nagra 2023). When exposed to neutron fluxes, ^{14}N impurities present in Zircaloy in the SFAs are activated, generating ^{14}C. ^{17}O could also be a precursor of ^{14}C in the oxide layer of the cladding due to the proximity of the UO_2/PuO_2 fuel to the cladding and the exposure of the latter to water coolant (Necib et al. 2018b, Gras 2014, Yim & Caron 2006). In contrast to reprocessed activated Zircaloy, which is stored in the L/ILW repository section and is exposed to highly alkaline porewater (pH ~ 12.5), activated Zircaloy as part of intact SFAs is exposed to near-neutral pH porewater (pH ~ 7.5) after canister breaching. In addition, it is exposed to stronger radiation prior to canister breaching (Nagra 2024f, Kosakowski et al. 2023, Nagra 2024n).

The speciation of ^{14}C compounds released from activated Zircaloy has mainly been studied under highly alkaline conditions (cf. Section 3.3.1.1). Only the study of Kaneko et al. (2002) allows an appraisal of the dependence on pH of the speciation of ^{14}C compounds released from activated Zircaloy. The results show that similar species (i.e., carboxylates, aldehydes and alcohols) are present both at pH 8 and 12.5. However, the total ^{14}C organic and inorganic concentrations were higher (by a maximum factor of 3) at highly alkaline pH. In the corrosion study of Sasoh (2008)

with non-activated Zircaloy powder (having a carbon content of 0.02 wt.%), a difference in the proportions of the individual stable carbon compounds within only a factor of 2 at pH 8 and 12.5 was reported, with overall higher concentrations in highly alkaline solution. This result is rather unexpected as the corrosion rates of metals are known to be higher under near-neutral conditions (Diomidis et al. 2023). Unfortunately, no result interpretation was given by Sasoh (2008).

Thermodynamic modelling about carbon speciation under HLW conditions suggested that, in case of complete thermodynamic equilibrium, CH_4 dominates the ^{14}C speciation, followed by carbonates and ethane (Wieland et al. 2023). The concentrations of other organic species possibly present (i.e., formate, acetate, oxalate, proprionate, ethane and propane) are at least three orders of magnitude lower than those of the predominant compounds. Assuming partial thermodynamic equilibrium, in which case no alkanes are expected to form, the predominant dissolved species are carboxylates (i.e., acetate, to a lesser extent formate) and alcohols (i.e., ethanol, propanol, butanol). On the basis of the thermodynamic modelling of the carbon speciation, it can be concluded that similar ^{14}C-bearing species would be released from activated Zircaloy irrespective of whether highly alkaline or near-neutral conditions prevail.

The effect of radiation on the speciation of ^{14}C compounds released from activated Zircaloy has not yet been studied experimentally. It is expected that the effect on long-term release is probably small, given that the dose rate from the SFAs will have dropped at the time of canister breaching and the outcome of release studies made with activated steel (cf. Section 3.3.1.1 and part "activated steel" below).

The rate of release of ^{14}C compounds from activated Zircaloy was experimentally determined mainly under highly alkaline conditions (Necib et al. 2018b, Necib et al. 2018a). Only in Kaneko et al. (2002), the total ^{14}C organic and ^{14}C inorganic contents were monitored over a period of 16 months in near-neutral solution. Similar rates of release were observed at both pH 8 and 12.5, with a faster release at pH 12.5 during the first two/three months followed by a slower one in the long term. The effect of radiation on the release rates of ^{14}C compounds has not yet been studied for activated Zircaloy.

Spent fuel

The second ^{14}C-bearing material in HLW is the fuel pellets with ~ 37% of the total ^{14}C inventory (Fig. 3-3) (Nagra 2023). ^{14}C is one of the main light and long-lived activation products present in SF (Johnson et al. 2023). Within the UO_2 or MOX matrix, a fraction of the ^{14}C inventory is segregated to grain boundaries and cracks. ^{14}C is also present in the gap between the fuel matrix and the cladding following in-reactor irradiation (Fig. 3-5).

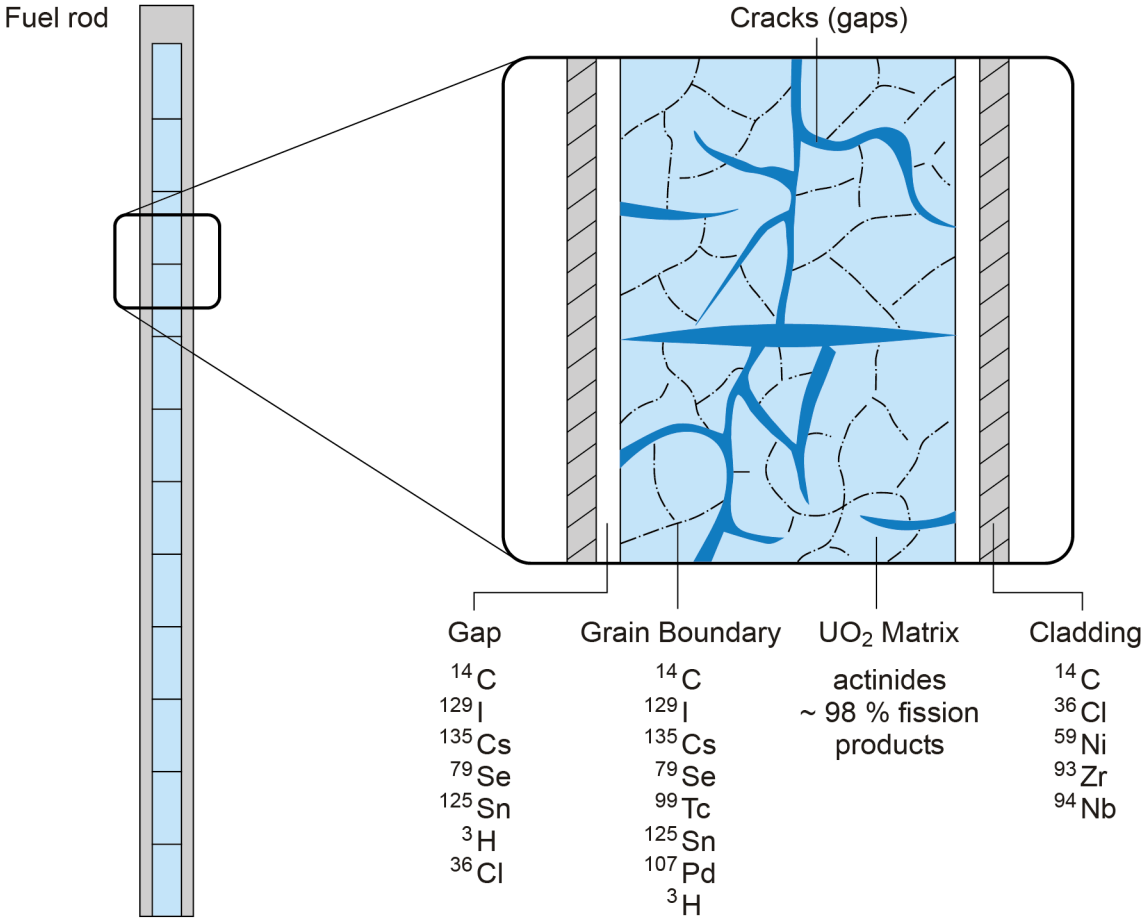

Fig. 3-5: Conceptual distribution of radionuclides considered for safety analysis in a SF rod after irradiation

Based on Johnson & Tait (1997).

In general, little information is available about the chemical forms of ^{14}C in UO_2 and MOX matrix and the speciation of ^{14}C upon release is rather uncertain (Johnson et al. 2023, Wieland et al. 2023). There is evidence to suggest that carbide, oxycarbide, elemental carbon or entrapped CO_2 or CH_4 could be the chemical form of ^{14}C produced by ^{14}N activation (Ferrari 1963, Hesböl et al. 1990, van Konynenburg 1994). However, the chemical form of ^{14}C generated from ^{17}O activation in UO_2 and MOX matrix remains unclear. There is experimental evidence that a thin oxidised layer exists on the UO_2 matrix due to the high sensitivity of U(IV) to oxidants (Johnson et al. 2023). The presence of H_2 at the interface of the UO_2 matrix in addition to the complete neutralisation of radiolytic oxidants also leads to the reduction of redox-sensitive radionuclides accommodated by the pre-oxidised layer (Spahiu 2021, Johnson et al. 2023). Based on this statement, Wieland et al. (2023) assumed that oxidised carbon species such as carbonates and carboxylic acids are expected to be the dominant species in the pre-oxidised layer, comparable to activated steel. These compounds are then released on contact with the solution if reduction to gaseous species (e.g., CH_4) is inhibited at the interface of the UO_2 matrix, i.e., if complete thermodynamic equilibrium is not reached. Under conditions of complete thermodynamic equilibrium, however, gaseous species could be released from the oxide layer of the UO_2 matrix (Wieland et al. 2023).

There is experimental evidence that ^{14}C-bearing gaseous species (e.g., CO_2, CO and CH_4) are either not present during rod puncture tests for fission gas or present only at very low levels (González-Robles et al. 2016, Kienzler et al. 2014) and that the vast majority of ^{14}C is retained in the matrix of the fuel (Johnson et al. 2023). These results suggest that ^{14}C compounds from the oxide layer are presumably water-soluble, oxidised compounds rather than gaseous species. It should be noted that the presence of a pre-oxidised layer is typical for fuel rods used in leaching experiments, which are often cut open several years before the leaching experiment occurs. However, the pre-oxidised layer is not expected to be present on the majority of the rods as they are expected to be disposed with intact cladding. As the chemical forms of carbon in the UO_2 matrix seem to be elemental carbon or carbide, and the presence of reactive H_2 at the interface between the UO_2 matrix and the solution ensures strongly reducing conditions, ^{14}C-bearing compounds released during the dissolution of the UO_2 matrix are expected to be reduced species. In their experiment on the dissolution of uranium monocarbide in water at neutral pH and 25 - 99 °C, Bradley & Ferris (1962) identified hydrous uranium oxide, H_2 and a mixture of gaseous HCs dominated by CH_4 with small amounts of C_2H_6 and saturated C3- to C6-HCs. Hence, dissolution of the SF is likely to result in ^{14}C being released predominantly as $^{14}CH_4$ during the dissolution of the SF, similar to long-term ^{14}C release from the bulk matrix of activated Zircaloy and steel.

The release of ^{14}C can be conceptualised to occur in two distinct steps, which are described in detail in Johnson et al. (2023). Upon contact with porewater, ^{14}C is rapidly released from the gaps between the pellets and the cladding, and cracks and grain boundaries from the SF. So far, few studies have quantified the initial fast release from SF (Johnson et al. 2023). The largest number of measurements of ^{14}C release were reported by Stroes-Gascoyne et al. (1994) on used CANDU fuel samples. In particular, this study reported an average fast release fraction of 2.7% of the total ^{14}C inventory. As the results for CANDU fuel show that ^{14}C release is independent of the linear power rating, these data are considered transferable from LWRs to SF. To date, only a few leaching tests have been carried out with LWR fuel (Wilson & Shaw 1987, Wilson 1990a, Wilson 1990b). These studies indicate rapid releases of 0.05% to 3.5% of the total ^{14}C inventory. Given the scarcity of data on ^{14}C release from LWR fuel, Johnson et al. (2023) have given the greatest weight to the dataset of Stroes-Gascoyne et al. (1994) and assumed that the initial fast release of ^{14}C is 3% of the total inventory, with an upper bound of 5%.

In the long term, ^{14}C release is expected to occur as a result of the dissolution of UO_2/PuO_2 crystalline lattice, generically called "matrix dissolution". The largest fraction of the ^{14}C inventory is expected to be released at the same fractional rate as the SF dissolves at. The latter process is controlled by the geochemical conditions existing when the disposal canister breaches, by the type of groundwater intruding, as well as by the radiation field of the SFAs (Johnson et al. 2023). The main component of the SF, UO_2, dissolves in water by releasing U(IV) species in solution. This process occurs with a certain rate, referred to as the rate of non-oxidative dissolution[8]. Non-oxidative dissolution occurs only in the complete absence of oxidants. By the time the disposal canister breaches, all O_2 present in the bentonite backfill is expected to be consumed (Giroud et al. 2018), resulting in an O_2-free and reducing environment saturated with H_2 from the anaerobic corrosion of the steel canisters.

In the pH range expected for the HLW near-field, UO_2 is sparingly soluble and U(IV) solutions in equilibrium have a concentration of ~ 3×10^{-9} M (Grenthe et al. 2020). As a result of the low solubility of UO_2 under relevant conditions, the solution inside the breached canister quickly becomes saturated with U(IV) and the non-oxidative dissolution rate approaches zero. Together

[8] There is also an oxidative dissolution of UO_2(s), during which various oxidants present in solution cause the oxidation of U(IV) atoms on the surface, followed by its release in solution as U(VI) or uranyl (UO_2^{2+}) species. However, due to the expected reducing conditions within the deep geological repository, oxidative dissolution rates are not applicable for safety assessment as outlined in Johnson et al. (2023).

with the expected lack of advective water flow in the bentonite backfill, this low solubility of UO_2 severely limits the effectiveness of the non-oxidative dissolution process and is irrelevant for the release of radionuclides from the disposal canister. Under such conditions, the release of actinides and of most fission products from UO_2 is controlled by their low solubility and diffusion. It should also be noted that high H_2 concentrations in porewater over hundreds of thousands of years, combined with other electrochemical effects on the surface of the fuel, leads to a persistent excess of H_2, which also inhibits SF dissolution.

Dissolution rates for both UO_2 and MOX were defined by Johnson et al. (2023), based on both experimental data, modelling and natural analogue studies. It should however be noted that a derivation of a dissolution rate of SF under relevant conditions cannot realistically be based only on direct measurements of radionuclide release rates from SF, as most measurements yielded zero or less-than zero as a result of detection limitations (Johnson et al. 2023).

Activated steel

Around 7% of the ^{14}C inventory present in HLW is associated with activated steel (Fig. 3-3) (Nagra 2023). Spacers and plates in SFAs are generally made of stainless steel (Nagra 2023). As for activated Zircaloy and as previously mentioned in Section 3.3.1.1, the production of ^{14}C in activated steel is mainly due to the presence of ^{14}N impurities (Yim & Caron 2006, Gras 2014). In the HLW section of the deep geological repository, activated steel is exposed to γ-radiation prior to the loss of canister containment and afterwards to near-neutral pH porewater (~ pH 7.5) (Nagra 2021b).

As for activated Zircaloy, the speciation of ^{14}C compounds released from activated steel was studied mainly under highly alkaline conditions (cf. Section 3.3.1.1). The effect of pH on the ^{14}C speciation was only studied by Heikola & Ollila (2018), using non-activated iron and steel powders. Similar carbon species were released at both pH 12.5 and 8.5. Concerning the release rate, higher concentrations (about a factor of two) were determined in both the liquid and gas phases under highly alkaline conditions, in a similar way as observed with activated Zircaloy (Sasoh 2008). No further explanation has been provided by Heikola & Ollila (2018).

The effect of radiation on the release of ^{14}C compounds can be assessed from the studies of Cvetković et al. (2018a), Cvetković et al. (2018b), Guillemot et al. (2022), Guillemot et al. (2023), Visser-Týnová et al. (2018a) and Visser-Týnová et al. (2018b) on non-activated iron powder and activated steel nuts with dose rates varying by two orders of magnitude difference between studies. Similar species were identified in the different experiments (i.e., carboxylates and carbonates in solution; small HCs in the gas phase with a predominance of CH_4). The concentration of oxidised ^{14}C compounds released to solution was the only difference noticed. Visser-Týnová et al. (2018a) and Visser-Týnová et al. (2018b) measured higher concentrations of oxygenated ^{14}C compounds in solution, with a majority of ^{14}C inorganics, released from activated steel with a dose rate that was two orders of magnitude higher than in the study of Cvetković et al. (2018b), Guillemot et al. (2022), and Guillemot et al. (2023). A higher γ-dose rate emitted from ^{60}Co (which is the main activation product in activated steel; Dey et al. 2020) is expected to produce more oxidants and radicals in solution, such as H_2O_2, $HO^{\bullet}$, $HO_2^{\bullet}$, by radiation, thus affecting the ^{14}C speciation by increasing the proportion of oxidised ^{14}C compounds (i.e., carboxylates, carbonates). It should be noted that the difference in dose rate did not seem to affect the rate of carbon release in the above studies, only its speciation: after the rapid release phase, both stable carbon compounds from non-activated iron powder and ^{14}C compounds from activated steel nuts were released at a slower rate, congruently with steel corrosion.

RP-HLW

Less than 1% of the total ^{14}C inventory in HLW is associated with RP-HLW (Fig. 3-3) (Nagra 2023). Studies on the release and selective retention of radionuclides during glass corrosion are generally rare. In particular, no experimental evidence on ^{14}C speciation and release from RP-HLW is currently available in the scientific literature. In the absence of measured data, it is usually assumed that ^{14}C is homogeneously distributed in the glass matrix because of intensive mixing prior to vitrification and is therefore released congruently with glass corrosion (Curti 2022).

Borosilicate glass corrosion rates under near-neutral conditions have recently been reviewed by Curti (2022). In particular, the review considered two reference types of glass (SON68 and MW) that are non-radioactive surrogates of the actual HLW glass produced in France and UK, respectively.

3.3.2.2 Approach to post-closure safety assessments

As with L/ILW (cf. Section 3.3.1.2), the approach to safety assessments is linked to knowledge about migration of ^{14}C within the repository system and to the assumptions that are made about this (see Chapter 4). Assuming an organic speciation of released ^{14}C-bearing compounds when information is missing, therefore overestimates ^{14}C release rates from the repository system, and such an assumption is conservative.

In the leaching experiments described in Section 3.3.2.1, three categories of carbon compounds released from various ^{14}C-bearing materials could be identified: dissolved organic species, dissolved inorganic species, and gaseous species (both organic and inorganic). Similar to as in the L/ILW near-field, the fractionation of carbon species between gas, liquid and solid phases depends on temperature, gas pressure, relative humidity, minerals present, as well as the salinity, pH and electrochemical potential of the liquid phase. Therefore, no a priori assignment of individual ^{14}C species to a specific phase (liquid or gaseous) can be made. A grouping of the various species identified in the experiments according to inorganic and organic species is hence also adopted here (cf. Fig. 3-4).

As for L/ILW, an experimentally observed or theoretically expected fast release of ^{14}C from HLW materials is well approximated by the assumption of an IRF. In contrast to L/ILW, where no period of containment was assumed, a period of complete containment for HLW is expected for a certain period of time, according to the provisional design of the HLW disposal canister (Nagra 2024b). This actually means that the IRF is released only at canister breaching, after that an important decay of ^{14}C had occurred. In the long-term, an CRF with corrosion or matrix dissolution is expected, similar to that observed for L/ILW (cf. Section 3.2.2.2).

The following sections are structured as follows:

- First, the assumptions on ^{14}C speciation and release for the main ^{14}C-bearing materials (material classes) in HLW are reported.
- Afterwards, an aggregation of these material classes to so-called release classes is made (Tab. 3-5). In this table, the release model is shown (IRF vs CRF), together with the respective release fractions for three scenarios, i.e., LB, best estimate and UB, which will be used in the probabilistic sensitivity and uncertainty analyses in Nagra (2024j). When experimental data are available, the best estimate corresponds to the values reported in the literature with a small conservative margin, as not many experiments have been done so far. The LB and UB encompass the range of measured values reported in the literature by one order of magnitude difference with the best estimate. In the absence of data, the best estimate is chosen in the middle of the whole possible range of values, in order to minimise potential error. The LB

and UB correspond to the most optimistic and pessimistic case, respectively. The ^{14}C speciation will not be varied in the sensitivity analysis, as the variation of this parameter towards a more conservative assumption negligibly impacts the dose release to the biosphere compared to other parameters. Therefore, just the best estimate value is given.

- Section 3.4 describes the ^{14}C source term approach for HLW AGTs.

Activated Zircaloy

For activated Zircaloy as part of SFAs, the same assumptions as for activated Zircaloy present in L/ILW are made (cf. Section 3.3.1.2). These comprise: (i) an IRF of 0.01% as best estimate, with an LB of 0.001% and an UB of 0.1%, under the chemical form of organics; and (ii) the remaining and main ^{14}C inventory is an CRF with corrosion (the corrosion rate of Zircaloy selected for RBG is available in Diomidis et al. 2023), under the chemical form of organics.

This approach is based on the experimental finding of Kaneko et al. (2002) showing that the speciation of released ^{14}C compounds depends only weakly on the pH conditions and that leaching rates are only slightly lower at neutral pH. Hence, the assumption held here for post-closure safety assessments is rather conservative.

Furthermore, the effect of higher radiation levels in HLW on the speciation and release of ^{14}C is expected to be negligible in the long term, given that the dose rate from the SFAs has dropped at the time of canister breaching and the studies on activated steel (cf. Section 3.3.2.1), where the difference in dose rate seems to affect only the ^{14}C speciation. More inorganic compounds were released when the dose rate increased. Considering only ^{14}C organics to be released from Zircaloy is therefore also rather conservative.

Spent fuel

For SF as a material, which comprises the fuel pellets and the gaps within rods, a reference IRF of 3% is assumed. The selected UB and LB values are 5% and 0.05%, based on the lowest and highest experimental results obtained for ^{14}C IRF (Stroes-Gascoyne et al. 1994).

The ^{14}C compounds instantaneously released from the fuel pellets are expected to be present in its pre-oxidised layer. Assuming the presence of a pre-oxidised layer from which ^{14}C compounds are instantaneously released is rather conservative, as this layer is not expected to be present on the majority of rods surrounded by intact cladding. Little information is available about the chemical forms of ^{14}C in UO_2 and MOX matrix and the speciation of ^{14}C upon release is rather uncertain. Based on expert judgements (Spahiu 2021, Johnson et al. 2023, Wieland et al. 2023), a 50% / 50% organic/inorganic speciation of the IRF is assumed.

The remainder and majority of the ^{14}C inventory in fuel pellets is assumed to be congruently released with the expected very slow dissolution of the UO_2 or MOX matrix. No reliable experimental rates for the dissolution process are available. Dissolution rates for both UO_2 and MOX are available in the review of Johnson et al. (2023), which combined experimental data, modelling and natural analogue studies. The speciation of the ^{14}C CRF is assumed to be 100% organic, based on experiments and expert judgements (Bradley & Ferris 1962, Johnson et al. 2023, Wieland et al. 2023).

Activated steel

For activated steel as part of SFAs, the same assumptions as for activated steel present in L/ILW are made (cf. Section 3.3.1.2). These comprise: (i) an IRF of 0.01% as best estimate, with an LB of 0.001% and an UB of 0.1%, under the chemical form of organics, and (ii) the remaining and main ^{14}C inventory is an CRF with corrosion (the corrosion rates of steels selected for RBG are available in Diomidis et al. 2023), under the chemical form of organics.

This approach is motivated by the experimental findings of Heikola & Ollila (2018) showing that the speciation of released ^{14}C compounds does not depend on pH conditions and that leaching rates are only slightly lower at neutral pH. Hence, the assumption held here for post-closure safety assessments is rather conservative.

The effect of higher radiation levels in HLW on the speciation and release of ^{14}C is expected to be negligible in the long term, given that the dose rate from the SFAs has dropped at the time of canister breaching. Furthermore, the studies on activated steel with different dose rate (Cvetković et al. 2018a, Cvetković et al. 2018b, Guillemot et al. 2022, Guillemot et al. 2023, Visser-Týnová et al. 2018a, Visser-Týnová et al. 2018b), seem to affect only the ^{14}C speciation. More inorganics compounds were released when the dose rate increased. Considering only ^{14}C organics to be released from activated steel is therefore also rather conservative.

RP-HLW

For RP-HLW, it is assumed that all ^{14}C is released congruently with the dissolution of the glass matrix, due to the intensive mixing during the vitrification process. Dissolution rates selected for RBG can be found in Curti (2022). No UB or LB are considered.

The speciation of the CRF is assumed to be 100% inorganic, given the high temperature and oxic conditions occurring during calcination of the radioactive solutions prior to vitrification.

Release classes

The above-mentioned ^{14}C-bearing materials with substantial contribution to the total HLW ^{14}C inventory are aggregated in Tab. 3-5 in so-called release classes, which specify the assumed release models (i.e., IRF *vs* CRF), release fractions (including LB, best estimate and UB) and speciation.

Tab. 3-5: ^{14}C speciation and rate of release for HLW

Release classes	**Release model**	**Release fraction (% IRF / CRF)**			**Speciation**	
					(% organic / inorganic)	
		LB	Best estimate	UB	Organics (CH_4, CAs, CO)	Inorganics (CO_2, CO_3^{2-})
SFAs (activated steel and Zircaloy)	Instant	0.001	0.01	0.1	100	0
	Congruent*	99.999	99.99	99.9	100	0
SF pellets	Instant	0.05	3	5	50	50
	Congruent	99.95	97	95	100	0
RP-HLW	Instant	/	0	/	0	0
	Congruent**	/	100	/	0	100

* the associated corrosion rates of metals selected for RBG are available in Diomidis et al. (2023).

** the associated dissolution rate of vitrified glass selected for RBG is available in Curti (2022).

App. B lists the materials to which ^{14}C is expected to be associated with, such as activated metals (i.e., steel, Zircaloy), SF pellets, contaminated (in-/organic and metallic) materials and RP-HLW. Each of these "^{14}C-bearing materials" will be linked via Tab. 3-5 to a "release class" that specifies the type of release (IRF and CRF, given as best estimate, LB and UB) and speciation of ^{14}C. App. B, together with Tab. 3-5, will be the basis for generating the ^{14}C source term (cf. Section 3.4) and dose calculations reported in the consequence analysis report (Nagra 2024j).

3.3.2.3 International approaches

In the post-closure safety assessments of WMOs, most of the information on the ^{14}C speciation and rate of release of HLW waste relates to SF. However, ^{14}C is not generally considered to be of concern due to the long containment of the ^{14}C provided by stable waste forms, long-lived disposal canisters and engineered barriers.

In RWM's analysis of gas generation from HLW and SF, the assumptions regarding speciation and release of ^{14}C were based on Nagra (2004) (Hoch et al. 2016b). ^{14}C release from the UO_2 fuel was assumed to be in an inorganic, non-volatile form. From the metallic components, the ^{14}C was assumed to be congruently released with corrosion as an organic gas phase (i.e., $^{14}CH_4$). Magnox SF provided the largest ^{14}C release per disposal canister. The IRF was ignored, and no water limitation was considered. In the dose calculations, releases were expressed in terms of simple analytic expressions that take into account both the inventory and corrosion rate. In the safety case for the deep geological repository system (RWM 2016b), an IRF followed by a slow release was assumed to solution for both vitrified waste and SF. The parameterisation was based on the CAST data available at that time. The IRFs used for ^{14}C are truncated normal distribution (i.e., mean = 20%; standard deviation = 24.3%; minimum = 0%; maximum = 100%) for SF from advanced gas-cooled reactors, 15% for SF from PWRs and MOX, truncated uniform (0%, 100%) for SF from Magnox SF and truncated triangular (minimum = 0.33%; best estimate = 1%; maximum = 3%) for vitrified waste (RWM 2016b). The solubility limit is assumed to be high with a best estimate at 3 mol/m^3, a minimum at 0.6 mol/m^3 and a maximum at 7 mol/m^3. No information is provided on speciation but RWM (2016b) appears to assume that the entire inventory of ^{14}C is potentially available for both aqueous and gaseous pathways.

The safety assessment of SKB for the HLW repository in a crystalline host rock is also based on CAST results (SKB 2010). The ^{14}C associated with the SF is assumed to be released using the standard two-stage model of an IRF and CRF of SF dissolution (Tab. 3-6) (SKB 2010). The IRF also includes the rapid release fraction from the cladding. However, the ^{14}C inventory from the SF is separated from the fuel rods. In the absence of literature data about the ^{14}C speciation from SF, SKB assumed that the ^{14}C compounds were present in dissolved forms (SKB 2010). However, SKB 2011 includes a "what-if?" type calculation for the release of a pulse of gas from a failed canister where the entire ^{14}C inventory is assumed to be released as $^{14}CH_4$.

Tab. 3-6: ^{14}C-IRF and corrosion release fraction used for the HLW repository in a crystalline host rock

From SKB (2010). Distributions are double triangular.

Type of reactor	IRF					
	LB	Reference	UB	LB	Reference	UB
BWR	0.085	0.086	0.09	0.65	0.66	0.68
PWR	0.11	0.11	0.11	0.57	0.60	0.62
Average	0.085	0.092	0.11	0.57	0.64	0.68

In their safety case for the operating licence application, Posiva (2021) highlights that ^{14}C release from SF is modelled as an IRF followed by a slow CRF of SF dissolution, similar to the approach used by SKB. The deterministic calculations assume that all ^{14}C is released to the liquid phase in organic form, resulting in the highest doses. The IRF values used are based on the CAST results and generally lower than those assumed in previous assessments. Probabilistic calculations used a range of speciation, based on CAST results (Tab. 3-7).

Tab. 3-7: Release parameters for ^{14}C used in the safety case for the operating licence application of Posiva

From Posiva (2021).

Component	Fraction of organic ^{14}C species released	Reference value for IRF	Distribution for IRF
UO_2 matrix	0 – 100%	5%	Triangular (1%, 3%, 10%)
Cladding	50 – 90%	5%	Log-uniform (0.1%, 10%)
Other metal parts	65 – 100%	n.a.	n.a.

n.a.: not available

3.4 ^{14}C source term workflow

This section summarises the workflow to derive the ^{14}C source term, based on the previous sections. The workflow is illustrated in Fig. 3-6 and applied to each AGT (both L/ILW and HLW) containing ^{14}C. The AGTs are listed in App. A (for L/ILW) and App. B (for HLW), together with the total ^{14}C activity and the material class(es). Each material class is linked to a release class that specifies IRF/CRF with respective speciations (cf. Tab. 3-4; Tab. 3-5). Given this, the individual steps to derive the ^{14}C source term are described and illustrated below with examples:

- First, the mean activity of a given AGT is split into IRF and CRF according to the release classes.

> Example: AGT with mean ^{14}C activity of 1×10^{12} Bq associated with activated steel. According to the release class "activated steel", the IRF and CRF for the reference case is 0.01% and 99.99%, respectively. Hence, the IRF amounts to 1×10^{8} Bq and the CRF to 9.999×10^{11} Bq.

The workflow now forks for the IRF and CRF. We first continue with the IRF:

- For the IRF, the activity is speciated into organic and inorganic fractions.

> Considering the same example above, the IRF speciation is 100% organic. Thus, the activity of organic species in the IRF amounts to 1×10^{8} Bq.

Concerning the IRF, the workflow (for one AGT) is already complete. The workflow continues for the CRF.

Each AGT consists of multiple components with a unique mass, geometry and material (Nagra 2023).

- First, relevant components are filtered based on two criteria: (i) they have to be part of the waste product; (ii) they have to match the material class.

> Example: If the material class in the AGT is "activated steel", then only components in the waste product that are composed of steel (e.g., stainless steel, carbon steel and iron) are filtered. In case of "mixed activated metals", all metallic components in the waste product are filtered.

- Second, the CRF activity is distributed on all filtered components proportional to their mass. A subworkflow is performed for each of the components. Each component has a defined material, with an associated corrosion or dissolution rate available in Diomidis et al. (2023), RWM (2016a) or Curti (2022). Together with the geometry of the component (e.g., plate, sphere, cylinder with respective parameters/dimensions, available in Nagra 2023), a fractional release rate (a^{-1}) over time can be calculated. The activity of a given component is speciated into organic and inorganic fractions and multiplied with the fractional release rate at each time step, leading to a congruent release rate (CRR) as a function of time (in Bq/a)[9].

> Example: a plate composed of carbon steel (best estimate corrosion rate of 1×10^{-3} mm/a in near-neutral condition), with a thickness of 1 mm. As the plate corrodes from both sides, the effective corrosion rate is 2×10^{-3} mm/a. Here, the fractional release rate is constant over time and is obtained by dividing the effective corrosion rate by the thickness. It equals to 2×10^{-3} a^{-1}. Each year, 0.2% of the plate is corroded. The corresponding inverse reflects the lifetime of the plate: after 500 years the plate is therefore completely corroded, and the fractional release rate drops to zero.
>
> The ^{14}C activity of the plate would, according to the release class of activated steel, be released as 100% organic species. Multiplying an example activity of 1×10^{9} Bq with the fractional release rate of 2×10^{-3} a^{-1}, the CRR over time is equal to 2×10^{6} Bq/a for the first 500 years and then drops to zero.

[9] The decay (after 2075) during containment (before release) is also accounted for.

The entire workflow described above will be repeated for all AGTs containing ^{14}C. To get the final model source term, all individual contributions to the IRF / CRR as both organic and inorganic ^{14}C species are summed up for both L/ILW and HLW. The derived ^{14}C source term will be used as an input for modelling the ^{14}C migration in the repository system and the geological environment (cf. Chapter 4).

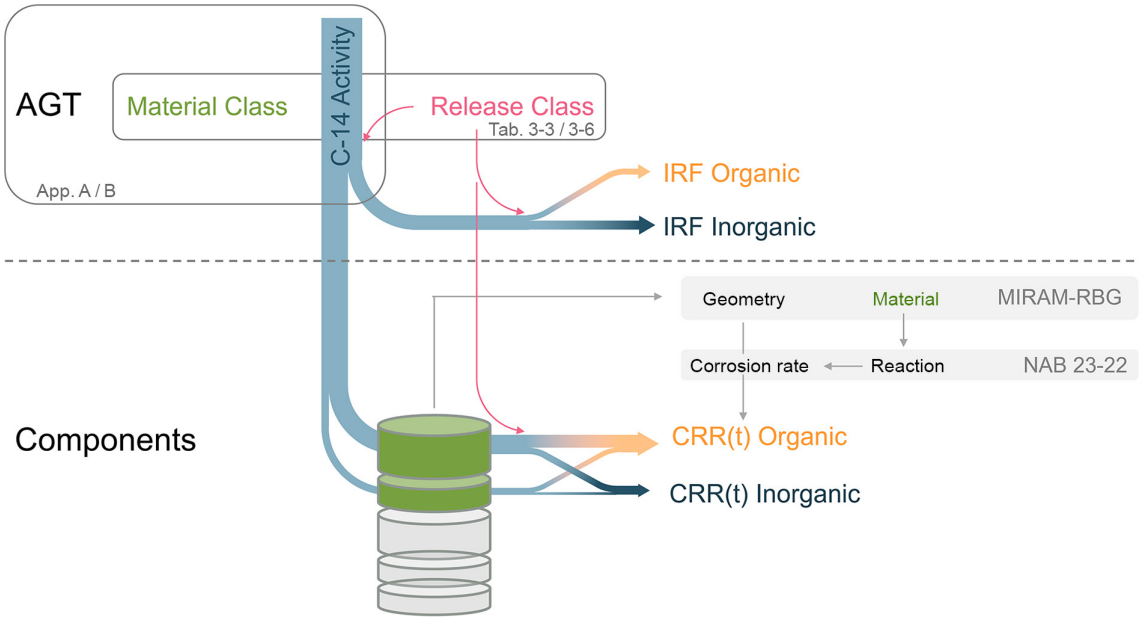

Fig. 3-6: Schematic illustration of the workflow on how to derive the ^{14}C source term

The pink arrows indicate where the release class controls the workflow: it defines, how a) the total activity is split into IRF/CRF and b) the IRF and CRF speciate into organic and inorganic species. The cylinders illustrate all components in the waste product. The green components are the ^{14}C-bearing components. The CRF is distributed on these green components proportional to their mass. Depending on the component's geometry and corrosion rate (which in turn depends on the material), a time-dependent fractional release rate can be determined (grey arrows). After multiplying with the organic/inorganic CRF, the time-dependent organic/inorganic CRR is obtained for a given component.

4 Migration of ^{14}C in the repository system and geological environment

After release of ^{14}C from the waste, there are two principal routes for its migration into and out of the repository system. Transport along the repository structures mainly occurs in gas phase as $^{14}CH_4$ (Section 4.1). Transport through the host rock and its confining units, regrouped under the term CRZ, mostly takes place in liquid phase as $^{14}CH_4$ and to a much smaller extent as LMW organics dissolved in porewater (Section 4.2). Accordingly, the release of ^{14}C from the repository system to the wider geological environment may take place near the underground access structures and at the interface of the confining units with the adjacent deep aquifers (Section 4.3).

The assessment of ^{14}C migration in the deep geological repository and surrounding geological environment requires information from different reports of the assessment basis and post-closure safety case (cf. Fig. 1-1). The evolution of a repository for both HLW and L/ILW in Opalinus Clay at the Haberstal site is described in Nagra (2024f). This report details the processes expected to occur during the construction, operation, closure and post-closure phase of the repository and also examines the safety-related impact of repository-induced effects on the geological barrier (e.g., thermal effects, the formation of an excavation damaged zone (EDZ), cement-clay interaction, and the effects of gas generation and gas pressure build-up). The assessment of the performance of the repository system is given in Nagra (2024m). The stratigraphy and lithology of the CRZ within the geological regions are summarised in the geosynthesis report (Nagra 2024d). Finally, a more focused appraisal of gas transport in the repository structures and surrounding rock is provided in the gas synthesis report (Nagra 2024i).

4.1 Migration of ^{14}C along repository structures

4.1.1 State of knowledge

During construction and ventilation of the deep geological repository, as well as after emplacement of the waste, backfill and sealing materials, a series of coupled hydro-chemo-mechanical processes will take place in the repository structures and at the interface with the host rock. A comprehensive review of the hydro-chemo-mechanical evolution in the repository structures is given in Nagra (2024f). The following section provides a general overview on the transport of ^{14}C along repository structures.

The excavation of the repository structures creates an EDZ where the hydraulic and mechanical properties of the rock are significantly altered. The construction and the subsequent ventilation of underground structures cause partial desaturation and depressurisation of the liner and the EDZ. After emplacement and backfilling of the repository, the liner and the EDZ will start to resaturate with porewater, which is associated with swelling and self-sealing of the EDZ. Porewater from the host rock will also migrate into the repository structures.

The bentonite of the HLW emplacement tunnels and the L/ILW and HLW sealing sections will saturate due to its high capillary suction and build up its swelling pressure. In particular, the bentonite of the V3 seal (located at the repository shafts; Fig. 2-1) is expected to saturate with porewater originating from the surrounding host rock, as well as more permeable overlying formations. The saturation and swelling of the bentonite will provide the sealing function of the V3 seal, limiting gas flow to the shaft during the time period relevant to ^{14}C release (Nagra 2024i).

The evolution of the saturation distribution in the L/ILW caverns and remaining backfilled structures will depend on the interplay between gravity and capillary suction. In the near-field, gas will be continuously generated from the corrosion of the various steel components and the degradation of organic materials in the waste, according to the availability of water. Gas pressure will increase and, due to the gas pressure gradient, gas will be transported through the backfill and sealing system maintaining a gas migration pathway along the repository structures for several tens of thousands of years (Nagra 2024i). Some partial desaturation of the backfill is expected due to the accumulation of gas in the tunnels and the resulting pressure build-up. In the post-closure phase, the gas generation rate from corrosion and degradation of organics will decline with time (Nagra 2024i). As the gas pressure decreases, the repository will therefore begin to resaturate and approach the hydrostatic pressure (Nagra 2024i).

Transport mechanisms for ^{14}C within repository structures will change with time according to the repository section considered (i.e., HLW *vs.* L/ILW). While with the provisional repository design the HLW near-field will resaturate with water within a few hundred years, the L/ILW near-field is expected to remain unsaturated for longer than 100,000 years (Nagra 2024f). Moreover, the HLW bentonite near-field exhibits relatively homogenous and isotropic porous media properties relevant to transport, whereas the cementitious near-field of the L/ILW repository section is more heterogeneous. Volatile ^{14}C species, such as $^{14}CH_4$ and LMW ^{14}C HCs, which are expected to be the dominant species in the long-term, will migrate along the repository structures through advection and diffusion in the gas phase. Dissolved ^{14}C species, mainly carboxylates, aldehydes, alcohols, carbonates and to a much lesser extent LMW ^{14}C HCs, are expected to migrate by diffusion and to some extent by porewater displacement, as a result of gas pressure build-up. However, ^{14}C mobility in both the liquid and gas phases will depend on the local and possibly variable degree of water saturation.

Sorption coefficients and retention processes for various ^{14}C species within repository structures are summarised in Wieland et al. (2023) and fully reported in Marques Fernandes et al. (2024) and Tits & Wieland (2023). Oxidised ^{14}C organics, such as aliphatic carboxylates and alcohols, are expected to sorb only weakly or not at all on HCP and clay minerals such as bentonite (Wieland et al. 2023, Marques Fernandes et al. 2024, Tits & Wieland 2023). The sorption of multidentate polycarboxylates is expected to be higher due to the specific structure of such molecules. $^{14}CH_4$ may principally sorb onto the surfaces of solid organic matter and minerals in bentonite and excavated clay rock or condense in micropores of clay particles (< 2 nm) (Marques Fernandes et al. 2024). As moisture greatly reduces the sorption capacity of these materials (Vinsot et al. 2017), sorption of $^{14}CH_4$ is therefore expected to be negligeable in post-closure conditions. No sorption of gaseous ^{14}C on cementitious materials is assumed, due to the absence of relevant quantities of organic matter (Wieland et al. 2023). $^{14}CO_2$ that may be released from activated steel, contaminated and vitrified waste will undergo isotope exchange with carbonate minerals in HCP and thus be retained very effectively (Tits & Wieland 2023). In the HLW near-field, $^{14}CO_2$ is however expected to sorb very weakly (Marques Fernandes et al. 2024).

Microbially-mediated conversion of organic ^{14}C species is expected to be inhibited in the HLW bentonite near-field due to small pore sizes and limited availability of water (Mijnendonckx et al. 2019). Very limited microbial activity leading to the conversion of organics is also expected for the L/ILW near-field due to persistent high pH conditions, while limited microbial life could exist locally in niches with lower pH conditions (Guillemot et al. 2023). In the remaining parts of the repository (i.e., EDZ, access tunnels and shafts), such conversion may occur.

4.1.2 Approach to post-closure safety assessments

Two complementary modelling approaches are adopted for the migration of ^{14}C within the repository system (including both the repository structures and CRZ) (Fig. 4-1):

1. Migration of volatile ^{14}C species: The expected initial presence and/or subsequent formation of gas phases within the repository system and any resulting transient water and gas flows during the period of assessments (i.e., 1 million years; cf. ENSI 2023) are explicitly taken into account. For the HLW repository section, the evolution of temperature as a result of heat emission and the associated influence on gas/water flows and ^{14}C migration is also explicitly modelled. Inorganic gaseous ^{14}C species (i.e., $^{14}CO_2$) are assumed to dissolve and react quickly with solid phases, thus such species are disregarded. Hence, a stylised organic volatile ^{14}C species ($^{14}C_{vol}$), mainly $^{14}CH_4$ (cf. Sections 3.3.1 and 3.3.2) is considered. $^{14}C_{vol}$ is assumed to be non-reactive and present in both the gas (preferably) and liquid phase, depending on its solubility and phase saturation. The approach accounts for both migration pathways: i) along repository structures (mainly in the gas phase) and ii) through CRZ (mainly in liquid phase).
2. Migration of dissolved ^{14}C species: The repository system is assumed to be water saturated and any water flow is hypothetised to be constant throughout the period of assessments (Nagra 2024j). A stylised inorganic ^{14}C species ($^{14}C_{inorg}$) includes inorganic ^{14}C species, while a stylised organic ^{14}C species ($^{14}C_{org}$) regroups various LMW ^{14}C organics[10]. Both stylised species are assumed not to be subject to any degradation. The individual molecules are assumed to either dissolve in porewater or adsorb onto solids. The transport of $^{14}C_{org}$ and $^{14}C_{inorg}$ is diffusion dominated. Given the high transport capacity of the CRZ for dissolved species, if compared with that of the pathway along repository structures (which would take longer to reach by diffusion and therefore would need more time), the latter pathway is disregarded (cf. Poller et al. 2014).

[10] $^{14}C_{inorg}$ includes dissolved $^{14}CO_2$ and $^{14}C_{org}$ integrates dissolved ^{14}C organics, mainly composed of $^{14}CH_4$, together with small amounts of ^{14}C-aliphatic carboxylates and ^{14}C-alcohols.

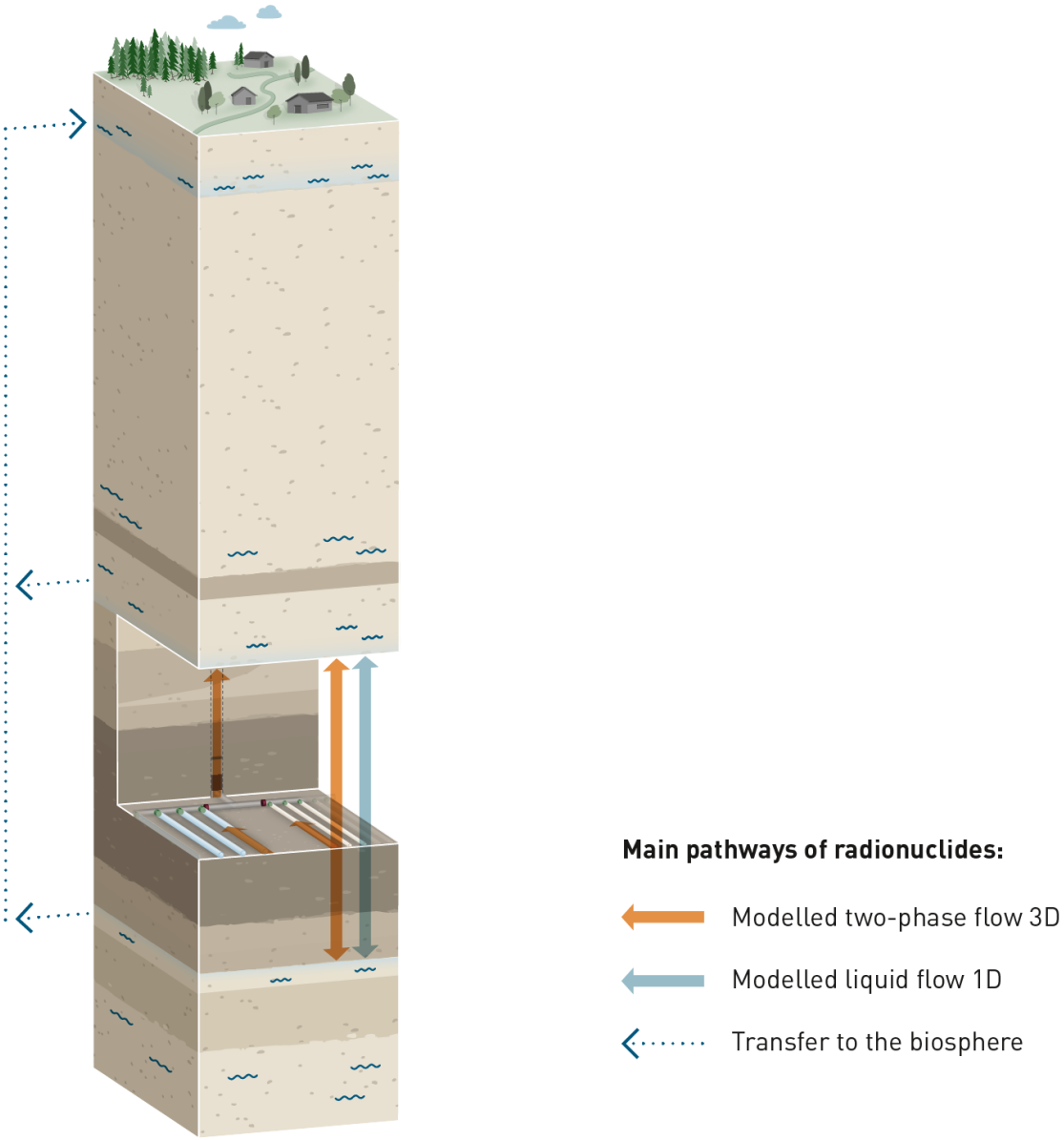

Fig. 4-1: Schematic representation of the two ^{14}C modelling approaches: 3D two-phase approach for modelling the migration of volatile ^{14}C species (thick orange arrow) and 1D single-phase liquid approach for modelling the migration of dissolved ^{14}C species (thick blue arrow)

The following overall assumptions are made regarding the assignment of the simplified release species, as introduced in Sections 3.3.1 and 3.3.2 to stylised model components (Fig. 4-2):

- Experimentally observed inorganic ^{14}C species are modelled with the stylised model component $^{14}C_{inorg}$ in the approach regarding the migration of dissolved ^{14}C species.
- Experimentally observed organic ^{14}C species are modelled with the stylised model component $^{14}C_{org}$ in the approach regarding the migration of dissolved ^{14}C species.

- Experimentally observed organic ^{14}C species are modelled with the stylised model component $^{14}C_{vol}$ in the approach regarding the migration of volatile ^{14}C species. Inorganic gaseous ^{14}C species are disregarded as they are assumed to dissolve and react quickly with solid phases.

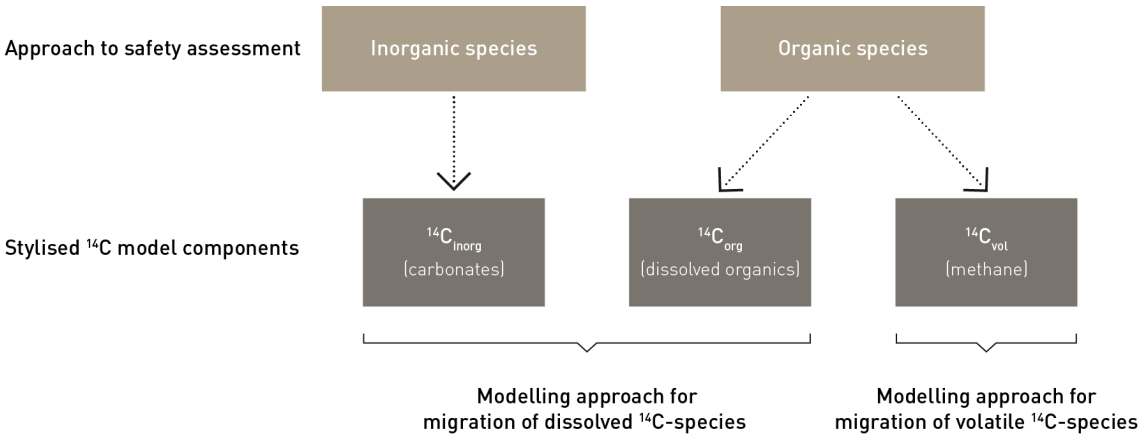

Fig. 4-2: Assignment of released ^{14}C species to stylised ^{14}C model components in the two modelling approaches for the migration of ^{14}C

The migration of ^{14}C-bearing species along repository structures is only relevant for volatile species. Therefore, only the approach regarding the migration of volatile ^{14}C-bearing species is described below. The migration of dissolved ^{14}C-bearing species is dominated by the diffusive transport through the CRZ; the pathway along repository structures can be disregarded. The respective approach is described in Section 4.2.2.

The migration of ^{14}C along repository structures is expected to occur almost exclusively in the form of volatile ^{14}C-bearing species moving through the repository within the gas phase. Therefore, the associated modelling approach takes the generation of gases in the repository along with the resulting transient two-phase (gas and water) flows explicitly into account. Given that the emission of heat from SF and RP-HLW affects the saturation of the HLW near-field and the evolution of the hydraulic pressure field both within and outside the HLW repository section, these processes are also explicitly considered.

The modelling approach used for migration of volatile ^{14}C species is called the macroelement approach. It is described in detail with the associated parameter values in the consequence analysis report (Nagra 2024j). The following paragraphs highlight the main aspects of this approach.

Several stylised phases prior to and within the period of ^{14}C release are identified:

- Initial conditions: No repository structures are present. The entire model domain is water saturated and free of ^{14}C species, hydrostatic conditions prevail, and the temperature field reflects the geothermal gradient. The initial conditions at the upper and lower boundaries of the model domain are retained as boundary conditions throughout the modelling period.
- Operational phase 1 (0 – 21 years): The access structures, the central area and operation / ventilation tunnels up to V2 seal are built instantaneously and thereafter ventilated for 21 years. Ventilation conditions are 1 bar, 28 °C and relative humidity of 60%.
- Operational phase 2 (21 – 36 years): All remaining repository structures including the emplacement drifts and caverns of the main and pilot repository are built instantaneously and ventilated for an additional 15 years.

- Post-closure phase (36 - 10^6 years): All repository structures are charged/backfilled instantaneously. All source terms are activated: i) gas from waste in emplacement drifts/caverns and construction materials in all tunnels (excluding shafts), ii) heat from HLW disposal canisters and iii) HLW and L/ILW ^{14}C source terms as described in Chapter 3.

Additional operational phases (or more detailed implementation of the repository timeline) may be considered in the model variants. It is assumed that all HLW disposal canisters will breach at the same time, after a certain containment period determined by its design. ^{14}C in SF and RP-HLW is therefore subject to radioactive decay before release starts. No period of complete containment is assumed for ^{14}C in L/ILW, since the 200 L steel drums, in which most of the L/ILW is stored, are not designed for a full containment of all radionuclides for a fixed time period and therefore not considered as a safety barrier (Nagra 2024f, Nagra 2024k).

The model domain encompasses the entire repository system, albeit in the following stylised manner. Similar and (quasi) symmetrically positioned repository structures along with the surrounding rock are aggregated to representative, 3D macroelements. Each macroelement represents the repository structure itself (tunnel or shaft) together with adjacent EDZ and CRZ. HLW emplacement drifts and L/ILW emplacement caverns are each modelled with a single macroelement. This implies that L/ILW is homogeneously distributed across all the caverns and no distinction between waste groups is made. All model units that represent different types of material within a macroelement are conceptualised as anisotropic and homogenous porous media. Fig. 4-3 shows an example macroelement of the emplacement caverns.

Extensive properties of the macroelements, such as volumes, areas and source terms, are multiplied by the respective number of aggregated structures/symmetry planes, whereas intensive properties/states, such as temperature, material properties and pressure gradients, remain unscaled. The macroelements of all repository structures (emplacement tunnels, V1 seals, branch tunnels, operation/ventilation tunnels, shafts) are linked together at the interface of the individual structures and the surrounding EDZ to allow for water and gas flow between the macroelements and hence enable ^{14}C transfer along repository structures. The rock parts of the respective macroelements are not connected, which reflects the expectation that these mostly remain water saturated and thus only allow for diffusion of dissolved ^{14}C in a plane perpendicular to the repository structures. An example schematic layout of a macroelement model is shown in Fig. 4-4.

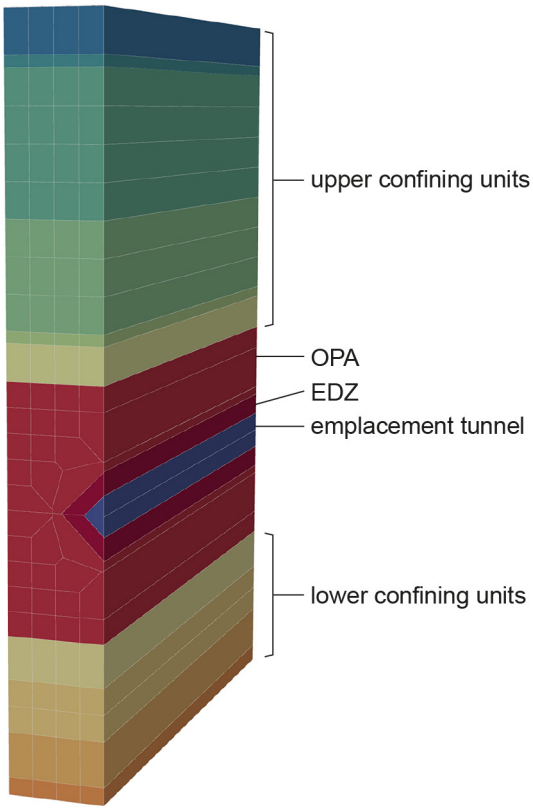

Fig. 4-3: Example 3D macroelement for the L/ILW emplacement caverns

Each macroelement consists of the repository structure (e.g., emplacement cavern), adjacent EDZ and CRZ (i.e., host rock and confining units). The macroelement only represents half of the repository structure to take advantage of the symmetry. To account for all 7 emplacement caverns, extensive properties (volumes, areas) are scaled by a factor of 7 (number of structures) times 2 (for the symmetry).

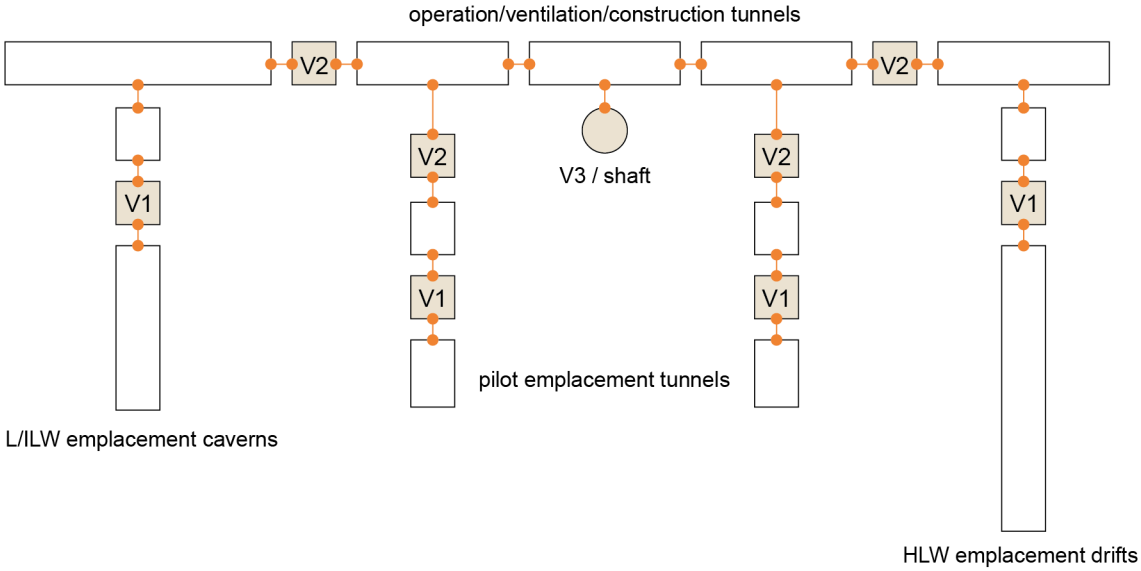

Fig. 4-4: Example schematic layout of a macroelement model

Macroelements are shown as boxes (seals in grey colour) and connections as orange lines/dots.

The macroelement approach allows for the coupled simulation of gas and water movements along with associated advective/diffusive transport of gaseous or dissolved ^{14}C within the model domain. Mechanical effects, such as bentonite swelling, pathway dilation or self-sealing, and chemical effects, such as cement degradation or local pore clogging, are either modelled indirectly (e.g., by assuming porosity and permeability values for swollen bentonite) or disregarded, if their effects on ^{14}C release rates from the repository system are judged to be negligible.

The modelling approach for the migration of volatile ^{14}C species is implemented in the TOUGH3 two-phase flow simulator and the corresponding EOS75r module (Jung et al. 2018). This module has been adapted from the official release of EOS7r, such that the original model component "air" uses the properties of H_2, which is the main gas component produced in the repository. Bulk gas is hence also modelled with the density and viscosity of H_2 gas. Another model component is taken to be the stylised volatile ^{14}C species ($^{14}C_{vol}$) with the properties of CH_4. Distribution of $^{14}C_{vol}$ between the liquid phase and the gas phase is assumed to follow Henry's Law. The associated distribution coefficient (Henry's coefficient) is set to a constant value of 0.0014 mol/kg/bar. Stable carbon species are not explicitly modelled. Since $^{14}C_{vol}$ is assumed to be non-reactive, no conversion processes other than radioactive decay are modelled, which is conservative. Conservatively, no sorption and no solubility limitation are modelled either, given the expected weak sorption of CH_4 (cf. Section 4.1.1).

In TOUGH3, the molecular diffusion coefficient for both the liquid and the gas phase is a global parameter, not a material parameter. Effective diffusion coefficients (depending on porosity, tortuosity and phase saturation) are calculated according to the Millington-Quirk model implemented in TOUGH3. The reference value for the molecular diffusion coefficient for the liquid phase is chosen such that the effective diffusion coefficient of $^{14}C_{vol}$ for the host rock in fully saturated state equals that of $^{14}C_{org}$ in the modelling approach for dissolved ^{14}C species. TOUGH3 / EOS75r has also been extended to account for anisotropy of diffusion coefficients and thermal conductivity. The relative permeability and capillary pressure relationships are parametrised according to the modified van Genuchten model, also implemented in TOUGH3.

The calculated flux of $^{14}C_{vol}$ at the upper and lower boundary of those macroelements that model repository structures represents the ^{14}C output from the CRZ. The respective flux at the upper boundary of those macroelements that model underground access structures (i.e., shafts, or alternatively a ramp) represents the ^{14}C output from repository structures. Both outputs are summed up to give the total ^{14}C output from the repository system. The mere summation of ^{14}C outputs at different locations is a conservative approach since the individual outputs may end up in different biosphere areas and/or undergo different travel times. Finally, the total output is multiplied by ^{14}C biosphere dose conversion factors (cf. Chapter 5) to yield the ^{14}C dose rate.

Major sources of uncertainty are managed via assumed parameter distributions and/or bandwidths that feed into probabilistic and deterministic uncertainty and sensitivity analyses. Exemplary parameters are IRF/CRF values, corrosion rates for different metals, permeability values for the different materials (notably of the host rock and of the sealing components), two-phase flow parameter values, porosity values, initial saturation of backfill materials and diffusion coefficients.

4.1.3 International approach

The information available on the migration of ^{14}C along repository structures in WMO safety assessments is rather limited. It is commonly assumed that $^{14}CO_2$ will react with cementitious materials and will be immobilised in the repository near-field, and ^{14}C carbonates will be exchanged with stable carbon, although this latter process is often conservatively ignored. $^{14}CH_4$ is treated as being mobile in both gaseous and aqueous forms and able to migrate through and out of the engineered barriers.

As an example, RWM's safety assessment for the groundwater pathway in higher strength and lower strength sedimentary host rocks considers the interaction between the radionuclides and the cementitious backfill but does not consider migration along the repository structures (RWM 2016c). The ^{14}C source term in the groundwater pathway model is characterised by a single compartment representing waste packages and backfill. Carbon (independent of speciation) is assumed to have a solubility of 0.01 mol/m^3 in backfill and to sorb with a 50th percentile value of 0.2 m^3/kg (log cumulative distribution ranges from 10^4 m^3/kg to 100 m^3/kg, again independent of speciation) (RWM 2016b). The rate at which water is released from the near-field to the host rock corresponds to the assumed flow rate through the representative vault defined in the model. There is no consideration of the EDZ or engineered structures outside the disposal vaults. RWM's safety assessment for the gas pathway assumes that $^{14}CO_2$ reacts with the cementitious backfill and $^{14}CH_4$ is transported with the bulk H_2 carrier gas as it is released to the host rock through the disposal vaults only. For high heat generating waste, diffusion of dissolved ^{14}C compounds through the bentonite buffer is included, assuming no sorption (RWM 2016c). The transport of gas is not assessed in the main safety assessment as Magnox SF, which is the only waste form judged likely to generate significant gaseous ^{14}C compounds, is not included in the reference cases. A more recent detailed modelling study (Swift et al. 2020) considered gas generation and migration in a repository for L/ILW based on Nagra's disposal concept. It shows that almost all the gas is transported along the engineered structures and released to the host rock and overlying strata through the seals and any associated EDZs.

In SKB's safety assessment for a L/ILW repository in a crystalline host rock (SR-PSU), a diffusive transport of dissolved ^{14}C compounds through the bentonite barrier of the silo has been assumed (SKB 2015a, SKB 2015b). It should also be noted that the inventory is restricted to ensure low gas pressures, avoiding any disruption of the barriers and therefore the need to assess gas migration. In the post-closure safety assessments for the deep geological disposal of ILW in a crystalline host rock (SE-SFL), SKB simulates aqueous transport of ^{14}C through the backfill

(cementitious or bentonite depending on the vault) but does not consider transport through the wider network of underground structures. The majority of the ^{14}C (> 90%) is assumed to decay before it reaches the host rock (SKB 2019a, SKB 2019b).

The Ontario Power Generation's deep geological repository in Canada was not intended to be backfilled, so gas was expected to mix throughout the repository (Quintessa et al. 2011). Physical segregation of H_2-generating waste (metals) from CO_2-generating waste (organic materials) was not considered, so the ^{14}C-containing gases could readily mix with the bulk H_2. As there was no cementitious backfill to react with it, $^{14}CO_2$ gas was considered to be present if no methanogenesis occurred. The concentration of dissolved ^{14}C-bearing inorganics was specified to be controlled by equilibrium with solid carbonate phases. A specific activity model was used in the assessment calculations to describe the partitioning of ^{14}C between liquid and gas phases. This model assumes that the partitioning of ^{14}C mirrors the behaviour of bulk stable carbon (i.e., ^{12}C) and uses the results of the detailed T2GGM model to determine ^{14}C mass flows out of the repository. However, it does not consider precipitation as calcite or exchange with carbonate rocks. The gaseous ^{14}C is only in the form of $^{14}CH_4$, due to microbially mediated methanogenesis converting all CO_2 to CH_4, using H_2 produced by metal corrosion.

Reference scenarios in most safety assessments do not explicitly consider migration of radionuclides through shafts and other access structures. This pathway is likely to be of relatively low importance for fractured crystalline host rocks through which gas and water can migrate relatively easily. So far, RWM does not include this pathway in their safety assessment models when considering a higher strength host rock (RWM 2016c). However, more recent modelling indicates that it may be the main pathway for the transport of gaseous ^{14}C compounds to the overlying geosphere in the lower strength sedimentary rock concept (Swift et al. 2020), which is based on Nagra's disposal concept. In the safety assessment of Ontario Power Generation's deep geological repository at the Bruce site (Quintessa et al. 2011), release of bulk gas containing ^{14}C from the repository was the main risk assessed in disruptive scenarios, in particular, a scenario where the shaft seals were assumed to be constructed poorly and fail. For seals, which should exhibit a very low gas permeability, the primary pathway for ^{14}C migration is via the EDZ (i.e., through the interfaces between engineered seals and the host rock). The rate of gas transport through the geosphere and shafts depends on the gas pressure in the repository, initial gas saturation conditions, and gas permeabilities of the shaft seals and host rock. This rate is underpinned by a coupled gas generation and two-phase flow transport code that represents the repository and geosphere in detail (Quintessa et al. 2011).

4.2 Migration of ^{14}C through the CRZ

4.2.1 State of knowledge

The construction of the repository induces pore pressure changes in the rock close to the underground openings. The subsequent ventilation of the underground structures at the prescribed temperature and relative humidity causes depressurisation and partial desaturation of the rock. The hydraulic gradient in the host rock towards the repository structures subsequently contributes to the resaturation of the EDZ and the hydration of bentonite in the HLW tunnels and the sealing sections of the repository after emplacement. In particular, the thermal pulse developing around the HLW tunnels in the early post-closure phase accelerates the hydration of the buffer around the HLW disposal canisters as a saturation front will develop due to the steep pressure gradient into high-suction bentonite material driving vapour diffusion and/or liquid flow (Nagra 2024f, Nagra 2024i).

The gases generated in the repository may go into the rock as gas phase but will predominantly dissolve in porewater[11]. Dissolved gas (mainly H_2) will be transported through the host rock predominantly via diffusion and to some extent with water displaced from the repository to the rock due to the gas pressure build-up in the underground structures. Depending on the hydraulic gradient across the CRZ, a small supplemental advective/dispersive component may be present. Within the period of assessments (i.e., 1 million years; cf. ENSI 2023), some dissolved gas may reach the over- and underlying confining units, depending on the amount of gas generated in the repository and the transport properties of the barriers. A continuous gas phase across the CRZ is considered unlikely, based on the two-phase flow properties of the Opalinus Clay (i.e., very low permeability and high capillarity) and the relatively high gas entry pressure (especially for the L/ILW repository section). In the late post-closure phase, gas pressures decrease and flow converges from the far field towards the repository as the underground structures saturate with porewater from the rock (Nagra 2024i).

According to the current knowledge about ^{14}C speciation and rate of release from the individual waste forms and the expected overall evolution of the repository, ^{14}C is expected to penetrate the intact CRZ primarily in the form of dissolved $^{14}CH_4$. Other LMW organics, such as carboxylates, aldehydes and alcohols, may also be present, but their fraction would be small. $^{14}CO_2$ is mainly released from L/ILW and expected to be largely retained in the L/ILW near-field by carbonation of cement and other reactions.

Oxidised ^{14}C-bearing organic compounds are expected to sorb very weakly onto minerals within the CRZ (Marques Fernandes et al. 2024, Tits & Wieland 2023). The sorption of multidentate polycarboxylates is expected to be higher due to the specific structure of such molecules. Microbially mediated degradation of organic ^{14}C species into thermodynamically stable end products $^{14}CH_4$ and $^{14}CO_2$ is expected to be inhibited in Opalinus Clay due to very low porosity and water availability (Guillemot et al. 2023). Microbes might, however, become metabolically active as soon as conditions improve (i.e., increase in pore space, water and substrate availability), for example in the EDZ. $^{14}CH_4$ may principally sorb onto the surfaces of solid organic matter (kerogen) and minerals, absorb into kerogen, or condense in micropores (< 2 nm). For the present host rock, sorption on solid organic matter is judged to be the dominant process. Moisture greatly reduces the sorption capacity of clay rock, thus sorption of $^{14}CH_4$ is expected to be negligeable (Vinsot et al. 2017, Van Loon & Chen unpublished). If $^{14}CO_2$ reaches the host rock, despite the high sorption occurring in the cementitious near-field of the L/ILW repository section, it would be effectively retained by isotope exchange with carbonate minerals present in Opalinus Clay (Marques Fernandes et al. 2024). More information about potential retention processes for various ^{14}C species is summarised in Wieland et al. (2023) and reported in Marques Fernandes et al. (2024).

4.2.2 Approach to post-closure safety assessments

The migration of ^{14}C-bearing species through the CRZ is in qualitative terms quite similar for the two modelling approaches introduced in Chapter 4.1.2, given that desaturated zones will only occur either close to the repository and in the EDZ in particular, or locally within the upper confining units in strata with storage capacity for gas. Overall ^{14}C transport rates through the CRZ are thus controlled by the diffusive transport capacity of vast saturated areas within this domain.

---

[11] For comparable volumes of a liquid phase and a gas phase in equilibrium, there are orders of magnitude more H_2 (and CH_4) in the gas phase. However, the total volume of water-saturated areas within the repository system (notably the host rock) is orders of magnitude higher than that of unsaturated areas (notably the L/ILW repository section), and diffusion of dissolved gases in the host rock is fast. Therefore, considerable amounts of gases are dissolved.

The modelling approach for migration of dissolved ^{14}C species is identical to that for the migration of all other relevant radionuclides. Details on this approach and the associated parameter values are documented in the consequence analysis report (Nagra 2024j). As the approach for volatiles ^{14}C species, the approach for dissolved ^{14}C species considers two distinct phases within the period of interest: i) a phase of complete containment (knowing that no containment is assumed for L/ILW after repository closure); and (ii) a subsequent phase of ^{14}C mobilisation and transport. The domain for modelling the migration of dissolved ^{14}C species is subdivided into the near-field, which encompasses the emplacement drifts and caverns, and the geosphere, which covers the CRZ. It should be noted that most of the transport distance (> 90%) resides in the CRZ. Nevertheless, the near-field can provide an effective first barrier for some radionuclides, including inorganic ^{14}C species (see below).

The near-field model for the L/ILW is a 2D cross-sectional representation of a single L/ILW cavern with averaged and homogeneously distributed inventory for each waste group and is implemented with the Versatile Performance Assessment Code (VPAC) code (Holocher et al. 2008). The HLW near-field is modelled with a 1D cylindrical geometry in the Source Term MANagement and prediction program (STMAN) code (Robinson 2022). Both near-field models include a representation of the EDZ to provide realistic conditions for the flux from the cement of the L/ILW cavern or the bentonite into the EDZ. This flux provides the input for the geosphere model, which is a network of 1D transport legs representing the EDZ, the host rock and the different lithofacial units within the confining units. The code used for the geosphere is PICNIC-TD (Robinson & Chittenden 2022). Fig. 4-5 shows a schematic view of a typical geosphere model developed for the Swiss repository concept.

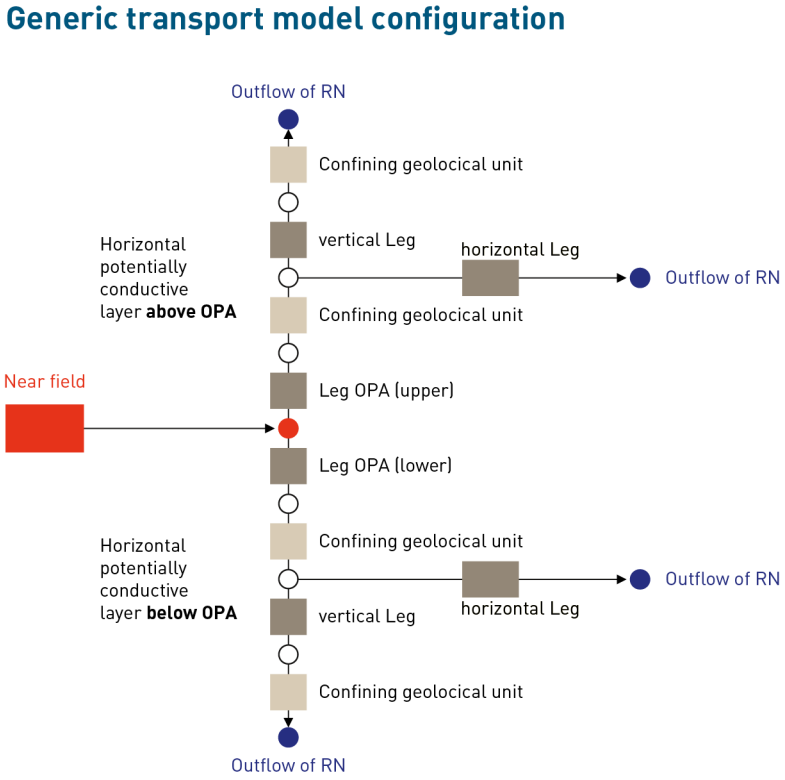

Fig. 4-5: Schematic view of a typical geosphere model in the modelling approach for migration of dissolved ^{14}C-bearing species

From Nagra (2024j).

Full water saturation and isothermal conditions are assumed in both the near-field domain and the geosphere domain. Model abstraction analyses to evaluate the conservatism of these assumptions are documented in Nagra (2024j).

The model components are a stylised inorganic ^{14}C species ($^{14}C_{inorg}$) and a stylised organic ^{14}C species ($^{14}C_{org}$). Initially, the concentration of the stylised model components is zero in the entire model domain. It should be noted that during the period of complete containment in the HLW disposal canisters, the model components are subject to radioactive decay.

In the L/ILW near-field model, the transport processes considered are advection, longitudinal and transverse dispersion, and diffusion. For the HLW near-field model, only diffusion is accounted for on the path from the waste through the bentonite buffer. For the geosphere model, advection, longitudinal dispersion and diffusion are considered. It should be noted that in the reference case, transport through the near-field and CRZ is dominated by diffusion. Transport parameters considered, e.g., effective diffusion coefficients and porosity, are specific to each model component and unit. The concentration of the model compounds at model boundaries that do not represent symmetry planes is zero. The flux of $^{14}C_{org}$ and $^{14}C_{inorg}$ from the cavern to the EDZ calculated within the near-field models is applied as a source term to the respective geosphere models.

Since the model components are assumed to not be subjected to any degradation (abiotic or biotic), no conversion process other than radioactive decay is modelled. Regarding interactions of the dissolved ^{14}C-bearing components with solids, fully reversible, linear sorption is assumed and quantified with component-specific and model unit-specific sorption coefficients (parameter K_d) according to the state of knowledge described above. Solubility limitation is explicitly modelled in the HLW near-field for $^{14}C_{inorg}$, which also requires the explicit modelling of stable carbon species. For the L/ILW near-field and the geosphere, the assumed sorption coefficient for $^{14}C_{inorg}$ represents a stylised approach to model the process of isotopic exchange of ^{14}C carbonates with accessible non-radioactive carbonate species (mostly calcite) (Marques Fernandes et al. 2024, Tits & Wieland 2023).

The calculated fluxes of the two components at the upper and lower boundaries of the geosphere models represent the ^{14}C output from the CRZ. In case of assumed horizontal water flow within individual strata of the confining units, a separate ^{14}C output from the CRZ is calculated and added to the total ^{14}C output. The summation of ^{14}C outputs at different locations represents a conservative approach, since the individual outputs may be released to different biosphere areas and/or with different travel times.

Major sources of uncertainty are managed via assumed parameter distributions and/or bandwidths that feed into probabilistic and deterministic uncertainty and sensitivity analyses. Exemplary parameters include the duration of complete containment, congruent release rates for different materials, water flow rates in the geosphere, transport parameters in the near-field and the geosphere, for example diffusion and sorption coefficients, and the thickness of rock formations in the geosphere. Parameter distributions are either uniform, log-uniform or log-normal.

4.2.3 International approach

For a repository constructed in low-permeability clay/mudrock or limestone formations, the host rock and immediately overlying rocks are generally considered to provide a significant barrier to the transport of ^{14}C in either aqueous or gaseous form. In contrast, for repositories in fractured crystalline rocks, the host rock provides little or no barrier to the transport of ^{14}C in either aqueous or gaseous form. This section particularly focuses on concepts for deep geological repository in sedimentary rocks.

RWM's recent ^{14}C integrated project focussed on a higher strength host rock but also includes limited consideration of a lower strength sedimentary host rock (i.e., clay) (RWM 2016b, RWM 2016c, RWM 2016d). ^{14}C can only migrate through the lower strength sedimentary host rock via aqueous diffusion or be transported in a carrier gas. It should however be noted that as the characteristics of the lower strength sedimentary host rock are based on those of the Opalinus Clay, the conclusions are similar to those from Nagra. Transport through the lower strength sedimentary host rock is modelled in GoldSim as diffusion (RWM 2016c), using transport parameters from RWM (2016d). Transport properties are independent of the speciation. RWM (2016d) also presents calculations carried out prior to 2010 for gas migration through a generic clay host rock. The results suggest that high gas pressures could develop in the host rock and gas could migrate through the host rock. The time taken for the gas to migrate though about 100 m of host rock was estimated to be about 20,000 years. However, these results are strongly dependent on the assumptions concerning gas generation (and therefore the pressure in the repository), and the characteristics of the rock, notably the gas entry pressure. The model did not include the various tunnels and engineered spaces that could serve as gas storage and there was no representation of the access drifts and shafts. Thus, the only route for gas migration from the disposal vaults was assumed to be through the host rock.

Ontario Power Generation's proposed deep geological repository for L/ILW in Canada will be located in a very low permeability limestone host rock. Aqueous transport through the host rock is modelled by diffusion. Its very low permeability, combined with significant void volume available in the repository to accommodate gas, limits ^{14}C migration. Once released into the gaseous phase, ^{14}C will partition between the gas and the coexisting liquid phase. No viable pathway through the host rock is considered for a relatively short-lived radionuclide such as ^{14}C (Quintessa et al. 2011).

4.3 Migration of ^{14}C in deep groundwater systems

4.3.1 State of knowledge

According to the current knowledge about migration of ^{14}C within the repository system (cf. Sections 4.1 and 4.2), only $^{14}C_{org}$ and $^{14}C_{vol}$ from the emplaced waste may enter the deep aquifers. The $^{14}C_{org}$ might reach the deep groundwater systems by diffusion, while $^{14}C_{vol}$ might enter the deep aquifers via two pathways: at the location of underground access structures, or more widely above and below the area affected by the repository. As discussed in Section 4.1.1 and detailed in the gas synthesis report (Nagra 2024i), the release of $^{14}C_{vol}$ through the access structures will be limited by the sealing function of the V3 seal. Hence, the consequence analysis does not rule out gas flow through the V3 seals (Nagra 2024j). Moreover, the EDZ around the shafts may form a preferential flow path for $^{14}C_{vol}$.

Above the repository as well as in the vicinity of the shafts, a part of the $^{14}CH_4$ mainly composing the $^{14}C_{vol}$ is assumed to dissolve in porewater (i.e., at the shaft interface to the rock/EDZ) and must be explicitly accounted for. Once in the deep groundwater systems, all $^{14}C_{vol}$ is assumed to be in dissolved form and is included in $^{14}C_{org}$. It is however not excluded that in these aquifers, dissolved $^{14}CH_4$ may form a gas phase again depending on its concentration and the local pressure, temperature and salinity conditions. The principal structure and expected evolution of deep groundwater systems passing through the geological siting regions are summarised in the geosynthesis report (Nagra 2024d), the hydrochemistry report (Gegg et al. 2019) and the groundwater modelling report (Nagra 2024e).

No oxidation of $^{14}C_{org}$ is expected to occur given that conditions in deep aquifers are observed to be methanogenic (Gegg et al. 2019, Nagra 2024e) and that O_2 brought into the repository by ventilation is expected to be consumed quickly after its closure by various biotic and abiotic redox

processes (Nagra 2024f). Given that present-day groundwaters contain substantial amounts of CH_4 (Nagra 2024e), the microbial-mediated oxidation of $^{14}CH_4$ to $^{14}CO_2$ is not expected either. Since clay mineral and organic content in the aquifers are relatively low (Nagra 2024d) and $^{14}C_{org}$ is assumed to sorb very weakly onto minerals (Marques Fernandes et al. 2024), retention of $^{14}C_{org}$ on solids present in deep groundwater system is expected to be negligible.

The relevant parameter for potential delay and hence decay of ^{14}C is the travel time from the repository to the deep aquifers and subsequently to the respective discharge area.

4.3.2 Approach to post-closure safety assessments

Given that the processes relevant to the release of $^{14}C_{vol}$ outside the repository through access structures are site-specific and very design-specific, potential delay and decay in safety assessments for the RBG are not taken into account. Similarly, potential delay and hence decay of $^{14}C_{org}$ along deep groundwater systems are also not taken into account. Transverse dispersion along such pathways, which would reduce the portion of released $^{14}C_{org}$ that enters the considered biosphere area, is also disregarded. These decisions are mainly based on the judgement that transport in fractured media is potentially fast, if matrix diffusion is weak and no retention or oxidation of $^{14}C_{org}$ is to be expected. In addition, the distance to potential discharge areas is short for some aquifers in some siting regions (Nagra 2024e, Nagra 2024d).

This approach is conservative and overestimates ^{14}C releases to the biosphere but conforms with the previous ones adopted in Nagra's safety assessments so far (Nagra 2002b, Nagra 2014a) and other WMOs (cf. Section 4.3.3).

4.3.3 International approach

In its dissolved chemical form, ^{14}C is generally treated in the same way as any other radionuclide in safety assessments for the groundwater pathway, taking sorption into account, where appropriate. Some safety assessments treat the inorganic and organic forms separately in the context of sorption when considering the sorption properties (SKB 2015a, SKB 2015b, SKB 2019a, SKB 2019b), while others do not distinguish the different chemical forms of ^{14}C (e.g., RWM 2016b).

Safety assessments often assume that ^{14}C in gaseous form is transported to the biosphere either instantly or within a very short period of time after leaving the repository or the host rock. This is a conservative, but not unreasonable assumption for a fractured crystalline geosphere. For example, SKB conservatively assumes that all ^{14}C is released from the L/ILW repository of SR-PSU as $^{14}CH_4$ and is transported out of the repository into the biosphere without significant radioactive decay (SKB 2015a). For the case of gas transport in the ILW repository of SE-SFL (also in crystalline host rock), it is assumed that half of the ^{14}C inventory is transported to the biosphere immediately on disposal canister failure and the other half is more gradually released on a timescale consistent with the generation of gas by corrosion of the canister insert (SKB 2011).

RWM's base assumption is that gas will be transported to the biosphere instantly after release from the repository, while noting that many geological environments provide ample opportunity for the gas to be trapped within the geosphere (RWM 2016d). In the absence of a site for the deep geological disposal of radioactive waste, RWM does not consider it appropriate to consider their safety assessment for any potential delay in ^{14}C migration in the geosphere.

The safety assessments for the Ontario Power Generation's deep geological repository in Canada assume that some gas (i.e., $^{14}CH_4$) reaches the shallow groundwater in case of severe failure of the shaft seals.

5 Migration of ^{14}C and radiation exposure in the biosphere

As described in the preceding chapters, there is potential for a fraction of the disposed ^{14}C inventory to reach the near-surface environment. Coming through a deep groundwater system, ^{14}C would be dissolved in groundwater and largely present as $^{14}CO_2$, $^{14}CH_4$ and ^{14}C bicarbonate, although some may be present as small organic molecules (e.g., carboxylic acids) (cf. Chapter 4). As they are discharged to the near-surface aquifers (Fig. 5-1), geochemical changes and microbial activities might induce oxidation of $^{14}CH_4$ and small ^{14}C organics to $^{14}CO_2$.

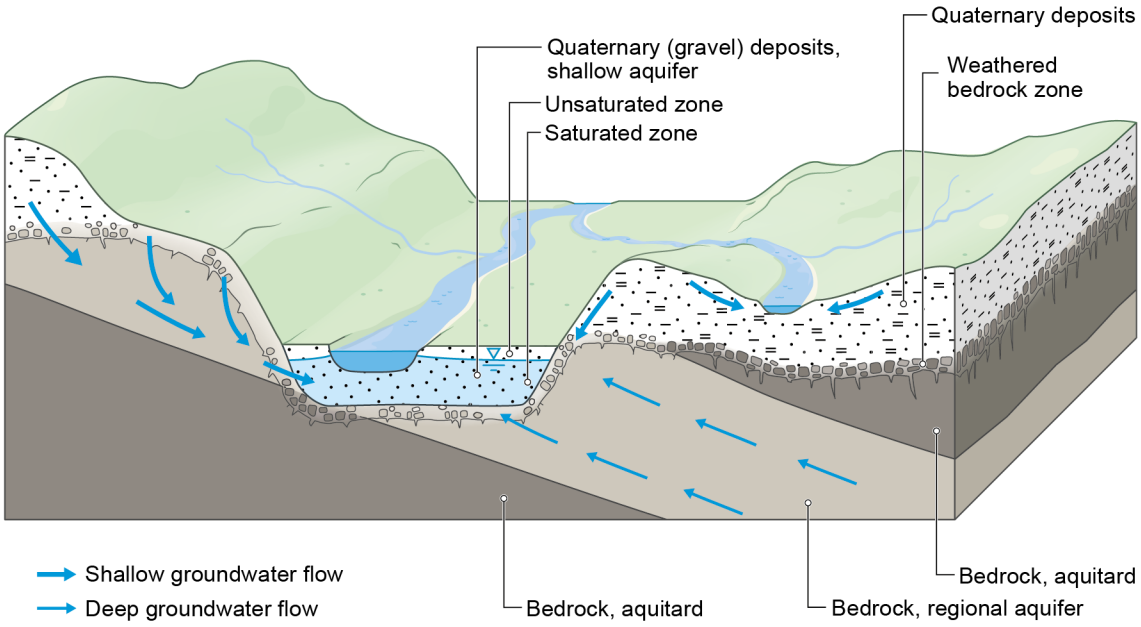

Fig. 5-1: Conceptual model of deep groundwater discharge to a valley in the context of Northern Switzerland

From Nagra (2024g).

The remainder of this chapter summarises how the potential significance of ^{14}C that may be released to the near-surface environment from a deep geological disposal facility is assessed. Section 5.1 describes how ^{14}C would behave in the near-surface (including a local shallow aquifer) and surface environments (collectively referred to as the "biosphere" in this context). Section 5.2 then describes how potential exposure to humans is evaluated to allow comparison against regulatory criteria. It should be noted that exposure is not certain to occur and is referred to as potential exposure.

5.1 Behaviour of ^{14}C released to the biosphere

5.1.1 State of knowledge

Even on timescales of several tens of thousands of years, the landscape in Northern Switzerland will continue to be dominated by valleys, with unconsolidated fluvioglacial deposits in the valley bottoms, hosting shallow groundwater aquifers (Nagra 2024g). As at the present day, the valley bottoms will have potential to be occupied by people, including those making use of local shallow

groundwater, producing food from agricultural use of the land and consuming fish from local surface waters. This would also be the case for moderately different climatic conditions that could occur during the period of assessments (i.e., 1 million years; cf. ENSI 2023), albeit different climatic conditions may entail different crop types, different agricultural patterns and different lifestyles. The climate in Northern Switzerland will evolve over the timescales of interest for assessing ^{14}C from geological disposal, with a potential period of warmer climate, as anthropogenic greenhouse gas emissions peak, followed by gradual cooling, influenced by orbital cycles and associated variations in insolation (Talento & Ganopolski 2021). Periglacial conditions or even glacial conditions are only expected to occur towards the end of the period of interest when a large fraction of the ^{14}C inventory will have already decayed.

Ultimately, the deep groundwater from the CRZ would most likely discharge to a local shallow aquifer, where groundwater and surface water flow would typically be dominated by catchment-scale hydrology (Fig. 5-1). In zones where mixing of deep groundwater with shallow groundwater occurs, pressure, salinity, redox conditions and temperature may change gradually or abruptly.

There is a small difference in molecular weight between ^{14}C and the lighter, stable ^{12}C, giving rise to distinctions in behaviour that are small relative to other sources of variability in carbon transport (for CH_4 the weight difference is ca. 10%; for inorganic carbon the difference is much lower). This difference in behaviour, due to isotopic fractionation/discrimination, is sufficiently small that the different ^{14}C forms can reasonably be expected to behave in the same way as the corresponding forms of stable carbon upon release to the biosphere. However, the fractional discrimination between isotopes is sufficient to allow distinctions in the ratio of stable ^{13}C to ^{12}C to be used to develop an understanding of some environmental processes. There is a large body of understanding in terms of the carbon cycle, which is important to ecology and central to climate science (e.g., Houghton 2003; Schlesinger & Bernhardt 2020; Wallmann & Aloisi 2012).

^{14}C occurs naturally in the environment because it is produced by the interaction of cosmic rays with the atmosphere and more recently by nuclear applications (notably atmospheric testing of nuclear weapons). Much is understood about the natural occurrence of ^{14}C in the biosphere (e.g., UNSCEAR 2010). For example, its presence forms the basis of the science of radiocarbon dating, whereby measuring the amount of ^{14}C in materials, coupled with knowledge of its half-life, allows the time at which the ^{14}C was fixed into organic molecules to be determined, providing insight into the age of the material.

These sources of understanding and information combine to support conceptualisation of how ^{14}C released to the biosphere in groundwater would behave in the long term.

Once released to the local shallow aquifer, dissolved ^{14}C originating from the deep geological repository would migrate with near-surface groundwater flows. Groundwater carrying dissolved ^{14}C then has potential to discharge to surface water in valley bottoms (including rivers and/or lakes), and potentially to soils/sediments adjacent to surface water. Consideration of typical hydrological settings in Northern Switzerland today provides a basis for understanding what may happen in the future and is discussed in Nagra (2024g).

The speciation of ^{14}C compounds initially present in deep groundwater systems may change as it enters and passes through the local shallow aquifer due to changes in geochemical conditions compared to deep groundwater. There is also potential for microbial processes to oxidise $^{14}C_{org}$ (dissolved $^{14}CH_4$ and small ^{14}C organics) and $^{14}C_{vol}$ ($^{14}CH_4$) to $^{14}C_{inorg}$ ($^{14}CO_2$) in the oxygenated conditions of the local shallow aquifer (Ward et al. 2017) or in oxygenated soils and sediments (Shaw & Thorne 2016). Once in near-surface aquifers, $^{14}C_{inorg}$ ($^{14}CO_2$ and ^{14}C bicarbonate dissolved in solution) is therefore expected to be predominantly present.

Volatile ^{14}C-bearing compounds may also degas as salinity, pressure and temperature change at mixing zones of deep groundwater with near-surface groundwater. At the water table, ^{14}C that outgases from near-surface groundwater may diffuse upward toward the soil atmosphere.

As ^{14}C passes through the local shallow aquifer, unsaturated zone, sediments and deeper soils, its transport will be retarded (held back) to some extent due to retention in the solid phase of the materials through which the groundwater or soil water passes, but the retardation remains difficult to model. Compared with other elements, the degree of retention of dissolved organic carbon can be expected to be minor. The degree of retention of dissolved inorganic carbon being influenced by factors such as the amount of calcium carbonate available for isotopic exchange and its associated solubility limit, which are both affected by the hydrogeochemistry (Hoch et al. 2016a; Sheppard et al. 1998).

Upon discharge to surface water, ^{14}C originating in shallow groundwater will disperse further and pass downstream. There may be some potential for ^{14}C to accumulate in aquatic bed sediments. Periods of high river flow rate in Northern Switzerland mean that finer sediments tend to get carried down-stream (Nagra 2024g), so potential for organic matter accumulation in riverbed sediments is limited if compared with the accumulation potential in agricultural soils. Depending on local conditions, there is also potential for groundwater carbon, including ^{14}C, to return to the atmosphere through CO_2 degassing in the vicinity of groundwater discharge to surface water, where it could be rapidly dispersed (Deirmendjian & Abril 2018) and to degas further downstream from the river water surface to the atmosphere.

Dissolved ^{14}C may reach soils with natural groundwater discharge, or due to irrigation with groundwater or surface water. Irrespective of the pathway to reaching the soil, concentrations of $^{14}CO_2$ in soil water and soil gas will equilibrate relatively quickly (Knoche 1980). In contrast, $^{14}CH_4$ is likely to remain largely in the gas phase in soils until it is oxidised to $^{14}CO_2$ by microbial processes. Field experiments have shown that CH_4 released to agricultural soils as gas can be completely oxidised by microbes to CO_2 over a length scale of a few tens of centimetres (Hoch 2014).

There is potential for ^{14}C in irrigation water to degas into the atmosphere; this may be limited for spray irrigation events, during which the water would only be airborne for a matter of seconds but will happen to a greater extent from irrigation water that is intercepted on the surfaces of plants and from the soil surface.

The extent to which ^{14}C reaching soils may be taken up by plants and animals and enter the human food chain is an important factor in understanding its behaviour in the biosphere. Aside from oxidation by methanotrophic microbes, CH_4 has limited interactions with organisms, whereas CO_2 is largely taken up by plants and assimilated into carbohydrates via photosynthesis, which forms a key step in the carbon cycle.

Soil gases will reach the plant canopy atmosphere above the soil by diffusion and through exchanges resulting from changes in atmospheric pressure. Air from the plant canopy atmosphere will then exchange with the above-canopy atmosphere. Although average wind speed profiles demonstrate a logarithmic decline towards the ground and vegetation surface, turbulent mixing driven by the rate of airflow extends into plant canopies (Fig. 5-2), which means that soil gases are subject to significant dispersion upon release from the soil surface (Foken et al. 2017). The areal extent of gaseous ^{14}C release from the soil will determine the degree of dilution in the above-canopy atmosphere, which acts as a boundary condition for the vertical concentration profile within the plant canopy.

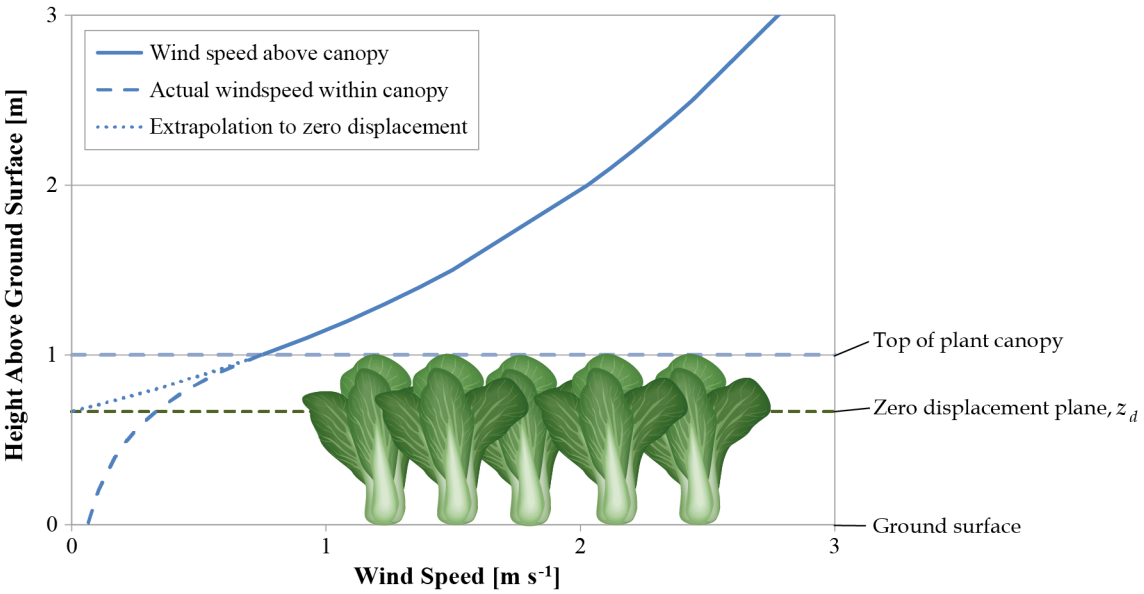

Fig. 5-2: Schematic illustration of wind speed above and within a plant canopy

From Walke & Thorne (2023).

This illustrates that the 'zero-displacement plane' is characterised by an extrapolation of the logarithmic decline of the above canopy wind speed. The zero-displacement plane does not characterise actual wind speed within the plant canopy. Although wind speed continues to decline within the plant canopy, turbulent mixing extends much further than the height of zero displacement.

Plants have evolved to effectively take up CO_2 from the canopy atmosphere via stomata, from where it diffuses to the sites of photosynthesis and the associated carbon is assimilated into organic compounds. Some CO_2 dissolved in soil water may be taken up by plants roots and transported to leaves in the transpiration stream. There is, therefore, potential for some of the CO_2 taken up via plant roots to also be assimilated into organic matter via photosynthesis in the leaves (Hoch 2014, Majlesi et al. 2019). Although only a small fraction of plant carbon may be derived from root uptake, the significant degree of dilution of carbon in soil gas released to the canopy atmosphere means that, in favourable circumstances (Ota & Tanaka 2019), root uptake may be an important process in terms of ^{14}C assimilation by plants.

Once incorporated into photosynthate, carbon can be released back to the canopy atmosphere and/or soil as CO_2 from respiration or may be used in the production of biomass. The part incorporated in biomass may be consumed by people or animals, or it may ultimately be returned to the soil as dead organic matter. As dead organic matter degrades, it will release carbon back to soil solution and soil gas. Detailed models for the degradation of organic matter in soils have been developed (e.g., Coleman & Jenkinson 1996). Relevant timescales range from seasonal variations in organic matter input to hundreds to thousands of years for degradation of chemically and physically stabilised organic matter.

5.1.2 Approach to post-closure safety assessments

Consistent with biosphere modelling for radioactive waste disposal in other national programmes (Lindborg et al. 2022), Nagra employs a compartment modelling approach to simulate radionuclide migration and their fate in the biosphere with the following characteristics:

- stable environmental conditions (including climate) are represented, suitable for long-term agricultural use by humans, so environmental change is not explicitly modelled, although different biosphere conditions (climate and morphology, e.g., drained wetlands) are represented;
- processes that operate within the compartments can be explicitly represented, including radioactive decay/in-growth, changes in speciation (e.g., due to microbial activity), partitioning between solid and liquid phases (sorption/retention), and partitioning between liquid and gas phases;
- the processes by which the radionuclides may be transferred between compartments or out of the biosphere area are explicitly represented.

By assigning properties to the compartments and quantitatively defining the transfer, retention and conversion processes, radionuclide behaviour in the biosphere can be simulated, allowing environmental concentrations and fluxes to be calculated, thus providing a basis for exposure assessment (the latter being described in Section 5.2).

Nagra's modelling approach has been developed and refined over the past thirty years or more and is reflected in the current version of the SwiBAC code (Nagra 2024g), which is based on the AMBER compartment modelling code (Quintessa 2023). The compartment model forming the basis of SwiBAC, allows concentrations in the local shallow aquifer, unsaturated zone, soil, sediments and surface water to be calculated following radionuclide releases to the biosphere in deep groundwater. Compartments are taken to be relatively homogeneous, with their dimensions determined from the characteristics of typical valleys in Northern Switzerland and resource areas for potential exposure groups. Many biosphere processes, such as uptake into crops, occur on timescales that are short relative to timescales of potential radionuclide releases, such that concentrations in plants and animals reach an equilibrium with concentrations in their surrounding environment. This allows concentrations in plants and animals to be determined using equilibrium concentration ratios and transfer factors from the literature.

The SwiBAC code is used to model a range of radioisotopes of repository-derived elements that may enter the biosphere with deep groundwater in the very long term. However, carbon is an element that forms a fundamental component of biological systems, such that, while it may be carried around the biosphere with the movement of groundwater and solids (as for other radionuclides), its behaviour is also subject to additional processes, including having potential to be present to a significant degree in the gas phase and to be taken up and incorporated into the food chain via photosynthesis. So, special considerations apply to modelling the behaviour of ^{14}C in the biosphere such that an additional model is used. Additional features implemented for modelling ^{14}C in the biosphere include:

- the topsoil is explicitly distinguished into soil solution, soil gas and organic matter, with retention of ^{14}C on soil solids represented;
- the atmosphere above the soil surface is explicitly represented and distinguished into the plant canopy atmosphere and the air above the plant canopy; and
- plants are explicitly represented and distinguished into above-ground and below-ground components.

Many of the processes represented in SwiBAC are also relevant to carbon dynamics in the biosphere and ^{14}C is taken to behave in the same way as stable carbon in the biosphere. The same underlying compartment model can, therefore, be used for ^{14}C released to the biosphere in deep groundwater, with adaptation/extension to include the additional features and processes relevant to carbon. The speciation of ^{14}C in groundwater and surface water is not explicitly distinguished; all forms are represented as having some limited degree of sorption onto solids based on carbonate exchange.

Nagra's biosphere model for ^{14}C released in groundwater is illustrated in Fig. 5-3, including the processes relevant to moving carbon between the compartments. By parameterising the amount of stable carbon in each compartment, and the transfer rate of stable carbon between the compartments, the model delivers the transfer rates needed to simulate the behaviour of ^{14}C in the biosphere. The approach of modelling ^{14}C behaviour in the biosphere based on the dynamics and balance for stable carbon is consistent with that adopted in other programmes (e.g., Saetre et al. 2013).

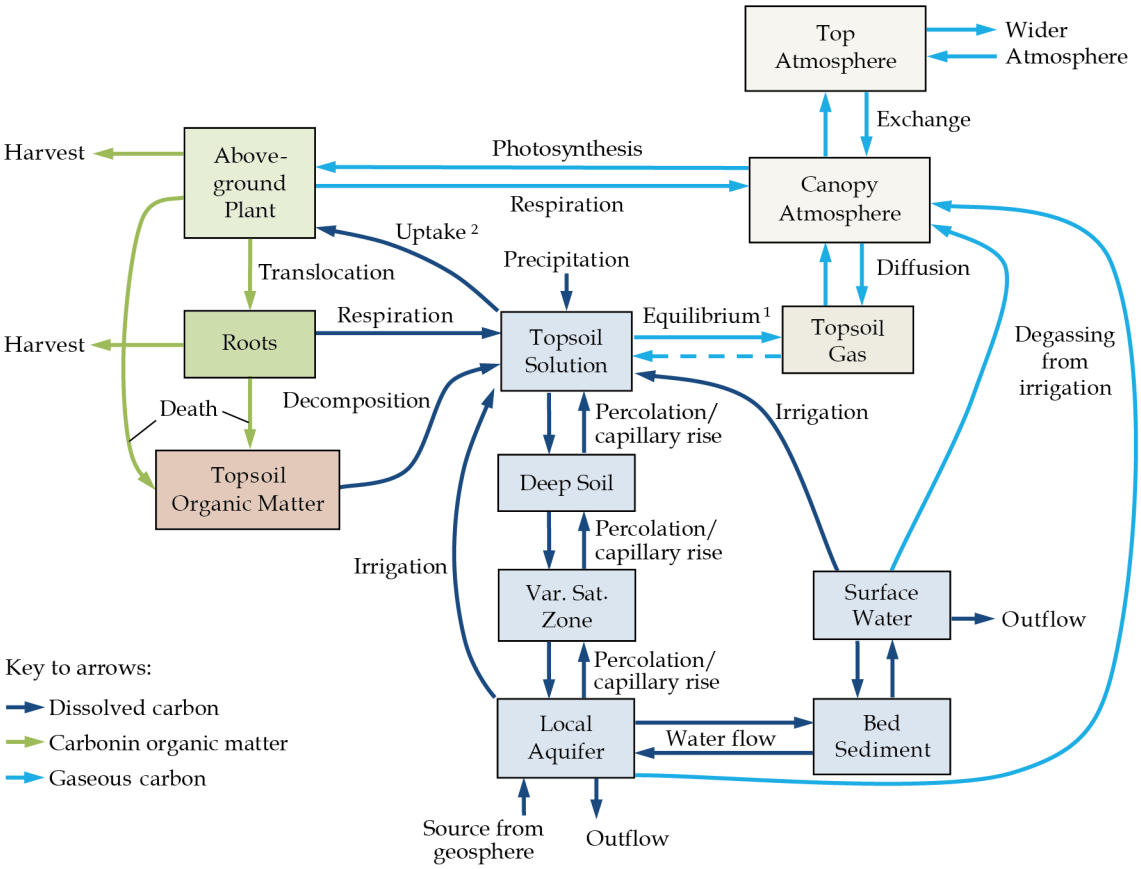

Fig. 5-3: Conceptualisation of Nagra's model for ^{14}C in the biosphere, which is based on stable carbon amounts and fluxes

From Walke & Thorne (2023) .

[1] Whilst conceptually carbon can be exchanged between the soil gas and solution, in practice release from the soil solution to soil gas is taken to dominate. [2] Carbon taken up from the topsoil solution by the plant for use in photosynthesis within the plant leaves is assumed not to interact with the roots. While, conceptually, potential for degassing from irrigation water intercepted on plant surface is recognised, it is parameterised as being zero in the modelling, as a conservative assumption.

Nagra's model for ^{14}C in the biosphere, therefore, enables the retention of ^{14}C in the different components of the surface and near-surface environment to be represented, taking account of the specific behaviour of carbon in the biosphere. The ^{14}C model is used to calculate parameter values that allow the retention of ^{14}C to be appropriately modelled in SwiBAC, including:

- the degree of sorption in the topsoil, taking account of retention in organic matter;
- the degree of loss from the topsoil to the atmosphere; and
- the degree of uptake by crops compared with the amount of ^{14}C in the soil.

This approach allows SwiBAC to adequately simulate the behaviour of ^{14}C alongside other radionuclides with potential to be released in the very long term. The resulting degree of retention and plant uptake modelled in SwiBAC is compared with that simulated by the ^{14}C model to build confidence and verify that its behaviour is appropriately captured.

SwiBAC is used to model other processes, including erosion, sediment movements, uptake from surface water by fish, and uptake from feed and drinking water by animals. SwiBAC is also used to model exposure rates to potentially exposed individuals (cf. Section 5.2).

Because carbon is a fundamental component of a wide variety of biogeochemical processes, its transport in the environment covers a wide range of timescales, from a few seconds for turbulent mixing in the plant canopy to hundreds of years for carbonate exchange in the local shallow aquifer. Not all of these processes need to be represented in the ^{14}C model, but judgements must be made as to which can be treated as being in equilibrium and which must be represented kinetically (e.g., in a compartment model). These judgements also need to be informed by the approach to assessing potential radiological exposures (cf. Section 5.2), bearing in mind that the focus tends to be on annual average effective doses. Variations on shorter than annual timescales are thus typically treated as being in equilibrium, using suitable time-averages for the parameters adopted, whereas longer-term variations are treated kinetically (though the rate constants adopted may themselves be time-averaged values).

For a constant rate of release of ^{14}C in groundwater to the near surface, concentrations will reach an equilibrium on timescales reflecting the rate of processes affecting the migration and turnover of carbon in the biosphere. Exchange between carbon dissolved in groundwater and that in the solid phase of the local shallow aquifer is the slowest process represented and has a characteristic time scale of hundreds of years, such that equilibrium is reached in the biosphere on a time scale approaching 1,000 years. This timescale is short relative to the period of interest (several tens of thousands of years) and the expected time scale of potential ^{14}C releases to the near-surface environment from the repository system (cf. Chapter 4). Assessment of ^{14}C exposures based on distributions in the biosphere that reflect long-term equilibrium provide an appropriate metric for comparison with dose constraints (cf. Section 5.2). Assessment of ^{14}C migration in the biosphere, therefore, aims to determine appropriate equilibrium concentrations for a constant release rate to the biosphere; calculations are undertaken for different climate conditions, which are reflected in hydrology and, therefore, have potential to affect the behaviour of ^{14}C.

Irrespective of whether processes are treated by equilibrium or kinetic approaches, it is important to recognise and represent the uncertainty relating to both our conceptual understanding of those processes and their parameterisation. Fortunately, the wealth of literature on the behaviour of stable carbon and its isotopes in the environment means that conceptual uncertainty in the key processes is limited and that extensive data are available for model parameterisation (Thorne et al. 2023).

Some uncertainties relating to ^{14}C behaviour in the biosphere are managed through making conservative or pessimistic assumptions, to help ensure that potential dose consequences are not underestimated. For example, 100% of $^{14}C_{vol}$ reaching the topsoil (e.g., in irrigation water) is assumed to be oxidised to $^{14}C_{inorg}$. This is conservative because the $^{14}C_{inorg}$ is then fully available for uptake by plants and ingestion of crops and animal products contaminated by uptake of ^{14}C are the main potential exposure pathways (cf. Section 5.2). Potential for ^{14}C in irrigation water (a key pathway to agricultural soils) to be lost to the atmosphere via degassing and isotopic exchange is recognised conceptually in Fig. 5-3, but conservatively parameterised as being zero in the modelling. Potential for ^{14}C to be lost via exchange between surface water and the atmosphere is similarly conservatively ignored. Plant characteristics for uptake by fruit are based on a low canopy height, more analogous to crops like strawberries rather than fruit trees; this is pessimistic because the height and degree of dispersion within fruit tree canopies would be significantly greater and would result in a lower degree of ^{14}C uptake after release to the plant canopy atmosphere.

5.1.3 International approach

The behaviour of ^{14}C in the biosphere is important to many types of radiological safety assessments, including those carried out relating to operational discharges from nuclear facilities as well as to potential discharges from radioactive waste disposal (Thorne et al. 2023). As a result, there have been many studies of its behaviour in the biosphere following discharge/release as well as international collaborative work to share understanding and help improve and refine assessment modelling (Bird 1996; IAEA 2012; Thorne et al. 2023).

Discussion of ^{14}C modelling in the soil-plant-atmosphere system and comparison of modelling approaches within the BIOPROTA international collaborative forum have contributed to improvements in modelling plant uptake, which contributes to ingestion exposures. In the past, assessment models conservatively treated much of the plant canopy atmosphere as being diffusively dominated. In practice, and in standard micrometeorological modelling, turbulent mixing with the above canopy atmosphere extends to close to the ground surface. Improved representation of the behaviour of ^{14}C between the soil, plant and atmosphere has led to reductions in the degree of accumulation in plants. Comparison with observational data has then helped build confidence in the updated models for plant uptake from the atmosphere (Limer et al. 2017).

Field research into the behaviour of ^{14}C released to soils formed part of an integrated project looking to improve operational and post-closure safety assessments relating to geological disposal of higher activity radioactive waste in the UK. The research confirmed that CH_4 released to soils can be effectively oxidised to CO_2 within agricultural soils (Hoch et al. 2014).

With accumulation in mire peat being important to the site context for assessments of shallow geological disposal of L/ILW and deep geological disposal of SF in Sweden, SKB place carbon balance modelling at the heart of post-closure biosphere modelling (Saetre et al. 2013, Avila et al. 2010). This includes explicit modelling of carbon uptake and retention in plants and animals.

These developments and wider discussion of ^{14}C behaviour in the biosphere and associated assessment within the BIOPROTA international collaborative forum have led to improvements in assessment models over the past decade. These improvements are reflected for the RBG in Nagra's post-closure safety assessments.

5.2 Radiation exposure of potentially exposed groups

5.2.1 State of knowledge

^{14}C decays to stable ^{14}N via beta decay, with a half-life of 5,700 years. Energy emitted during the decay of ^{14}C incorporated in the body will deliver a radiation dose to tissues. Such a dose results in a risk of inducing cancer or other health effects. Radiation exposure can occur externally, as ^{14}C reaching surface soil (e.g., in irrigation water) decays and emits radiation that results in exposure to nearby individuals. Alternatively, it can occur internally, if ^{14}C is ingested with water and food, via inadvertent ingestion of soil (e.g., as soil contamination of foods) or inhaled as gas or bound to dust particles in the air. However, because of the low energy of the beta emissions from ^{14}C decay, external exposure is seldom of relevance. Radiation exposure is measured as effective dose in Sieverts (Sv).

The International Commission on Radiological Protection (ICRP) has set out general principles for the disposal of long-lived solid radioactive waste (ICRP 1998; ICRP 2013). More details of how the biosphere should be addressed in post-closure safety assessments is given in the enhanced BIOMASS assessment methodology developed under Phase II of the IAEA MODARIA Programme (Lindborg et al. 2022).

The ICRP also provides effective dose per unit intake values for various forms of carbon, and these provide the basis for the values given in the Swiss Radiological Protection Ordinance (RPO) (ICRP 2012), which are reproduced in Tab. 5-1. A notable area of pessimism relates to uncertainty concerning the effective dose coefficients associated with intake of ^{14}C (Thorne et al. 2023). The ICRP is in the process of updating its biokinetic modelling for ^{14}C, with the expectation that the revised dose coefficient for ingestion will be about 30% of the current value (Harrison & Leggett 2016). Furthermore, the ingestion dose coefficient assumes complete absorption of carbon following ingestion. This assumption is appropriate to ^{14}C incorporated into foods, but is pessimistic for ^{14}C in drinking water, in which ^{14}C may be present primarily as dissolved CO_2 or dissolved bicarbonate/carbonate. Although transfer across the gut may be close to complete for these forms, almost all the ^{14}C will subsequently be lost through exhalation as CO_2 without first having been metabolised and incorporated into body tissues (i.e., before being able to deliver much of the effective dose accounted for by the ingestion dose coefficient). It is estimated that a more realistic effective dose coefficient for ^{14}C in drinking water in bicarbonate form would be about a factor of 40 lower than the current value (Harrison & Leggett 2016). Effective dose coefficients for ingestion and inhalation are complemented by those for external irradiation, which are available from US Environment Protection Agency (EPA 2019) guidance and are expressed as Sv/a per Bq/m^3 in the soil.

Tab. 5-1: Effective dose coefficients for ^{14}C from the Swiss RPO

From (KEV 2004). Values based on ICRP (2012).

Exposure pathway	Value in RPO	Note
Inhalation	5.8×10^{-10} Sv/Bq	Based on inhalation of particulate organic ^{14}C (e.g., in particulate dust resuspended from soil).
Ingestion	5.8×10^{-10} Sv/Bq	Assumes 100% absorption from the gastrointestinal tract.

Given that ^{14}C occurs naturally in the environment, it contributes a fraction of natural background radiation exposure. In Switzerland, the average natural background exposure rate from all radionuclides and from external exposure is in the range of approximately 1 to 14 mSv/a (ENSI 2023). ENSI (2023) refer to a period of assessments of up to one million years, during which assessed doses should remain below 0.1 mSv/a, representing a small fraction of the natural background exposure rate (Nagra 2024j). The rate of release of any ^{14}C reaching the biosphere from geological disposal can be expected to change slowly over the time scale of a human lifetime, such that annual average doses to adults, representative of the more highly exposed individuals in a population, provide an adequate basis for comparison with the dose constraint, consistent with recommendations in ICRP (2013). Assessments consider individuals of potentially exposed groups representative of the more highly exposed individuals in the population. The habits and characteristics assumed for the individuals are chosen on the basis of reasonably conservative and plausible assumptions.

5.2.2 Approach to post-closure safety assessments

Nagra's biosphere assessment focuses on the geographical area local to potential contaminant releases, where radionuclide concentrations would be at their highest (cf. Section 5.1). Attention is focused on releases to valleys likely to receive direct deep groundwater discharges (in contrast, lakes are typically underlain by impermeable sediments). The assessment is based on self-sufficient agricultural systems, for which the range of potential exposure pathways is greatest and where people may make maximal use of local food and water resources (Nagra 2024g). The exposure pathways considered in Nagra's biosphere assessment are shown in Fig. 5-4.

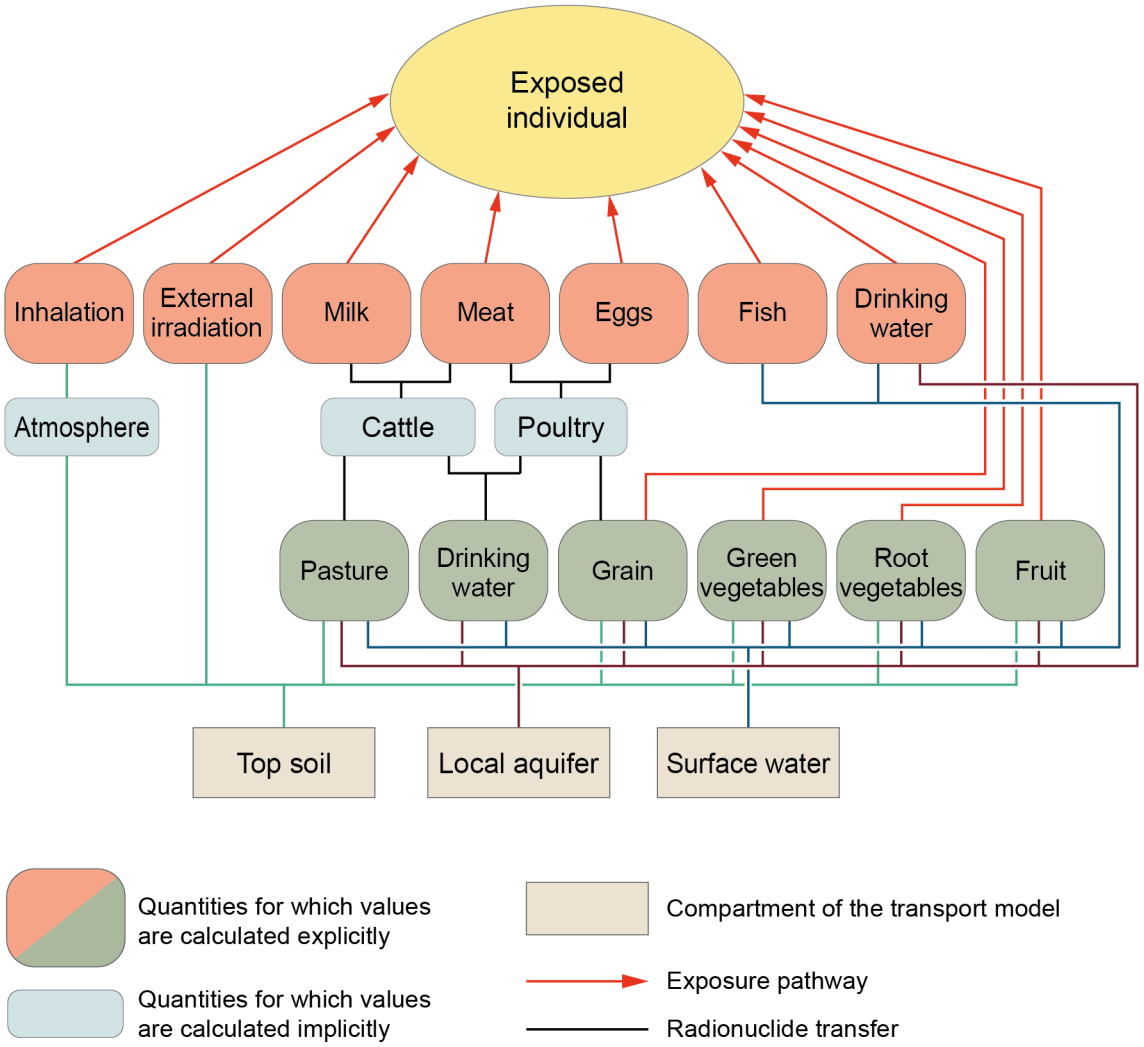

Fig. 5-4: Potential exposure pathways included in Nagra's biosphere modelling

From Nagra (2024g).

A single potential exposure group is considered. To ensure that they are representative of the more highly exposed individuals in the population, pessimistic assumptions are used in defining their habits, including an assumption that they are self-sufficient and draw maximally on locally, potentially contaminated food and water. On this basis, they are assumed to:

- spend 100% of their time in the biosphere area receiving ^{14}C contaminated deep groundwater;
- obtain 100% of their drinking water from a groundwater well within the shallow local aquifer receiving ^{14}C contaminated deep groundwater;
- consume 100% of their crops and animal produce from that grown or reared within the biosphere area; and
- consume fish from a local river receiving the shallow groundwater discharge.

As described above, the SwiBAC code models the migration and retention of ^{14}C in the biosphere and delivers calculated concentrations in the local shallow groundwater, surface water, surface soil, atmosphere, crops, animal produce and fish. SwiBAC also calculates total potential effective dose rates to the potential exposure group by combining the concentrations with exposure group habits (occupancies, ingestion rates, inhalation rates) and the recommended ingestion, inhalation and external dose coefficients.

SwiBAC provides the effective dose rate for ^{14}C (Sv/a) for a constant unit release rate of ^{14}C in groundwater to the local shallow aquifer (Bq/a). The dynamics of the biosphere model (especially retention within the local shallow aquifer) mean that an equilibrium is reached between a constant radionuclide release rate in groundwater to the biosphere and the resulting effective dose rate after a period of about 1,000 years (cf. Section 5.1). The effective dose rate at equilibrium per unit release rate to the biosphere is then used as a biosphere dose conversion factor (BDCF, Sv per Bq) for deep groundwater-mediated ^{14}C input to the biosphere. Input of ^{14}C originating in the deep geological repository is expected to occur over a protracted period, such that use of a BDCF is reasonable and not overly pessimistic. In this way, doses to a person representative of the potentially exposed group are evaluated by simply multiplying the calculated ^{14}C release rate to the biosphere (Bq/a) by the BDCF.

The overall workflow calculating effective dose rates for ^{14}C is illustrated in Fig. 5-5.

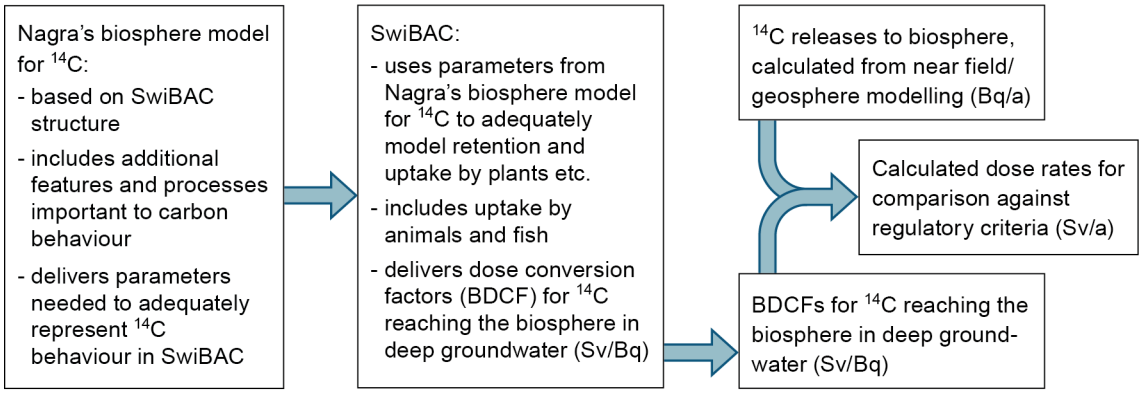

Fig. 5-5: Workflow showing how Nagra's model for ^{14}C in the biosphere is used

From Nagra (2024g).

Assessments are made on the pessimistic assumption that 100% of the radionuclides reaching the biosphere in deep groundwater (including ^{14}C) are discharged to a single biosphere area with dimensions ca. 2.3 km^2. Retention, dispersion and degassing within the pathway from depth to the near surface are conservatively disregarded.

On the basis of modelling the behaviour of ^{14}C in the biosphere described in Section 5.1.2 and assessing potential exposures, as described above, the BDCF for ^{14}C released to the near surface in groundwater is 3.6×10^{-16} Sv/Bq for reference (equivalent to present-day) climate conditions. The main contributions arise from ingestion of animal produce (49%), drinking water (29%) and irrigated crops (20%).

In addition to a reference case, biosphere modelling includes consideration of alternative conditions, exploring alternative biosphere configurations and climate conditions (Nagra 2024g). The alternative conditions affect dynamics within the biosphere and the range of potential exposure pathways that are relevant and, therefore, affect calculated BDCFs.

- The BDCF for groundwater releases to an area of former wetland that has been drained for agriculture are about a factor of 0.4 lower than the reference case, at 2.2×10^{-16} Sv/Bq.
- The BDCF for a warmer-drier climate, which requires a higher rate of irrigation, is about a factor of 2.6 higher than the reference case, at 9.24×10^{-16} Sv/Bq.
- The BDCF for cold climate conditions, which may arise in the very long term as a result of glacial-interglacial climate cycling, is about a factor of thirty-six lower than the reference case, at 1.0×10^{-17} Sv/Bq.

Given the possibility for degassing of ^{14}C reaching the local shallow aquifer from depth, a side calculation has been explored in which the source term is directed to the topsoil rather than the local aquifer; i.e., equivalent to 100% of the ^{14}C degassing and reaching the topsoil without delay or retardation. In this situation, the BDCF for ^{14}C would be a factor of 2.8 higher for reference conditions, which is taken as a bounding case.

As with modelling the behaviour of ^{14}C in the biosphere (cf. Section 5.1), much is understood about potential uptake of ^{14}C and associated exposures. Assessment of doses to humans representative of more highly exposed individuals provides some confidence that results are not underestimated. Indeed, the assumption of a completely self-sufficient lifestyle in the reference case is particularly pessimistic in comparison with present-day habits.

5.2.3 International approach

Assessment of ^{14}C doses remains a topic of interest to radioactive waste management organisations and is the subject of ongoing international workshops and collaborative studies including, for example, those undertaken through the BIOPROTA international collaborative forum (e.g., Thorne et al. 2023). Informed by these studies, Nagra's approach to representing ^{14}C in exposure assessments has been maintained to be consistent with the latest modelling by other radioactive waste management organisations.

When the updated ICRP recommendations are finalised, then it is notable that BDCFs for ^{14}C will be reduced by about 70% compared to the above, consistent with the expected reduction in the recommended ingestion dose coefficient.

6 Conclusions

^{14}C is a key volatile radionuclide that can be released from a deep geological repository for radioactive waste. Hence, the potential radiological impact of ^{14}C is reassessed for the radiological consequence analyses in the framework of RBG documentation. This report provides, based on the current scientific understanding, the basis for radiological consequence for ^{14}C from its source term via its mobilisation from the emplaced radioactive waste to its migration within the repository system, host rock and confining units and its release to the biosphere, including the potential exposure of humans to ^{14}C. This study especially includes:

- The estimation of the ^{14}C content of individual waste package types, notably from activation measurements and calculations;
- The determination of ^{14}C speciation and rate of release from the ^{14}C-carrying materials both emplaced in the L/ILW and HLW disposal sections;
- The development of a modelling approach for the migration of ^{14}C in both dissolved and gaseous forms along the repository structures and through the CRZ, taking gas pressure and thermal processes explicitly into account;
- The assessment of transport of ^{14}C within deep groundwater systems that pass through the geological siting regions, while acknowledging that the provisional design of shafts and other underground structures are site-specific;
- The refinement of the biosphere model for the ^{14}C release to the biosphere and assessment of ^{14}C radiation exposure by integrating the behaviour of ^{14}C in the canopy layer of agricultural systems and updating BDCFs according to regulatory requirements, respectively.

Compared to previous safety assessments for deep geological repositories, the treatment of ^{14}C in the post-closure safety assessment for the RBG is more detailed, taking account of recent scientific knowledge based on experimental data. In particular, it is less conservative in terms of the ^{14}C inventory and source term and more realistic regarding ^{14}C migration in the geological environment, as ^{14}C compounds released both in liquid and gas phases are considered. Nagra's approach is generally in line with other disposal programmes, based on a similar knowledge base. Differences relate primarily to the waste inventory, repository concept, WMO-specific factors relating to the stage of the programme/purpose of the post-closure safety assessments, and interpretation of some of the less well-understood scientific results.

7 References

Abrahamsen, L., Arnold, T., Brinkmann, H., Leys, N., Merroun, M., Mijnendonckx, K., Moll, H., Polvika, P., Ševců, A., Small, J., Vikman, M. & Wouters, K. (2015): A review of anthropogenic organic wastes and their degradation behaviour. MIND D1.1.

Andra (2005): Référentiel de comportement des colis de déchets à haute activité et à vie longue. Andra Technical Report C.RP.ASCM.04.0017.A. Andra, Paris.

Aomi, M., Baba, T., Miyashita, T., Kamimura, K., Yasuda, T., Shinohara, Y. & Takeda, T. (2008): Evaluation of hybride reorientation behavior and mechanical properties for high-burnup fuel Cladding Tubes in Interim Dry Storage. Journal of ASTM International 5/9, 1-21. DOI: 10.1520/JAI101262.

Avila, R., Ekström, P.-A. & Åstrand, P.-G. (2010): Landscape dose conversion factors used in the safety assessment SR-Site. Technical Report TR-10-06. Swedish Nuclear Fuel and Waste Management SKB, Stockholm.

BFE (2008): Sachplan Geologische Tiefenlager: Konzeptteil. BFE 2. April 2008 (Revision vom 30. November 2011). Departement für Umwelt, Verkehr, Energie und Kommunikation UVEK, Bern.

Bird, G. (1996): Validation test for carbon-14 migration and accumulation in a Canadian shield lake. BIOMOVS II Technical Report TR14. BIOMOVS II Steering Committee, Stockholm.

Bourgeois, M. (2000): Retraitement du combustible. Principales opérations. Génie nucléaire, BN3650-1. DOI: 10.51257/a-v1-bn3650.

Bradley, M.J. & Ferris, L.M. (1962): Hydrolysis of uranium carbides between 25 and 100°. I. Uranium monocarbide. Inorganic Chemistry 1/3, 683-687. DOI: 10.1021/ic50003a047.

Bucur, C., Florea, I., Reiller, P.E. & Dumitrescu, D. (2018): ^{14}C content in candu spent fuel ion exchange resins and its release under alkaline conditions. Radiocarbon 60/6, 1797-1808. DOI: 10.1017/RDC.2018.83.

Caes, S., Druyts, F. & Thomas, P. (2018): Release and speciation of carbon from Zircaloy-4 in anaerobic and highly alkaline conditions: Comparison of simple immersion and potentiostatic corrosion tests. Radiocarbon 60/6, 1787-1796. DOI: 10.1017/RDC.2018.105.

Cloet, V., Lothenbach, B., Lura, P., Kosakowski, G., Curti, E., Wieland, E., Lanyon, G.W., Diomidis, N. & Leupin, O.X. (2019): Cementitious backfill for a high-level waste repository: Impact of repository-induced effects. Nagra Arbeitsbericht NAB 18-41.

Cloet, V., Schwyn, B. & Wieland, E. (2014): Geochemische Nahfeld-Daten zu den SMA und ATA für die provisorischen Sicherheitsanalysen in SGT Etappe 2. Nagra Arbeitsbericht NAB 14-52 Rev. 1.

Coleman, K. & Jenkinson, D.S. (1996): RothC-26.3 - A Model for the turnover of carbon in soil. *In:* Powlson, D.S. (ed.): Evaluation of Soil Organic Matter Models. Using Existing Long-Term Datasets. (NATO ASI Series, 38). Springer, Berlin, Heidelberg, 237-246.

Curti, E. (2022): Aqueous Corrosion of Vitrified Nuclear Waste: Current Process Understanding, Literature Review and Recommended Rates. Nagra Arbeitsbericht NAB 23-09. Nagra, Wettingen, Switzerland.

Cvetković, B.Z., Salazar, G., Kunz, D., Szidat, S., Wieland, E., Rothardt, J., Büttler, A. & Schlotterbeck, G. (2018a): Formation of low-molecular-weight organic compounds during anoxic corrosion of zero-valent iron. Environmental Engineering Science 35/5, 447-461. DOI: 10.1089/ees.2017.0216.

Cvetković, B.Z., Salazar, G., Kunz, D., Tits, J., Szidat, S. & Wieland, E. (2018b): Quantification of dissolved organic ^{14}C-containing compounds by accelerator mass spectrometry in a corrosion experiment with irradiated steel. Radiocarbon 60/6, 1711-1727. DOI: 10.1017/RDC.2018.90.

Deirmendjian, L. & Abril, G. (2018): Carbon dioxide degassing at the groundwater-stream-atmosphere interface: Isotopic equilibration and hydrological mass balance in a sandy watershed. Journal of Hydrology 558, 129-143. DOI: 10.1016/j.jhydrol.2018.01.003.

Dey, R., Sarkar, T., Subramanian, C., Anand, S., Singh, K.D. & Kulkarni, M.S. (2020): Temporal evolution of activation products in a Zircaloy-4 guide tube and the estimation of its external gamma dose rate for decommissioning activities. Journal of Radiological Protection 40/1, 197-214. DOI: 10.1088/1361-6498/ab55c9.

Diomidis, N., Guillemot, T. & King, F. (2023): Definition of Reference Corrosion Rates for Performance and Safety Assessments. Nagra Arbeitsbericht NAB 23-22. Nagra, Wettingen, Switzerland.

Druyts, F., Caes, S. & Thomas, P. (2018): Carbon-14 release and speciation from carbon steel in highly alkaline conditions. Radiocarbon 60/6, 1683-1690. DOI: 10.1017/RDC.2018.92.

EMRAS (2012): A summary report of the results of the Environmental Modelling for Radiation Safety (EMRAS) Programme (2003-2007). IAEA-TECDOC-1678. IAEA.

ENSI (2010): Sicherheitstechnisches Gutachten zum Vorschlag geologischer Standortgebiete. Sachplan geologische Tiefenlager, Etappe 1 ENSI 33/070. Eidgenössisches Nuklearsicherheitsinspektorat ENSI, Brugg.

ENSI (2017): Sicherheitstechnisches Gutachten zum Vorschlag der in Etappe 3 SGT weiter zu untersuchenden geologischen Standortgebiete. Sachplan geologische Tiefenlager, Etappe 2 ENSI 33/540. Eidgenössisches Nuklearsicherheitsinspektorat ENSI, Brugg.

ENSI (2018): Präzisierungen der sicherheitstechnischen Vorgaben für Etappe 3 des Sachplans geologische Tiefenlager. Sachplan geologische Tiefenlager, Etappe 3. ENSI 33/649. Eidgenössisches Nuklearsicherheitsinspektorat ENSI, Brugg.

ENSI (2020a): Geologische Tiefenlager. Erläuterungsbericht zur Richtlinie ENSI-G03/d. Eidgenössisches Nuklearsicherheitsinspektorat ENSI, Brugg.

ENSI (2020b): Geologische Tiefenlager. Richtlinie für die schweizerischen Kernanlagen ENSI-G03/d. Eidgenössisches Nuklearsicherheitsinspektorat ENSI, Brugg.

ENSI (2023): Geologische Tiefenlager. Ausgabe Dezember 2020 (Änderung vom 1. November 2023). Richtlinie für die schweizerischen Kernanlagen ENSI-G03/d. Eidgenössisches Nuklearsicherheitsinspektorat ENSI, Brugg.

EPA (2019): External Exposure to Radionuclides in Air, Water and Soil. External Dose Rate Coefficients for General Application EPA-402/R19/002, Federal Guidance Report 15. Environmental Protection Agency EPA, Washington, D.C.

Evans, J.C., Lepel, E.L., Sanders, R.W., Wilkerson, C.L., Silker, W., Thomas, C.W., Abel, K.H. & Robertson, D.R. (1984): Long-Lived Activation Products in Reactor Materials. NUREG/CR-3474.

FEPC & JAEA (2007): Second progress report on research and development for TRU waste disposal in Japan. JAEA-Review 2007-010, FEPC TRU-TR2-2007-01.

Ferrari, H.M. (1963): Nitrogen release from UO_2 pellets at elevated temperatures. Nuclear Science and Engineering 17/4, 503-512. DOI: 10.13182/NSE63-A18440.

Foken, T., Nappo, C.J. & Klein, P. (2017): Micrometeorology. 2nd ed. Springer, Berlin, Germany.

Gegg, L., Kuster, A.M., Deplazes, G., Madritsch, H. & Buechi, M.W. (2019): Quaternary Borehole QBO Gebenstorf-Brüel (QGBR). Nagra Arbeitsbericht NAB 19-02.

Giroud, N., Tomonaga, Y., Wersin, P., Briggs, S., King, F., Vogt, T. & Diomidis, N. (2018): On the fate of oxygen in a spent fuel emplacement drift in Opalinus Clay. Applied Geochemistry 97, 270-278. DOI: 10.1016/j.apgeochem.2018.08.011.

González-Robles, E., Metz, V., Wegen, D.H., Herm, M., Papaioannou, D., Bohnert, E., Gretter, R., Müller, N., Nasyrow, R., Weerd, W. de, Wiss, T. & Kienzler, B. (2016): Determination of fission gas release of spent nuclear fuel in puncturing test and in leaching experiments under anoxic conditions. Journal of Nuclear Materials 479, 67-75. DOI: 10.1016/j.jnucmat.2016.06.035.

Gras, J.-M. (2014): State of the art of ^{14}C in Zircaloy and Zr alloys. ^{14}C release from zirconium alloy hulls. CAST Deliverable D3.1. European Union EU, Brussels.

Grenthe, I., Gaona, X., Plyasunov, A.V., Rao, L., Runde, W.H., Grambow, B., Konings, R.J.M., Smith, A.L. & Moore, E.E. (2020): Second update on the Chemical Thermodynamics of Uranium, Neptunium, Plutonium, Americium And Technetium. (Chemical Thermodynamics, 14). Edited by Ragoussi M.-E., J.S. Martinez & D. Costa. Nuclear Energy Agency of the OECD NEA, Boulogne-Billancourt.

Guillemot, T., Kunz, D., Salazar, G., Rauber, M., Szidat, S. & Wieland, E. (2021): Long-term monitoring of dissolved and gaseous C-14 bearing carbon compounds during anoxic alkaline corrosion of irradiated steel. Nagra Arbeitsbericht NAB 21-26. Nagra, Wettingen, Switzerland.

Guillemot, T., Salazar, G., Rauber, M., Kunz, D., Szidat, S. & Wieland, E. (2022): Carbon-14 release and speciation during corrosion of irradiated steel under radioactive waste disposal conditions. Science of the Total Environment 817, 152596. DOI: 10.1016/j.scitotenv.2021.152596.

Guillemot, T., Wieland, E., Mosberger, L. & Warthmann, R. (2023): Degradation of Organic Materials in a L/ILW Repository. Nagra Technical Report NTB 23-11.

Hall, G.R., Klaschka, J.T., Nellestyn, A. & Streat, M. (1970): Thermal stability of ion exchange resins. *In:* SCI (ed.): Ion exchange in the process industries: papers read at the conference held at Imperial College of Science and Technology. London, July 16-18, 1969 with discussions that followed. Society of Chemical Industry SCI, London, 62-70.

Harrison, J.D. & Leggett, R.W. (2016): Appropriate selection of dose coefficients in radiological assessments: C-14 and Cl-36: Response to the letter of G Smith and M Thorne (2015, Journal of Radiological Protection 35, 737-40). Journal of Radiological Protection 36/2, 388-390. DOI: 10.1088/0952-4746/36/2/388.

Heikola, T. & Ollila, K. (2018): Release and speciation of carbon from stainless steel under mildly and highly alkaline, reducing conditions. CAST Deliverable D2.9. European Union EU, Brussels.

Hélie, M. (2004): Dossiers de synthèse sur le comportement à long terme des colis: Dossier de référence phénoménoligique CSD-C 2004. CEA Technical Report Réf. RT DPC/SCCME 04-685-A. Commissariat à l'Énergie Atomique CEA, Paris.

Hesböl, R., Puigdomenech, I. & Evans, S. (1990): Source terms, isolation and radiological consequences of carbon-14 waste in the Swedish SFR repository. SKB Technical Report TR 90-02. Swedish Nuclear Fuel and Waste Management SKB, Stockholm.

Hoch, A.R. (2014): Uptake of Gaseous Carbon-14 in the Biosphere: Development of an Assessment Model. AMEC Report NPO004437, AMEC/004041/007, Issue 2. Radioactive Waste Management RWM, Oxfordshire.

Hoch, A.R., Lever, D. & Shaw, G.G. (2014): Uptake of Carbon-14 in the Biosphere: Summary Report. AMEC Report NPO004437, AMEC/004041/008, Issue 2. Radioactive Waste Management RWM, Oxfordshire.

Hoch, A.R., Rochelle, C.A., Humphreys, P.N., Lloyd, J.R., Heath, T.G. & Thatcher, K.E. (2016a): Carbon-14 Project Phase 2 – Formation of a Gas Phase and its Migration. AMEC Report RP50, AMEC/200047/007, Issue 1. Radioactive Waste Management RWM, Oxfordshire.

Hoch, A.R., Swift, B., Smart, N. & Smith, P. (2016b): Gas Generation from HLW and Spent Fuel. AMEC Report NPO004726, AMEC/005126/001, Issue 4. Radioactive Waste Management RWM, Oxfordshire.

Holocher, J., Mayer, G., Namar, R., Siegel, P., Hubschwerlen, N. & Colenco, A.-F. (2008): VPAC - a numerical model for groundwater flow and radionuclide transport. Nagra Arbeitsbericht NAB 08-05.

Houghton, R.A. (2003): 8.10 – The Contemporary Carbon Cycle. *In:* Schlesinger, W.H. (ed.): Biogeochemistry. (Treatise on Geochemistry, 8). Elsevier, Amsterdam, 473-513.

HSK (2000): Anforderungen der HSK an das Projekt eines Lagers für schwach- und mittelaktive Abfälle (SMA) am Wellenberg. HSK 30/15. Hauptabteilung für die Sicherheit der Kernanlagen HSK, Villigen.

HSK (2005): Gutachten zum Entsorgungsnachweis der Nagra für abgebrannte Brennelemente, verglaste hochaktive sowie langlebige mittelaktive Abfälle (Projekt Opalinuston). HSK 35/99. Hauptabteilung für die Sicherheit der Kernanlagen HSK, Würenlingen.

IAEA (1998): Waterside Corrosion of Zirconium Alloys in Nuclear Power Plants. IAEA-TECDOC-996. International Atomic Energy Agency IAEA, Wien.

IAEA (2012): Environmental Modelling for Radiation Safety (EMRAS). A Summary Report of the Results of the EMRAS Programme (2003-2007) IAEA-TECDOC-1678. International Atomic Energy Agency IAEA, Vienna.

ICRP (1998): Radiation Protection Recommendations as Applied to the Disposal of Long-lived Solid Radioactive Waste. ICRP Publication 81. (Vol. 28/4). Edited by J. Valentin. International Commission on Radiological Protection ICRP, Oxford.

ICRP (2012): Compendium of Dose Coefficients based on ICRP Publication 60. ICRP Publication 119. (Vol. 41, Supplement 1). Edited by C.H. Clement. International Commission on Radiological Protection ICRP, Oxford.

ICRP (2013): Radiological Protection in Geological Disposal of Long-lived Solid Radioactive Waste. ICRP Publication 122. (Vol. 42/3). Edited by C.H. Clement. International Commission on Radiological Protection ICRP, Oxford.

Johnson, L. & Schwyn, B. (2008): Proceedings of a Nagra / RWMC workshop on the release and transport of C-14 in repository environments. Nagra Arbeitsbericht NAB 08-22.

Johnson, L.H., Curti, E. & Spahiu, K. (2023): A Radionuclide Release Model for Spent UO2 and MOX Fuel for Safety Assessment with Application to Waste to be Disposed of in a Deep Geological Repository in Switzerland. Nagra Arbeitsbericht NAB 23-10. Nagra, Wettingen, Switzerland.

Johnson, L.H. & Tait, J.C. (1997): Release of segregated nuclides from spent fuel. SKB Technical Report TR 97-18. Swedish Nuclear Fuel and Waste Management SKB, Stockholm.

Jung, Y., Pau, G.S.H., Finsterle, S. & Doughty, C. (2018): TOUGH3 User's Guide. Version 1.0. Energy Geosciences Division, Lawrence Berkeley National Laboratory, University of California.

Kaneko, S., Tanabe, H., Sasoh, M., Takahashi, R., Shibano, T. & Tateyama, S. (2002): A study on the chemical forms and migration behavior of carbon-14 leached from the simulated hull waste in the underground condition. MRS Online Proceedings Library 757/38, 621-626. DOI: 10.1557/PROC-757-II3.8.

KEG (2003): Kernenergiegesetz (KEG) vom 21. März 2003, Stand am 1. Januar 2024. Systematische Sammlung des Bundesrechts SR 732.1, Schweiz.

KEV (2004): Kernenergieverordnung (KEV) vom 10. Dezember 2004, Stand am 1. Januar 2024. Systematische Sammlung des Bundesrechts SR 732.11, Schweiz.

Kienzler, B., Bohnert, E., González-Robles, E., Herm, M., Gaona, X. & Borkel, C. (2014): Thermodynamic considerations on the speciation of ^{14}C in spent nuclear fuel. *In:* Kienzler, B., Metz, V., Duro, L. & Valls, A. (eds.): 2nd Annual Workshop Proceedings of the Collaborative Project "Fast/Instant Release of Safety Relevant Radionuclides from Spent Nuclear Fuel". KIT Scientific Reports KIT-SR 7676. 7th EC FP CP FIRST-Nuclides. Antwerp, November 5-7, 2013. Karlsruher Institut für Technologie KIT, Karlsruhe, 45-52.

Knoche, W. (1980): Chemical Reactions of CO_2 in Water. *In:* Bauer, C., Gros, G. & Bartels, H. (eds.): Biophysics and Physiology of Carbon Dioxide. (Proceedings in Life Sciences). Springer, Berlin, Heidelberg, 3-11.

Kosakowski, G., Churakov, S.V., Glaus, M., Guillemot, T., Hummel, W., Kulik, D., Ma, B., Martin, L., Miron, D. & Prasianakis, N.L. (2023): Geochemical Evolution of the L/ILW Near-Field. Nagra Technical Report NTB 23-03.

Lever, D. & Vines, S. (2015): The carbon-14 IPT: An integrated approach to geological disposal of UK wastes containing carbon-14. Mineralogical Magazine 79/6, 1641-1650. DOI: 10.1180/minmag.2015.079.6.40.

Lindborg, T., Brown, J., Griffault, L., Ikonen, A., Kautsky, U., Sanae, S., Smith, G., Smith, K., Thorne, M. & Walke, R. (2022): Safety assessments undertaken using the BIOMASS methodology: Lessons learnt and methodological enhancements. Journal of Radiological Protection 42/2. DOI: 10.1088/1361-6498/ac563c.

Magnusson, Å. & Stenström, K. (2005): ^{14}C produced in Swedish nuclear power reactors – measurements on spent ion exchange resins, various process water systems and ejector off-gas. SKB Report R-05-78. Swedish Nuclear Fuel and Waste Management SKB, Stockholm.

Majlesi, S., Juutilainen, J., Kasurinen, A., Mpamah, P., Trubnikova, T., Oinonen, M., Martikainen, P. & Biasi, C. (2019): Uptake of soil-derived carbon into plants: Implications for disposal of nuclear waste. Environmental Science & Technology 53/8, 4198-4205.

Marques Fernandes, M., Marinich, O., Miron, G.D., Kulik, D.A., Baeyens, B., Wüst, R.A.J., Becker, J. & Li, X. (2024): Sorption Databases for Opalinus Clay, Confining Geological Units, and Bentonite: Methods, Concepts, and Upscaling of Data. Nagra Technical Report NTB 23-06.

Marsden, B., Hopkinson, K. & Wickham, A.J. (2002): The chemical form of carbon-14 within graphite. Report N° SA/RJCB/RD03612001/R01, Issue 4. Serco.

Mibus, J., Diomidis, N., Wieland, E. & Swanton, S. (2018): Final synthesis report on results from WP2. CAST Deliverable D2.18. European Union EU, Brussels.

Mijnendonckx, K., Small, J.S., Abrahamsen-Mills, L., Pedersen, K. & Leys, N. (2019): MIND project: Final integration and evaluation report. MIND Deliverable D3.7. European Commission, Horizon2020.

Miyauchi, Y., Yamashita, Y., Sakurai, J. & Sasoh, M. (2011): Nuclide release behaviour from activated stainless steel and measurement of Kd-value. Session ID B23. Annual / Fall Meetings of Atomic Energy Society of Japan (2011).

Nagra (1985): Project Gewähr 1985: Nuclear Waste Management in Switzerland: Feasibility Studies and Safety Analyses. Nagra Project Report NGB 85-09.

Nagra (1994): Endlager für Schwach - und mittelaktive Abfälle (Endlager SMA): Bericht zur Langzeitsicherheit des Endlagers SMA am Standort Wellenberg (Gemeinde Wolfenschiessen, NW). Nagra Technischer Bericht NTB 94-06.

Nagra (2002a): Project Opalinus Clay: Models, codes and data for safety assessment: Demonstration of disposal feasibility for spent fuel, vitrified high-level waste and long-lived intermediate-level waste (Entsorgungsnachweis). Nagra Technical Report NTB 02-06.

Nagra (2002b): Project Opalinus Clay. Safety report: Demonstration of disposal feasibility for spent fuel, vitrified high-level waste and long-lived intermediate-level waste (Entsorgungsnachweis). Nagra Technical Report NTB 02-05.

Nagra (2004): Effects of Post-disposal Gas Generation for Spent Fuel, High-level Waste and Long-lived Intermediate Level Waste Sited in Opalinus Clay. Nagra Technical Report NTB 04-06. Nagra, Wettingen, Switzerland.

Nagra (2008a): Entsorgungsprogramm 2008 der Entsorgungspflichtigen. Nagra Technischer Bericht NTB 08-01.

Nagra (2008b): Vorschlag geologischer Standortgebiete für ein SMA- und ein HAA-Lager: Begründung der Abfallzuteilung, der Barrierensysteme und der Anforderungen an die Geologie (Bericht zur Sicherheit und Machbarkeit). Nagra Technischer Bericht NTB 08-05.

Nagra (2009): The Nagra Research, Development and Demonstration (RD&D) Plan for the Disposal of Radioactive Waste in Switzerland. Nagra Technical Report NTB 09-06.

Nagra (2014a): Provisional Safety Analyses for SGT Stage 2. Models, Codes and General Modelling Approach. Nagra Technical Report NTB 14-09.

Nagra (2014b): SGT-Etappe 2: Vorschlag weiter zu untersuchender geologischer Standortgebiete mit zugehörigen Standortarealen für die Oberflächenanlage: Charakteristische Dosisintervalle und Unterlagen zur Bewertung der Barrierensysteme. Nagra Technischer Bericht NTB 14-03.

Nagra (2016): The Nagra Research, Development and Demonstration (RD&D) Plan for the Disposal of Radioactive Waste in Switzerland. Nagra Technical Report NTB 16-02.

Nagra (2021a): Entsorgungsprogramm 2021 der Entsorgungspflichtigen. Nagra Technischer Bericht NTB 21-01.

Nagra (2021b): The Nagra Research, Development and Demonstration (RD&D) Plan for the Disposal of Radioactive Waste in Switzerland. Nagra Technical Report NTB 21-02.

Nagra (2021c): Verschlusskonzept für ein geologisches Tiefenlager. Nagra Arbeitsbericht NAB 21-12.

Nagra (2023): Modellhaftes Inventar für radioaktive Materialien - MIRAM-RBG. Nagra Technischer Bericht NTB 22-05. Nagra, Wettingen, Switzerland.

Nagra (2024a): Abfallzuteilung und Betrachtungszeiträume für den Standortvergleich und Nachweiszeitraum für den Sicherheitsnachweis für das geologische Tiefenlager. Nagra Arbeitsbericht NAB 24-05.

Nagra (2024b): Design and Performance Assessment of HLW Disposal Canisters. Nagra Technical Report NTB 24-20.

Nagra (2024c): Development of Safety Scenarios. Nagra Technical Report NTB 24-21.

Nagra (2024d): Geosynthesis of Northern Switzerland. Nagra Technischer Bericht NTB 24-17.

Nagra (2024e): Hydrogeological Model of Northern Switzerland. Nagra Arbeitsbericht NAB 24-16.

Nagra (2024f): Phenomenological Description of the Evolution of a Combined Geological Repository for Radioactive Waste in Opalinus Clay. Nagra Arbeitsbericht NAB 24-20 rev.1.

Nagra (2024g): Post-Closure Biosphere Assessment. Nagra Arbeitsbericht NAB 24-06.

Nagra (2024h): Post-closure safety report. Nagra Technical Report NTB 24-10.

Nagra (2024i): Production and Fate of Gases in a Combined Repository. Nagra Technical Report NTB 24-23.

Nagra (2024j): Radiological Consequence Analysis for a Deep Geological Repository in Northern Switzerland. Nagra Technical Report NTB 24-18.

Nagra (2024k): Safety and Repository Concept and Provisional Design. Nagra Arbeitsbericht NAB 24-18.

Nagra (2024l): Safety Assessment Methodology. Nagra Technical Report NTB 24-19.

Nagra (2024m): Synthesis of the Performance Assessment for a Combined Repository. Nagra Technical Report NTB 24-22.

Nagra (2024n): The Geochemical Evolution of the HLW Repository Near-Field. Nagra Technical Report NTB 23-02 rev.1.

Nagra (2025a): Rahmenbewilligungsgesuch für das geologische Tiefenlager – Begründung der Standortwahl. Nagra Technischer Bericht NTB 24-03.

Nagra (2025b): Rahmenbewilligungsgesuch für das geologisches Tiefenlager – Sicherheitsbericht. Nagra Technischer Bericht NTB 24-01.

Necib, S., Ambard, A., Bucur, C., Caes, S., Cochin, F., Fulger, M., Gras, J.-M., Herm, M., Kasprzak, L., Legand, S., Metz, V., Perrin, S., Sakuragi, T. & Suzuki-Muresan, T. (2018a): Final report on ^{14}C behaviour in Zr fuel clad wastes under disposal conditions. CAST Deliverable D3.20. European Union EU, Brussels.

Necib, S., Bucur, C., Caes, S., Cochin, F., Cvetković, B.Z., Fulger, M., Gras, J.-M., Herm, M., Kasprzak, L., Legand, S., Metz, V., Perrin, S., Sakuragi, T. & Suzuki-Muresan, T. (2018b): Overview of ^{14}C release from irradiated Zircaloys in geological disposal conditions. Radiocarbon 60/6, 1757-1771. DOI: 10.1017/RDC.2018.137.

Ota, M. & Tanaka, T. (2019): Importance of root uptake of $^{14}CO_2$ on ^{14}C transfer to plants impacted by below-ground $^{14}CH_4$ release. Journal of Environmental Radioactivity 201, 5-18.

Poller, A., Smith, P., Mayer, G. & Hayek, M. (2014): Modelling of Radionuclide Transport along the Underground Access Structures of Deep Geological Repositories. Nagra Technical Report NTB 14-10.

Poncet, B. & Petit, L. (2009): EDF analysis on the origins of ^{14}C in UNGG cores. 8th EPRI International decommissioning and radioactive waste workshop - Carbowaste session (2009).

Posiva (2021): Source terms for the safety case in support of the operating licence application. Posiva 2021-11. Posiva, Oy, Olkiluoto.

Quintessa (2023): Amber 6.7 Reference Manual. (QPUB-AMBER-1, Version 6.7). Quintessa Limited, available online at available online at www.quintessa.org/amber.

Quintessa, Geofirma Engineering & SENES Consultants (2011): Post-closure Safety Assessment. NWMO DGR-TR-2011-25. R000. (OPG's Deep Geologic Repository for Low and Intermediate Level Waste). Nuclear Waste Management Organization NWMO, Toronto.

Rizzato, C., Shcherbina, N. & Reiller, P.E. (2017): Compilation and comparaison of data on ^{14}C from spent ion-exchange resins. CAST Deliverable D4.8. European Union EU, Brussels.

Rizzo, A., Bruni, S., Gessi, A., Marghella, G., Moretti, L., Telloli, C., Rizzato, C. & Luce, A. (2018): Morphological study of ionic exchange resins to support the ^{14}C release investigation from radioactive wastes-EURATOM CAST project. Radiocarbon 60/6, 1809-1817. DOI: 10.1017/RDC.2018.136.

Robinson, P. (2022): STMAN 5: User Guide and Theoretical Background for Version 5.10. Nagra Arbeitsbericht NAB 22-10.

Robinson, P. & Chittenden, N. (2022): PICNIC-TD: User Guide for Version 1.5.1. Nagra Arbeitsbericht NAB 22-11.

RWM (2016a): Geological Disposal. Carbon-14 Project Phase 2: Overview Report. NDA Report NDA/RWM/137. Radioactive Waste Management RWM, Oxfordshire.

RWM (2016b): Geological Disposal. Disposal System Safety Case: Data Report. NDA Report DSSC/422/01. Radioactive Waste Management RWM, Oxfordshire.

RWM (2016c): Geological Disposal. Generic Post-closure Performance Modelling. NDA Report NDA/RWM/138. Radioactive Waste Management RWM, Oxfordshire.

RWM (2016d): Geological Disposal. Generic Post-closure Safety Assessment. NDA Report DSSC/321/01. Radioactive Waste Management RWM, Oxfordshire.

Saetre, P., Nordén, S., Keesmann, S. & Ekström, P.-A. (2013): The Biosphere model for radionuclide transport and dose assessment in SR-PSU. SKB Report R-13-46. Updated 2017-09. Swedish Nuclear Fuel and Waste Management SKB, Stockholm.

Sakuragi, T. (2017): Final report on Zr alloys corrosion studies at RWMC. CAST Deliverable D3.19. European Union EU, Brussels.

Sakuragi, T., Tanabe, H., Hirose, E., Sakashita, A. & Nishimura, T. (2014): Estimation of Carbon 14 Inventory in Hull and End-Piece Wastes From Japanese Commercial Reprocessing Operation. ICEM2013-96110. *In:* Kok, K.D. (ed.): Proceedings of the ASME 15th International Conference on Environmental Remediation and Radioactive Waste Management, vol. 1. Brussels, September 8-12, 2013. American Society of Mechanical Engineers ASME, New York.

Sakuragi, T. & Yamashita, Y. (2020): Instant release fractions for ^{14}C, ^{60}Co, and ^{125}Sb from irradiated Zircaloy oxide film. MRS Advances 5/1-2, 9-17. DOI: 10.1557/adv.2019.486.

Sasoh, M. (2008): The study for the chemical forms of C-14 released from activated metals. *In:* Johnson, L. & Schwyn, B.: Proceedings of a Nagra / RWMC workshop on the release and transport of C-14 in repository environments. Nagra Arbeitsbericht NAB 08-22.

Schlesinger, W.H. & Bernhardt, E.S. (2020): Biogeochemistry. An analysis of global change. 4th ed. Academic Press, Amsterdam.

Shaw, G.G. & Thorne, M.C. (2016): The oxidation of methane in soil as a factor in determining the radiological impact of a geological disposal facility. AMEC Report RWM005675, AMEC/200047/001 Issue 1. Radioactive Waste Management RWM, Harwell.

Sheppard, S.C., Ticknor, K.V. & Evenden, W.G. (1998): Sorption of inorganic 14C on to calcite, montmorillonite and soil. Applied Geochemistry 13/1, 43-47. DOI: 10.1016/S0883-2927(97)00052-8.

SKB (2010): Data report for the safety assessment SR-Site. SKB Technical Report TR-10-52. Updated 2014-01. Swedish Nuclear Fuel and Waste Management SKB, Stockholm.

SKB (2011): Long-term safety for the final repository for spent nuclear fuel at Forsmark. Main report of the SR-Site project. SKB Technical Report TR-11-01. Updated 2015-05. Swedish Nuclear Fuel and Waste Management SKB, Stockholm.

SKB (2015a): Radionuclide transport and dose calculations for the safety assessment SR-PSU. SKB Technical Report TR-14-09. Revised edition. Swedish Nuclear Fuel and Waste Management SKB, Stockholm.

SKB (2015b): Safety analysis for SFR Long-term safety: Main report for the safety assessment SR-PSU. SKB Technical Report TR-14-01. Updated 2017-04. Swedish Nuclear Fuel and Waste Management SKB, Stockholm.

SKB (2019a): Post-closure safety for a proposed repository concept for SFL: Main report for the safety evaluation SE-SFL. SKB Technical Report TR-19-01. Updated 2020-02. Swedish Nuclear Fuel and Waste Management SKB, Stockholm.

SKB (2019b): Radionuclide transport and dose calculations for the safety evaluation SE-SFL. SKB Technical Report TR-19-06. Swedish Nuclear Fuel and Waste Management SKB, Stockholm.

Smith, H.D. & Baldwin, D.L. (1993): An investigation of thermal release of carbon-14 from PWR Zircaloy spent fuel cladding. Journal of Nuclear Materials 2000/1, 128-137. DOI: 10.1016/0022-3115(93)90016-R.

Spahiu, K. (2021): State of the Knowledge (SoK) Report. Spent Nuclear Fuel Domain 3.1.1. European Joint Programme on Radioactive Waste Management EURAD.

Stroes-Gascoyne, S., Tait, J.C., Porth, R.J., McConnell, J.L. & Lincoln, W.J. (1994): Release of ^{14}C from the gap and grain-boundary regions of used candu fuels to aqueous solutions. Waste Management 14/5, 385-392. DOI: 10.1016/0956-053X(94)90043-4.

Swanton, S., Baston, G.M.N. & Smart, N.R. (2015): Rates of steel corrosion and carbon-14 release from irradiated steels – state of the art review. CAST Deliverable D2.1. European Union EU, Brussels.

Swift, B. (2016): Specification for SMOGG Version 7.0: A Simplified Model of Gas Generation from Radioactive Wastes. AMEC Report RWM007409, AMEC/204651/001, Issue 2. Radioactive Waste Management RWM, Oxfordshire.

Swift, B., Hoch, A.R., Tstsopoulos, V., Lanyon, B. & Marschall, P. (2020): GDF Pre-closure to Post-closure Waste-derived Gas Generation and Migration. NDA Report RWM/Contr/20/024, Issue 2. (Contractor Report to RWM). Radioactive Waste Management RWM, Oxfordshire.

Swift, B., Swanton, S., Miller, W. & Towler, G. (2016): Carbon-14 Project Phase 2. Irradiated Graphite Wastes. AMEC Report RP50, AMEC/200047/004, Issue 2. Radioactive Waste Management RWM, Oxfordshire.

Takahashi, R., Sasoh, M., Yamashita, Y., Tanabe, H. & Sakuragi, T. (2014): Improvement of Inventory and Leaching Rate Measurements of C-14 in Hull Waste, and Separation of Organic Compounds for Chemical Species Identification. Materials Research Society Symposium Proceedings 1665, 139-148. DOI: 10.1557/opl.2014.639.

Talento, S. & Ganopolski, A. (2021): Reduced-complexity model for the impact of anthropogenic CO_2 emissions on future glacial cycles. Earth System Dynamics 12/4, 1275-1293. DOI: 10.5194/esd-12-1275-2021.

Tanabe, H., Nishimura, T., Kaneko, M., Sakuragi, T., Nasu, Y. & Asano, H. (2009): Characterization of Hull Waste in Underground Conditions. *In:* OECD (ed.): Mobile Fission and Activation Products in Nuclear Waste Disposal. Workshop Proceedings NEA No. 6310. La Baule, January 16-19, 2007. Organisation for Economic Co-operation and Development OECD, Paris, 207-220.

Thorne, M., Ikonen, A. & Smith, K. (2023): Transport of C-14 in terrestrial and aquatic environments. BIOPROTA project report Technical Report TR 23-24. Swedish Nuclear Fuel and Waste Management SKB.

Tits, J. & Wieland, E. (2023): Radionuclide Retention in the Cementitous Near-field of a Repository for Low- and Intermediate-level Waste: Development of the Cement Sorption Database. Nagra Technical Report NTB 23-07.

Toulhoat, N., Moncoffre, N., Narkunas, E., Poskas, P., Bucur, C., Ichim, C., Petit, L., Schumacher, S., Catherin, S., Capone, M., Shcherbina, N., Bukaemskiy, A., Rodríguez Alcalá, M., Magro, E., Márquez, E.M., Piña, G., Fachinger, J., Fugaru, V., Norris, S. & Zlobenko, B. (2018): Final report on results from Work Package 5: Carbon-14 in irradiated graphite. CAST Deliverable D5.19. European Union EU, Brussels.

UNSCEAR (2010): Sources and Effects of Ionizing Radiation. United Nations Scientific Committee on the Effects of Atomic Radiation. UNSCEAR 2008 Report to the General Assembly with Scientific Annexes. Volume I. United Nations UN, New York.

van Konynenburg, R.A. (1994): Behavior of carbon-14 in waste packages for spent fuel in a tuff repository. Waste Management 14/5, 363-383. DOI: 10.1016/0956-053X(94)90042-6.

Van Loon, L.R. & Chen, Y. (unpublished): Sorption of methane on Opalinus Clay. PSI internal communication. Paul Scherrer Institut PSI, Villigen.

Van Loon, L.R. & Hummel, W. (1995): The Radiolytic and Chemical Degradation of Organic Ion Exchange Resins under Alkaline Conditions: Effect on Radionuclide Speciation. PSI Bericht Nr. 95-13. PSI, Villigen.

Večerník, P., Bucur, C., Comte, J., Legand, S., Rizzato, C., Shcherbina, N. & Reiller, P.E. (2018): Final Report on Leaching and Desorption Experiments of ^{14}C from Spent Ion Exchange Resins. CAST Deliverable D4.6. European Union EU, Brussels.

Vinsot, A., Appelo, C., Lundy, M., Wechner, S., Cailteau-Fischbach, C., Donato, P. de, Pironon, J., Lettry, Y., Lerouge, C., Cannière, P. de, Vinsot, A., Appelo, C.A.J., Lundy, M., Wechner, S., Cailteau-Fischbach, C., Donato, P. de, Pironon, J., Lettry, Y., Lerouge, C. & Cannière, P. de (2017): Natural gas extraction and artificial gas injection experiments in Opalinus Clay, Mont Terri rock laboratory (Switzerland). Swiss Journal of Geosciences 110/1, 375-390. DOI: 10.1007/s00015-016-0244-1.

Visser-Týnová, E., Stijkel, M.P., Swanton, S., Otlet, B. & Walker, J. (2018a): C-14 release and speciation from irradiated stainless steel under alkaline reducing conditions. CAST Deliverable D2.8. European Union EU, Brussels.

Visser-Týnová, E., Swanton, S., Williams, S.J., Stijkel, M.P., Walker, A.J. & Otlet, R.L. (2018b): ^{14}C release from irradiated stainless steel. Radiocarbon 60/6, 1671-1681. DOI: 10.1017/RDC.2018.134.

Walke, R. & Thorne, M. (2023): Biosphere Modelling for C-14: Description of the Nagra Model. Nagra Arbeitsbericht NAB 23-25.

Walke, R., van Dorp, F. & Keesmann, S. (2013): Biosphere Modelling for C-14: Description of the Nagra Model. Nagra Arbeitsbericht NAB 12-26.

Wallmann, K. & Aloisi, G. (2012): The Global Carbon Cycle. Geological Processes. *In:* Knoll, A.H., Canfield, D. & Konhauser, K. (eds.): Fundamentals of Geobiology. Wiley-Blackwell, Chichester, West Sussex, 20-35.

Ward, N.D., Bianchi, T.S., Medeiros, P.M., Seidel, M., Richey, J.E., Keil, R.G. & Sawakuchi, H.O. (2017): Where Carbon Goes When Water Flows: Carbon Cycling across the Aquatic Continuum. Frontiers in Marine Science 4. DOI: 10.3389/fmars.2017.00007.

Wareing, A., Abrahamsen, L., Banford, A., Metcalfe, M. & Lensa, W. (2013): Treatment and Disposal of Irradiated Graphite and Other Carbonaceous Waste. Final Publishable CARBOWASTE Report. CARBOWASTE-1306-D-0.3.12.

Wieland, E., Curti, E., Miron, G.D., Tits, J., Van Loon, L.R. & Guillemot, T. (2023): Carbon-14 Sources, Speciation and Release from Radioactive Waste in the context of a Deep Geological Repository. Nagra Technical Report NTB 22-04 rev.1. Nagra, Wettingen, Switzerland.

Wieland, E. & Kosakowski, G. (2020): Review of the compositions of hydrated cements and cement-type pore water at different stages of the cement degradation. Nagra Arbeitsbericht NAB 20-12.

Yamaguchi, T., Tanuma, S., Yatsutomi, I., Nakayama, T., Tanabe, H., Katsurai, K., Kawamura, W., Maeda, K., Kitao, H. & Saigusa, M. (1999): C-14 release behaviour of radionuclides in hull wastes. Radioactive Waste management and Environmental Remediation (ICEM1999), ASME, Nagoya, Japan (1999).

Yamashita, Y., Tanabe, H., Sakuragi, T., Takahashi, R. & Sasoh, M. (2014): C-14 Release Behavior and Chemical Species from Irradiated Hull Waste under Geological Disposal Conditions. MRS Online Proceedings Library 1665, 187-194. DOI: 10.1557/opl.2014.645.

Yim, M.-S. & Caron, F. (2006): Life cycle and management of carbon-14 from nuclear power generation. Progress in Nuclear Energy 48/1, 13181. DOI: 10.1016/j.pnucene.2005.04.002.

App. A ^{14}C activity, speciation and rate of release from individual L/ILW waste package types

Waste package type	^{14}C associated materials*	^{14}C activity (Bq)**	CRF***		IRF***	
			organics	inorganics	organics	inorganics
J-B-000007A	contaminated waste	1.04×10^{9}	0	0	50	50
J-B-000008A	contaminated waste	9.89×10^{8}	0	0	50	50
J-B-000009A	contaminated waste	5.66×10^{11}	0	0	50	50
J-B-000010A	contaminated waste	8.80×10^{9}	0	0	50	50
J-B-000014	contaminated waste	3.91×10^{10}	0	0	50	50
J-B-000034	IERs from PWR	4.59×10^{10}	0	0	30	70
J-B-000038	IERs from PWR	8.14×10^{10}	0	0	30	70
J-B-000041	IERs from PWR	1.96×10^{10}	0	0	30	70
J-B-000042	IERs from PWR	1.24×10^{10}	0	0	30	70
J-B-000043	IERs from PWR	1.88×10^{11}	0	0	30	70
J-B-000044	IERs from PWR	6.81×10^{10}	0	0	30	70
J-B-000045	IERs from PWR	7.80×10^{10}	0	0	30	70
J-B-000046	IERs from PWR	6.95×10^{10}	0	0	30	70
J-B-000047	IERs from PWR	6.05×10^{10}	0	0	30	70
J-B-000049	IERs from PWR	1.28×10^{9}	0	0	30	70
J-B-000050	IERs from PWR	2.03×10^{10}	0	0	30	70
J-B-000051	IERs from PWR	7.12×10^{9}	0	0	30	70
J-B-000052	IERs from PWR	9.90×10^{9}	0	0	30	70
J-B-000054	IERs from PWR	1.42×10^{8}	0	0	30	70
J-B-000055	contaminated waste	1.35×10^{11}	0	0	50	50
J-B-000056	contaminated waste	2.04×10^{9}	0	0	50	50
J-B-000057	contaminated waste	5.19×10^{9}	0	0	50	50
J-B-000058	contaminated waste	6.65×10^{9}	0	0	50	50
J-B-000059	contaminated waste	1.80×10^{10}	0	0	50	50
J-B-000060	contaminated waste	3.33×10^{10}	0	0	50	50
J-B-000061	contaminated waste	2.56×10^{9}	0	0	50	50
J-B-000062	contaminated waste	2.99×10^{10}	0	0	50	50
J-B-000063	contaminated waste	3.08×10^{9}	0	0	50	50
J-B-000065	contaminated waste	4.61×10^{8}	0	0	50	50
J-B-000066	contaminated waste	1.76×10^{11}	0	0	50	50
J-B-000067	contaminated waste	1.86×10^{10}	0	0	50	50

Waste package type	^{14}C associated materials*	^{14}C activity (Bq)**	CRF***		IRF***	
			organics	inorganics	organics	inorganics
J-B-000069	contaminated waste	1.61×10^{11}	0	0	50	50
J-B-000072	IERs from PWR	1.80×10^{10}	0	0	30	70
J-B-000073	contaminated waste	1.43×10^{10}	0	0	50	50
J-B-000075	contaminated waste	6.08×10^{11}	0	0	50	50
J-B-000078	products from incineration/plasma furnace	8.60×10^{3}	0	0	0	100
J-B-000079	products from incineration/plasma furnace	6.81×10^{4}	0	0	0	100
J-B-000080	products from incineration/plasma furnace	1.87×10^{4}	0	0	0	100
J-B-000081	products from incineration/plasma furnace	4.98×10^{4}	0	0	0	100
J-B-000082	products from incineration/plasma furnace	1.17×10^{6}	0	0	0	100
J-B-000083	products from incineration/plasma furnace	8.02×10^{3}	0	0	0	100
J-B-000085	products from incineration/plasma furnace	1.07×10^{4}	0	0	0	100
J-B-000086	products from incineration/plasma furnace	1.29×10^{5}	0	0	0	100
J-B-000087	products from incineration/plasma furnace	1.44×10^{4}	0	0	0	100
J-B-000088	IERs from PWR	2.93×10^{9}	0	0	30	70
J-B-000093	contaminated waste	1.98×10^{11}	0	0	50	50
J-B-000094	contaminated waste	1.29×10^{10}	0	0	50	50
J-B-000095	contaminated waste	7.07×10^{10}	0	0	50	50
J-B-000098	contaminated waste	3.27×10^{10}	0	0	50	50
J-B-000099	IERs from PWR	1.42×10^{9}	0	0	30	70
J-B-000100	contaminated waste	6.46×10^{9}	0	0	50	50
J-B-000101	contaminated waste	4.85×10^{9}	0	0	50	50
J-B-000102	contaminated waste	8.67×10^{6}	0	0	50	50

Waste package type	^{14}C associated materials*	^{14}C activity (Bq)**	CRF***		IRF***	
			organics	inorganics	organics	inorganics
J-B-000103	contaminated waste	5.90×10^{8}	0	0	50	50
J-B-000108	IERs from PWR	4.88×10^{9}	0	0	30	70
J-B-000109	IERs from PWR	2.45×10^{7}	0	0	30	70
J-B-000110	IERs from PWR	5.03×10^{9}	0	0	30	70
J-B-000111	contaminated waste	8.65×10^{8}	0	0	50	50
J-B-000112	contaminated waste	8.65×10^{8}	0	0	50	50
J-B-000113	contaminated waste	8.60×10^{8}	0	0	50	50
J-B-000114	contaminated waste	8.60×10^{8}	0	0	50	50
J-B-000115	contaminated waste	1.59×10^{11}	0	0	50	50
J-B-000116	IERs from PWR	2.36×10^{10}	0	0	30	70
J-B-000118	contaminated waste	4.61×10^{10}	0	0	50	50
J-B-000119	contaminated waste	2.78×10^{9}	0	0	50	50
J-B-000120	contaminated waste	1.02×10^{9}	0	0	50	50
J-B-000121	contaminated waste	1.26×10^{8}	0	0	50	50
J-B-000122	contaminated waste	1.95×10^{9}	0	0	50	50
J-B-000123	contaminated waste	2.63×10^{9}	0	0	50	50
J-B-000124	contaminated waste	1.28×10^{8}	0	0	50	50
J-B-000125	contaminated waste	4.28×10^{6}	0	0	50	50
J-B-000127	contaminated waste	2.56×10^{7}	0	0	50	50
J-B-000128	contaminated waste	2.51×10^{8}	0	0	50	50
J-B-000129	contaminated waste	2.51×10^{8}	0	0	50	50
J-B-000130	contaminated waste	1.47×10^{8}	0	0	50	50
J-B-910001	IERs from PWR	3.72×10^{9}	0	0	30	70
J-B-910002	contaminated waste	7.11×10^{9}	0	0	50	50
J-B-910003	contaminated waste	5.15×10^{10}	0	0	50	50
J-B-910010	products from incineration/plasma furnace	1.82×10^{4}	0	0	0	100
J-B-920001	activated steel	7.58×10^{11}	99.99	0	0.01	0
J-B-9320141	activated steel	1.03×10^{10}	99.99	0	0.01	0
J-B-9320151	activated steel	2.68×10^{10}	99.99	0	0.01	0
J-B-9320152	activated steel	7.77×10^{10}	99.99	0	0.01	0
J-B-9320161	activated steel	1.50×10^{11}	99.99	0	0.01	0
J-B-9320162	activated steel	6.74×10^{10}	99.99	0	0.01	0

Waste package type	^{14}C associated materials*	^{14}C activity (Bq)**	CRF***		IRF***	
			organics	inorganics	organics	inorganics
J-B-9320171	activated steel	1.08×10^{12}	99.99	0	0.01	0
J-B-9320181	activated steel	9.07×10^{11}	99.99	0	0.01	0
J-B-9320182	activated steel	1.50×10^{11}	99.99	0	0.01	0
J-B-9320183	activated steel	4.52×10^{12}	99.99	0	0.01	0
J-B-9320191	activated steel	1.53×10^{13}	99.99	0	0.01	0
J-B-9320211	contaminated and activated steel	1.80×10^{9}	49.995	0	25.005	25
J-B-9320221	activated steel	4.10×10^{5}	99.99	0	0.01	0
J-B-9320222	activated steel	6.30×10^{4}	99.99	0	0.01	0
J-B-9320223	activated steel	2.73×10^{4}	99.99	0	0.01	0
J-B-9320224	activated steel	2.76×10^{3}	99.99	0	0.01	0
J-B-9320231	activated steel	1.27×10^{9}	99.99	0	0.01	0
J-B-9320232	activated steel	3.47×10^{4}	99.99	0	0.01	0
J-B-9320233	activated steel	2.55×10^{9}	99.99	0	0.01	0
J-B-932024	activated steel	3.72×10^{9}	99.99	0	0.01	0
J-B-932025	activated steel	6.72×10^{10}	99.99	0	0.01	0
J-B-9320301	activated steel and activated concrete	3.79×10^{10}	49.995	0	12.505	12.5
J-B-9321011	products from incineration/plasma furnace	7.08×10^{8}	0	0	0	100
J-B-9321201	contaminated waste	7.31×10^{7}	0	0	50	50
J-B-9321203	contaminated waste	8.35×10^{9}	0	0	50	50
J-B-9321204	contaminated waste	4.18×10^{11}	0	0	50	50
J-B-9321301	contaminated waste	2.96×10^{7}	0	0	50	50
J-B-9321303	contaminated waste	4.94×10^{8}	0	0	50	50
J-B-9321304	contaminated waste	4.94×10^{10}	0	0	50	50
J-B-9321311	contaminated waste	7.76×10^{7}	0	0	50	50
J-B-9321320	contaminated waste	2.75×10^{8}	0	0	50	50
J-B-932200	products from incineration/plasma furnace	1.54×10^{5}	0	0	0	100
J-B-932201	contaminated waste	1.30×10^{9}	0	0	50	50
J-B-932202	contaminated waste	1.59×10^{9}	0	0	50	50
J-B-932203	contaminated waste	9.05×10^{9}	0	0	50	50
J-B-932210	IERs from PWR	1.42×10^{10}	0	0	30	70

Waste package type	^{14}C associated materials*	^{14}C activity (Bq)**	CRF***		IRF***	
			organics	inorganics	organics	inorganics
J-B-932211	IERs from PWR	6.37×10^{10}	0	0	30	70
J-G-000003	contaminated waste	1.59×10^{8}	0	0	50	50
J-G-000004	contaminated waste	2.51×10^{7}	0	0	50	50
J-G-000005	contaminated waste	1.26×10^{9}	0	0	50	50
J-G-000006	contaminated waste	8.90×10^{7}	0	0	50	50
J-G-000007	contaminated waste	7.72×10^{8}	0	0	50	50
J-G-000008	contaminated waste	1.66×10^{7}	0	0	50	50
J-G-000009	contaminated waste	2.02×10^{8}	0	0	50	50
J-G-000010	contaminated waste	8.69×10^{7}	0	0	50	50
J-G-000011	contaminated waste	3.69×10^{8}	0	0	50	50
J-G-000012	contaminated waste	1.01×10^{7}	0	0	50	50
J-G-000013	contaminated waste	1.92×10^{9}	0	0	50	50
J-G-000014	contaminated waste	1.05×10^{9}	0	0	50	50
J-G-000015	contaminated waste	2.80×10^{7}	0	0	50	50
J-G-000016	contaminated waste	5.25×10^{6}	0	0	50	50
J-G-000017	contaminated waste	1.77×10^{7}	0	0	50	50
J-G-000018	contaminated waste	4.01×10^{6}	0	0	50	50
J-G-000019	contaminated waste	9.65×10^{6}	0	0	50	50
J-G-000020	contaminated waste	2.43×10^{6}	0	0	50	50
J-G-000021	contaminated waste	1.24×10^{8}	0	0	50	50
J-G-000022	contaminated waste	2.02×10^{8}	0	0	50	50
J-G-000023	contaminated waste	5.77×10^{8}	0	0	50	50
J-G-000024	IERs from PWR	1.07×10^{11}	0	0	30	70
J-G-000025	IERs from PWR	5.67×10^{6}	0	0	30	70
J-G-000026	contaminated waste	3.05×10^{7}	0	0	50	50
J-G-000027	contaminated waste	6.09×10^{6}	0	0	50	50
J-G-000028	IERs from PWR	1.99×10^{8}	0	0	30	70
J-G-000029	IERs from PWR	4.24×10^{7}	0	0	30	70
J-G-000030	contaminated waste	2.87×10^{8}	0	0	50	50
J-G-000031	contaminated waste	6.08×10^{8}	0	0	50	50
J-G-000032	contaminated waste	3.95×10^{7}	0	0	50	50
J-G-000033	contaminated waste	4.68×10^{6}	0	0	50	50
J-G-000035	contaminated waste	9.15×10^{6}	0	0	50	50
J-G-000036	contaminated waste	2.69×10^{6}	0	0	50	50

Waste package type	^{14}C associated materials*	^{14}C activity (Bq)**	CRF***		IRF***	
			organics	inorganics	organics	inorganics
J-G-000037	contaminated waste	7.38×10^{7}	0	0	50	50
J-G-000038	contaminated waste	1.51×10^{8}	0	0	50	50
J-G-000039	contaminated waste	4.22×10^{7}	0	0	50	50
J-G-000042	IERs from PWR	1.06×10^{6}	0	0	30	70
J-G-000043	IERs from PWR	4.31×10^{8}	0	0	30	70
J-G-000044	contaminated waste	9.25×10^{6}	0	0	50	50
J-G-000045	contaminated waste	5.05×10^{7}	0	0	50	50
J-G-000046	activated steel	1.59×10^{9}	99.99	0	0.01	0
J-G-000047	contaminated waste	1.75×10^{6}	0	0	50	50
J-G-000049	contaminated waste	1.21×10^{9}	0	0	50	50
J-G-000050	contaminated waste	2.76×10^{9}	0	0	50	50
J-G-000051	contaminated waste	8.14×10^{8}	0	0	50	50
J-G-000052	contaminated waste	3.08×10^{8}	0	0	50	50
J-G-000055	contaminated waste	1.68×10^{7}	0	0	50	50
J-G-000056	contaminated waste	1.42×10^{7}	0	0	50	50
J-G-000057	contaminated waste	4.36×10^{6}	0	0	50	50
J-G-000059	contaminated waste	5.69×10^{7}	0	0	50	50
J-G-000060	contaminated waste	2.20×10^{8}	0	0	50	50
J-G-000061	products from incineration/plasma furnace	9.10×10^{4}	0	0	0	100
J-G-000062	products from incineration/plasma furnace	4.62×10^{5}	0	0	0	100
J-G-000063	products from incineration/plasma furnace	2.16×10^{5}	0	0	0	100
J-G-000064	products from incineration/plasma furnace	6.71×10^{5}	0	0	0	100
J-G-000065	products from incineration/plasma furnace	4.33×10^{4}	0	0	0	100
J-G-000066	products from incineration/plasma furnace	2.30×10^{5}	0	0	0	100
J-G-000067	products from incineration/plasma furnace	3.21×10^{4}	0	0	0	100

Waste package type	^{14}C associated materials*	^{14}C activity (Bq)**	CRF***		IRF***	
			organics	inorganics	organics	inorganics
J-G-000068	products from incineration/plasma furnace	2.85×10^{5}	0	0	0	100
J-G-000069	products from incineration/plasma furnace	8.36×10^{5}	0	0	0	100
J-G-000070	products from incineration/plasma furnace	3.82×10^{4}	0	0	0	100
J-G-000071	products from incineration/plasma furnace	3.24×10^{5}	0	0	0	100
J-G-000072	products from incineration/plasma furnace	1.79×10^{5}	0	0	0	100
J-G-000073	products from incineration/plasma furnace	1.65×10^{6}	0	0	0	100
J-G-000079	contaminated waste	3.06×10^{10}	0	0	50	50
J-G-000080	contaminated waste	1.12×10^{9}	0	0	50	50
J-G-000081	contaminated waste	6.26×10^{7}	0	0	50	50
J-G-000082	IERs from PWR	3.45×10^{10}	0	0	30	70
J-G-000087	activated steel	3.79×10^{11}	99.99	0	0.01	0
J-G-000088	activated steel	6.10×10^{9}	99.99	0	0.01	0
J-G-000089	activated steel	2.64×10^{10}	99.99	0	0.01	0
J-G-000090	contaminated waste	2.17×10^{10}	0	0	50	50
J-G-000091	contaminated waste	1.19×10^{9}	0	0	50	50
J-G-000093	IERs from PWR	1.89×10^{11}	0	0	30	70
J-G-910001	IERs from PWR	4.73×10^{9}	0	0	30	70
J-G-910002	contaminated waste	2.16×10^{9}	0	0	50	50
J-G-910003	contaminated waste	9.95×10^{10}	0	0	50	50
J-G-910010	products from incineration/plasma furnace	2.00×10^{5}	0	0	0.00	100
J-G-910011	contaminated waste	6.78×10^{7}	0	0	50	50
J-G-9320141	activated steel	5.90×10^{8}	99.99	0	0.01	0
J-G-9320142	activated steel	6.74×10^{9}	99.99	0	0.01	0
J-G-9320143	activated steel	1.18×10^{9}	99.99	0	0.01	0
J-G-9320144	activated steel	2.67×10^{9}	99.99	0	0.01	0

Waste package type	^{14}C associated materials*	^{14}C activity (Bq)**	CRF***		IRF***	
			organics	inorganics	organics	inorganics
J-G-9320151	activated steel	1.05×10^{10}	99.99	0	0.01	0
J-G-9320152	activated steel	3.44×10^{10}	99.99	0	0.01	0
J-G-9320153	activated steel	1.81×10^{9}	99.99	0	0.01	0
J-G-9320161	activated steel	5.17×10^{11}	99.99	0	0.01	0
J-G-9320162	activated steel	4.87×10^{9}	99.99	0	0.01	0
J-G-9320171	activated steel	9.18×10^{10}	99.99	0	0.01	0
J-G-9320181	activated steel	3.41×10^{12}	99.99	0	0.01	0
J-G-9320211	activated steel	2.12×10^{8}	99.99	0	0.01	0
J-G-9320212	activated steel	1.85×10^{10}	99.99	0	0.01	0
J-G-9320221	activated steel	7.60×10^{7}	99.99	0	0.01	0
J-G-9320222	activated steel	2.39×10^{8}	99.99	0	0.01	0
J-G-9320223	activated steel	3.83×10^{9}	99.99	0	0.01	0
J-G-9320224	activated steel	4.69×10^{8}	99.99	0	0.01	0
J-G-9320225	activated steel	4.00×10^{9}	99.99	0	0.01	0
J-G-9320226	activated steel	1.75×10^{8}	99.99	0	0.01	0
J-G-9320231	activated steel	1.71×10^{9}	99.99	0	0.01	0
J-G-9320232	activated steel	1.04×10^{9}	99.99	0	0.01	0
J-G-9320233	activated steel	1.13×10^{8}	99.99	0	0.01	0
J-G-9320234	activated steel	2.62×10^{9}	99.99	0	0.01	0
J-G-9320301	activated steel and activated concrete	2.23×10^{10}	50.00	0	12.51	13
J-G-9320302	activated steel and activated concrete	1.22×10^{8}	49.995	0	12.505	12.5
J-G-9321001	contaminated waste	7.72×10^{6}	0	0	50	50
J-G-9321011	products from incineration/plasma furnace	1.75×10^{5}	0	0	0	100
J-G-9321014	products from incineration/plasma furnace	1.38×10^{10}	0	0	0	100
J-G-9321015	products from incineration/plasma furnace	1.38×10^{11}	0	0	0	100
J-G-9321201	contaminated waste	2.17×10^{5}	0	0	50	50
J-G-9321204	contaminated waste	2.24×10^{9}	0	0	50	50
J-G-9321205	contaminated waste	5.50×10^{10}	0	0	50	50

Waste package type	^{14}C associated materials*	^{14}C activity (Bq)**	CRF***		IRF***	
			organics	inorganics	organics	inorganics
J-G-9321301	contaminated waste	5.78×10^{4}	0	0	50	50
J-G-9321304	contaminated waste	1.06×10^{9}	0	0	50	50
J-G-9321305	contaminated waste	1.22×10^{10}	0	0	50	50
J-G-9321310	contaminated waste	9.47×10^{5}	0	0	50	50
J-G-932200	products from incineration/plasma furnace	1.66×10^{5}	0	0	0	100
J-G-932201	contaminated waste	2.15×10^{8}	0	0	50	50
J-G-932202	contaminated waste	1.59×10^{8}	0	0	50	50
J-G-932203	contaminated waste	2.64×10^{9}	0	0	50	50
J-G-932210	IERs from PWR	1.21×10^{9}	0	0	30	70
J-G-932211	IERs from PWR	5.38×10^{9}	0	0	30	70
J-L-000003	contaminated waste	2.75×10^{7}	0	0	50	50
J-L-000004	IERs from BWR	1.57×10^{10}	0	0	10	90
J-L-000005	activated Zr	1.13×10^{11}	99.99	0	0.01	0
J-L-000006	contaminated waste	3.77×10^{9}	0	0	50	50
J-L-000012	products from incineration/plasma furnace	2.10×10^{6}	0	0	0	100
J-L-000015	IERs from BWR	3.33×10^{9}	0	0	10	90
J-L-000017	IERs from BWR	2.63×10^{10}	0	0	10	90
J-L-000018	IERs from BWR	1.31×10^{6}	0	0	10	90
J-L-000019	IERs from BWR	1.82×10^{9}	0	0	10	90
J-L-000022	products from incineration/plasma furnace	2.03×10^{7}	0	0	0	100
J-L-000023	products from incineration/plasma furnace	1.37×10^{4}	0	0	0	100
J-L-000024	products from incineration/plasma furnace	7.36×10^{2}	0	0	0	100
J-L-000025	products from incineration/plasma furnace	1.64×10^{6}	0	0	0	100
J-L-000026	products from incineration/plasma furnace	1.62×10^{7}	0	0	0	100

Waste package type	^{14}C associated materials*	^{14}C activity (Bq)**	CRF***		IRF***	
			organics	inorganics	organics	inorganics
J-L-000027	products from incineration/plasma furnace	2.71×10^{6}	0	0	0	100
J-L-000028	products from incineration/plasma furnace	2.46×10^{5}	0	0	0	100
J-L-000029	products from incineration/plasma furnace	3.52×10^{6}	0	0	0	100
J-L-000030	contaminated waste	4.56×10^{6}	0	0	50	50
J-L-000033	contaminated waste	4.40×10^{2}	0	0	50	50
J-L-000034	contaminated waste	1.26×10^{7}	0	0	50	50
J-L-000035	contaminated waste	4.23×10^{5}	0	0	50	50
J-L-000036	contaminated waste	7.10×10^{5}	0	0	50	50
J-L-000037	contaminated waste	2.01×10^{5}	0	0	50	50
J-L-000038	contaminated waste	1.62×10^{7}	0	0	50	50
J-L-000043	contaminated waste	3.48×10^{4}	0	0	50	50
J-L-000046	IERs from BWR	3.95×10^{10}	0	0	10	90
J-L-000060	activated steel	1.92×10^{11}	99.99	0	0.01	0
J-L-000061	activated Zr	1.12×10^{10}	99.99	0	0.01	0
J-L-000062	activated steel	1.71×10^{9}	99.99	0	0.01	0
J-L-000063	activated steel	1.57×10^{10}	99.99	0	0.01	0
J-L-000064	activated steel	4.84×10^{10}	99.99	0	0.01	0
J-L-000065	activated steel	1.27×10^{12}	99.99	0	0.01	0
J-L-000066	activated steel	4.11×10^{11}	99.99	0	0.01	0
J-L-000090	contaminated waste	4.17×10^{8}	0	0	50	50
J-L-910001	IERs from BWR	8.85×10^{9}	0	0	10	90
J-L-910002	contaminated waste	1.01×10^{8}	0	0	50	50
J-L-910003	contaminated waste	5.34×10^{9}	0	0	50	50
J-L-910006	contaminated waste	7.76×10^{5}	0	0	50	50
J-L-910008	contaminated waste	7.56×10^{6}	0	0	50	50
J-L-910010	products from incineration/plasma furnace	4.13×10^{5}	0	0	0	100
J-L-9320131	activated steel	3.25×10^{9}	99.99	0	0.01	0
J-L-9320132	activated steel	8.80×10^{8}	99.99	0	0.01	0

Waste package type	^{14}C associated materials*	^{14}C activity (Bq)**	CRF***		IRF***	
			organics	inorganics	organics	inorganics
J-L-9320133	activated steel	$1.67E+^{10}$	99.99	0	0.01	0
J-L-9320134	activated steel	2.90×10^{9}	99.99	0	0.01	0
J-L-9320135	activated steel	9.28×10^{7}	99.99	0	0.01	0
J-L-9320141	activated steel	5.99×10^{9}	99.99	0	0.01	0
J-L-9320142	activated steel	1.67×10^{9}	99.99	0	0.01	0
J-L-9320143	activated steel	8.08×10^{10}	99.99	0	0.01	0
J-L-9320144	activated steel	7.59×10^{9}	99.99	0	0.01	0
J-L-9320145	activated steel	4.36×10^{8}	99.99	0	0.01	0
J-L-9320151	activated steel	1.28×10^{11}	99.99	0	0.01	0
J-L-9320152	activated steel	4.16×10^{9}	99.99	0	0.01	0
J-L-9320153	activated steel	5.97×10^{10}	99.99	0	0.01	0
J-L-9320154	activated steel	2.78×10^{10}	99.99	0	0.01	0
J-L-9320155	activated steel	7.73×10^{9}	99.99	0	0.01	0
J-L-9320161	activated steel	5.11×10^{11}	99.99	0	0.01	0
J-L-9320162	activated steel	2.15×10^{10}	99.99	0	0.01	0
J-L-9320163	activated steel	4.58×10^{9}	99.99	0	0.01	0
J-L-9320164	activated steel	1.08×10^{10}	99.99	0	0.01	0
J-L-9320165	activated steel	6.75×10^{10}	99.99	0	0.01	0
J-L-9320166	activated steel	8.62×10^{9}	99.99	0	0.01	0
J-L-9320171	activated steel	1.04×10^{12}	99.99	0	0.01	0
J-L-9320172	activated steel	1.15×10^{11}	99.99	0	0.01	0
J-L-9320173	activated steel	9.03×10^{11}	99.99	0	0.01	0
J-L-9320211	activated steel	6.11×10^{6}	99.99	0	0.01	0
J-L-9320212	activated steel	2.66×10^{5}	99.99	0	0.01	0
J-L-9320213	activated steel	1.46×10^{9}	99.99	0	0.01	0
J-L-9320221	activated steel	1.42×10^{7}	99.99	0	0.01	0
J-L-9320222	activated steel	4.31×10^{8}	99.99	0	0.01	0
J-L-9320223	activated steel	4.30×10^{8}	99.99	0	0.01	0
J-L-9320224	activated steel	1.09×10^{7}	99.99	0	0.01	0
J-L-9320225	activated steel	1.83×10^{8}	99.99	0	0.01	0
J-L-9320226	activated steel	7.14×10^{7}	99.99	0	0.01	0
J-L-9320227	activated steel	3.96×10^{8}	99.99	0	0.01	0
J-L-9320228	activated steel	1.56×10^{7}	99.99	0	0.01	0
J-L-9320231	activated steel	2.81×10^{7}	99.99	0	0.01	0

Waste package type	^{14}C associated materials*	^{14}C activity (Bq)**	CRF***		IRF***	
			organics	inorganics	organics	inorganics
J-L-9320232	activated steel	3.24×10^{8}	99.99	0	0.01	0
J-L-9320233	activated steel	2.39×10^{8}	99.99	0	0.01	0
J-L-9320234	activated steel	2.92×10^{8}	99.99	0	0.01	0
J-L-9320235	activated steel	4.69×10^{7}	99.99	0	0.01	0
J-L-9320301	activated steel and activated concrete	2.44×10^{7}	49.995	0	12.505	12.5
J-L-9320302	activated steel and activated concrete	2.09×10^{7}	49.995	0	12.505	12.5
J-L-9320303	activated steel and activated concrete	5.38×10^{9}	49.995	0	12.505	12.5
J-L-9321002	contaminated metals	6.43×10^{6}	0	0	50	50
J-L-9321003	contaminated metals	4.49×10^{5}	0	0	50	50
J-L-9321004	contaminated metals	6.40×10^{9}	0	0	50	50
J-L-9321012	products from incineration/plasma furnace	1.65×10^{7}	0	0	0	100
J-L-9321013	products from incineration/plasma furnace	4.27×10^{8}	0	0	0	100
J-L-9321014	products from incineration/plasma furnace	6.75×10^{9}	0	0	0	100
J-L-9321022	contaminated waste	3.29×10^{8}	0	0	50	50
J-L-9321024	contaminated waste	1.32×10^{9}	0	0	50	50
J-L-9321201	contaminated waste	7.57×10^{4}	0	0	50	50
J-L-9321202	contaminated waste	2.10×10^{7}	0	0	50	50
J-L-9321203	contaminated waste	4.98×10^{8}	0	0	50	50
J-L-9321204	contaminated waste	4.10×10^{10}	0	0	50	50
J-L-9321301	contaminated waste	8.26×10^{3}	0	0	50	50
J-L-9321302	contaminated waste	5.78×10^{6}	0	0	50	50
J-L-9321303	contaminated waste	5.78×10^{7}	0	0	50	50
J-L-9321304	contaminated waste	5.78×10^{9}	0	0	50	50
J-L-9321310	contaminated waste	3.61×10^{5}	0	0	50	50
J-L-932200	products from incineration/plasma furnace	3.64×10^{5}	0	0	0	100
J-L-932201	contaminated waste	5.07×10^{6}	0	0	50	50

Waste package type	^{14}C associated materials*	^{14}C activity (Bq)**	CRF***		IRF***	
			organics	inorganics	organics	inorganics
J-L-932202	contaminated waste	4.77×10^{7}	0	0	50	50
J-L-932203	contaminated metals	2.42×10^{8}	0	0	50	50
J-L-932210	IERs from BWR	8.77×10^{7}	0	0	10	90
J-L-932211	IERs from BWR	3.99×10^{8}	0	0	10	90
J-M-000049	contaminated waste	1.82×10^{6}	0	0	50	50
J-M-000050	activated steel	4.06×10^{9}	99.99	0	0.01	0
J-M-000051	activated steel	2.79×10^{8}	99.99	0	0.01	0
J-M-000054	contaminated waste	9.20×10^{6}	0	0	50	50
J-M-000055	contaminated waste	6.06×10^{6}	0	0	50	50
J-M-000061	IERs from BWR	2.56×10^{8}	0	0	10	90
J-M-000064	IERs from BWR	6.15×10^{10}	0	0	10	90
J-M-000066	IERs from BWR	4.63×10^{8}	0	0	10	90
J-M-000070	IERs from BWR	7.63×10^{8}	0	0	10	90
J-M-000071	contaminated waste	2.70×10^{7}	0	0	50	50
J-M-000072	products from incineration/plasma furnace	9.44×10^{5}	0	0	0	100
J-M-000073	products from incineration/plasma furnace	3.03×10^{5}	0	0	0	100
J-M-000074	products from incineration/plasma furnace	1.38×10^{5}	0	0	0	100
J-M-000075	products from incineration/plasma furnace	2.37×10^{6}	0	0	0	100
J-M-000076	products from incineration/plasma furnace	1.50×10^{6}	0	0	0	100
J-M-000077	products from incineration/plasma furnace	9.50×10^{4}	0	0	0	100
J-M-000078	products from incineration/plasma furnace	1.01×10^{5}	0	0	0	100
J-M-000079	products from incineration/plasma furnace	1.04×10^{5}	0	0	0	100

Waste package type	^{14}C associated materials*	^{14}C activity (Bq)**	CRF***		IRF***	
			organics	inorganics	organics	inorganics
J-M-000080	products from incineration/plasma furnace	1.49×10^{6}	0	0	0	100
J-M-000081	products from incineration/plasma furnace	7.18×10^{5}	0	0	0	100
J-M-000082	products from incineration/plasma furnace	1.23×10^{6}	0	0	0	100
J-M-000083	products from incineration/plasma furnace	2.43×10^{2}	0	0	0	100
J-M-000084	products from incineration/plasma furnace	3.92×10^{5}	0	0	0	100
J-M-000085	products from incineration/plasma furnace	4.51×10^{5}	0	0	0	100
J-M-000086	products from incineration/plasma furnace	8.69×10^{4}	0	0	0	100
J-M-000087	products from incineration/plasma furnace	4.33×10^{5}	0	0	0	100
J-M-000088	IERs from BWR	1.11×10^{10}	0	0	10	90
J-M-000089	IERs from BWR	1.15×10^{12}	0	0	10	90
J-M-000090	IERs from BWR	9.46×10^{5}	0	0	10	90
J-M-000091	IERs from BWR	1.54×10^{11}	0	0	10	90
J-M-000092	IERs from BWR	4.67×10^{10}	0	0	10	90
J-M-000094	activated Zr	2.25×10^{11}	99.99	0	0.01	0
J-M-000096	activated Zr	9.82×10^{10}	99.99	0	0.01	0
J-M-000097	contaminated waste	2.72×10^{10}	0	0	50	50
J-M-000098	contaminated waste	2.18×10^{9}	0	0	50	50
J-M-000099	contaminated waste	2.34×10^{9}	0	0	50	50
J-M-000100	activated steel	4.52×10^{7}	99.99	0	0.01	0
J-M-000102	contaminated waste	3.27×10^{6}	0	0	50	50
J-M-000103	activated steel	5.66×10^{10}	99.99	0	0.01	0
J-M-000104	IERs from BWR	1.68×10^{7}	0	0	10	90
J-M-000105A	IERs from BWR	3.77×10^{9}	0	0	10	90

Waste package type	^{14}C associated materials*	^{14}C activity (Bq)**	CRF***		IRF***	
			organics	inorganics	organics	inorganics
J-M-000107	contaminated waste	1.02×10^{5}	0	0	50	50
J-M-000108	contaminated waste	1.23×10^{6}	0	0	50	50
J-M-000109	contaminated waste	2.67×10^{6}	0	0	50	50
J-M-000110	contaminated waste	5.32×10^{5}	0	0	50	50
J-M-000111	contaminated waste	9.85×10^{6}	0	0	50	50
J-M-000112	contaminated waste	6.24×10^{4}	0	0	50	50
J-M-000113	contaminated waste	3.57×10^{5}	0	0	50	50
J-M-000114	contaminated waste	6.29×10^{4}	0	0	50	50
J-M-000116	contaminated waste	3.04×10^{6}	0	0	50	50
J-M-000119	IERs from BWR	5.71×10^{10}	0	0	10	90
J-M-000122	activated steel	2.10×10^{11}	99.99	0	0.01	0
J-M-910001	IERs from BWR	3.61×10^{8}	0	0	10	90
J-M-910002	contaminated waste	1.22×10^{8}	0	0	50	50
J-M-910003	contaminated waste	1.17×10^{6}	0	0	50	50
J-M-910010	products from incineration/plasma furnace	1.49×10^{3}	0	0	0	100
J-M-920001	activated steel	3.59×10^{11}	99.99	0	0.01	0
J-M-920002	activated steel	3.58×10^{10}	99.99	0	0.01	0
J-M-9320001	activated steel	2.19×10^{10}	99.99	0	0.01	0
J-M-9320002	activated steel	2.08×10^{10}	99.99	0	0.01	0
J-M-9320003	activated steel	9.08×10^{9}	99.99	0	0.01	0
J-M-9320004	activated steel	1.11×10^{10}	99.99	0	0.01	0
J-M-9320005	activated steel	2.89×10^{9}	99.99	0	0.01	0
J-M-9320006	activated steel	5.20×10^{10}	99.99	0	0.01	0
J-M-9320007	activated steel	9.07×10^{9}	99.99	0	0.01	0
J-M-9320008	activated steel	7.42×10^{10}	99.99	0	0.01	0
J-M-9320009	activated steel	1.66×10^{10}	99.99	0	0.01	0
J-M-9320010	activated steel	7.99×10^{8}	99.99	0	0.01	0
J-M-9320011	activated steel	2.01×10^{9}	99.99	0	0.01	0
J-M-9320012	activated steel	2.24×10^{9}	99.99	0	0.01	0
J-M-9320131	activated steel	8.66×10^{10}	99.99	0	0.01	0
J-M-9320132	activated steel	2.19×10^{11}	99.99	0	0.01	0
J-M-9320133	activated steel	2.76×10^{12}	99.99	0	0.01	0

Waste package type	^{14}C associated materials*	^{14}C activity (Bq)**	CRF***		IRF***	
			organics	inorganics	organics	inorganics
J-M-9320211	activated steel and activated concrete	2.34×10^{9}	49.995	0	12.505	12.5
J-M-9320212	activated steel	1.06×10^{6}	99.99	0	0.01	0
J-M-9320221	activated steel	9.44×10^{8}	99.99	0	0.01	0
J-M-9320222	activated steel	2.76×10^{8}	99.99	0	0.01	0
J-M-9320223	activated steel	7.70×10^{6}	99.99	0	0.01	0
J-M-9320224	activated steel	3.24×10^{9}	99.99	0	0.01	0
J-M-9320225	activated steel	2.98×10^{7}	99.99	0	0.01	0
J-M-9320301	activated steel and activated concrete	1.45×10^{6}	49.995	0	12.505	12.5
J-M-9320302	activated steel and activated concrete	1.34×10^{7}	49.995	0	12.505	12.5
J-M-9321011	products from incineration/plasma furnace	1.85×10^{4}	0	0	0	100
J-M-9321201	contaminated waste	1.88×10^{4}	0	0	50	50
J-M-9321202	contaminated waste	5.34×10^{4}	0	0	50	50
J-M-9321203	contaminated waste	7.90×10^{5}	0	0	50	50
J-M-9321204	contaminated waste	5.02×10^{6}	0	0	50	50
J-M-9321205	contaminated waste	1.88×10^{8}	0	0	50	50
J-M-9321311	contaminated waste	5.87×10^{4}	0	0	50	50
J-M-9321320	contaminated waste	1.46×10^{4}	0	0	50	50
J-M-932200	products from incineration/plasma furnace	1.59×10^{5}	0	0	0	100
J-M-932201	contaminated waste	9.21×10^{4}	0	0	50	50
J-M-932202	contaminated waste	1.97×10^{6}	0	0	50	50
J-M-932203	contaminated waste	3.48×10^{5}	0	0	50	50
J-N-900001	contaminated waste	4.22×10^{4}	0	0	50	50
J-N-900003	contaminated waste	1.63×10^{7}	0	0	50	50
J-N-900004	products from incineration/plasma furnace	1.15×10^{4}	0	0	0	100
J-N-900005	contaminated waste	1.42×10^{5}	0	0	50	50
J-N-900501B	contaminated waste	1.90×10^{5}	0	0	50	50

Waste package type	^{14}C associated materials*	^{14}C activity (Bq)**	CRF***		IRF***	
			organics	inorganics	organics	inorganics
J-N-900503	products from incineration/plasma furnace	3.69×10^{4}	0	0	0	100
J-N-900504	contaminated waste	6.41×10^{5}	0	0	50	50
J-N-900505	contaminated waste	6.10×10^{7}	0	0	50	50
J-N-910001	contaminated waste	2.93×10^{3}	0	0	50	50
J-N-910002	contaminated waste	1.42×10^{4}	0	0	50	50
J-N-910004	products from incineration/plasma furnace	9.63×10^{4}	0	0	0	100
J-N-910005	products from incineration/plasma furnace	3.22×10^{4}	0	0	0	100
J-N-910007	contaminated waste	1.20×10^{10}	0	0	50	50
J-N-920001	products from incineration/plasma furnace	1.65×10^{4}	0	0	0	100
J-P-000164	activated steel	1.25×10^{11}	99.99	0	0.01	0
J-P-000164B	activated steel	9.96×10^{10}	99.99	0	0.01	0
J-P-001001	contaminated waste	6.66×10^{6}	0	0	50	50
J-P-001004	contaminated waste	2.06×10^{6}	0	0	50	50
J-P-001007	contaminated waste	7.32×10^{8}	0	0	50	50
J-P-001008	contaminated waste	1.74×10^{4}	0	0	50	50
J-P-001009	contaminated waste	1.83×10^{4}	0	0	50	50
J-P-001020	contaminated waste	1.78×10^{8}	0	0	50	50
J-P-001021	contaminated waste	3.74×10^{8}	0	0	50	50
J-P-001030	contaminated waste	4.68×10^{10}	0	0	50	50
J-P-001031	contaminated waste	7.45×10^{7}	0	0	50	50
J-P-001033	contaminated waste	3.27×10^{8}	0	0	50	50
J-P-001050	products from incineration/plasma furnace	1.59×10^{6}	0	0	0	100
J-P-001052	products from incineration/plasma furnace	4.58×10^{5}	0	0	0	100
J-P-001054	products from incineration/plasma furnace	8.46×10^{5}	0	0	0	100

Waste package type	^{14}C associated materials*	^{14}C activity (Bq)**	CRF***		IRF***	
			organics	inorganics	organics	inorganics
J-P-001055	products from incineration/plasma furnace	9.87×10^{5}	0	0	0	100
J-P-001080	products from incineration/plasma furnace	2.23×10^{5}	0	0	0	100
J-P-001081	products from incineration/plasma furnace	4.24×10^{4}	0	0	0	100
J-P-001082	products from incineration/plasma furnace	1.54×10^{4}	0	0	0	100
J-P-001083	products from incineration/plasma furnace	2.71×10^{7}	0	0	0	100
J-P-001084	products from incineration/plasma furnace	3.49×10^{5}	0	0	0	100
J-P-001100	contaminated waste	2.55×10^{10}	0	0	50	50
J-P-001102	contaminated waste	8.11×10^{7}	0	0	50	50
J-P-001103	contaminated waste	4.49×10^{11}	0	0	50	50
J-P-001110	contaminated waste	5.46×10^{11}	0	0	50	50
J-P-001111	contaminated waste	4.74×10^{11}	0	0	50	50
J-P-001112	contaminated waste	2.41×10^{11}	0	0	50	50
J-P-001113#	contaminated waste	1.07×10^{12}	0	0	49	51
J-P-001114S	contaminated waste	1.60×10^{11}	0	0	50	50
J-P-001114T	contaminated waste	6.40×10^{11}	0	0	50	50
J-P-001115#	contaminated waste	2.44×10^{11}	0	0	23	77
J-P-001116S	contaminated waste	2.05×10^{11}	0	0	50	50
J-P-001116T	contaminated waste	9.98×10^{11}	0	0	50	50
J-P-001117S	contaminated waste	4.00×10^{11}	0	0	50	50
J-P-001117T	contaminated waste	2.00×10^{12}	0	0	50	50
J-P-001120	contaminated waste	1.50×10^{9}	0	0	50	50
J-P-001123	contaminated waste	3.03×10^{6}	0	0	50	50
J-P-001124	contaminated waste	3.29×10^{3}	0	0	50	50
J-P-001202	contaminated waste	5.15×10^{10}	0	0	50	50
J-P-001211	contaminated waste	1.29×10^{11}	0	0	50	50
J-P-001212	contaminated waste	1.88×10^{11}	0	0	50	50

Waste package type	^{14}C associated materials*	^{14}C activity (Bq)**	CRF***		IRF***	
			organics	inorganics	organics	inorganics
J-P-001214	contaminated waste	3.39×10^{11}	0	0	50	50
J-P-001251#	contaminated waste	1.71×10^{12}	0	0	21	79
J-P-001253	contaminated waste	8.06×10^{9}	0	0	50	50
J-P-001261#	contaminated waste	9.55×10^{11}	0	0	50	50
J-P-001400	contaminated waste	2.21×10^{11}	0	0	50	50
J-P-001401	contaminated waste	1.78×10^{6}	0	0	50	50
J-P-001600	contaminated waste	7.19×10^{10}	0	0	50	50
J-P-002010S	contaminated waste	5.17×10^{4}	0	0	50	50
J-P-002010T	contaminated waste	5.91×10^{5}	0	0	50	50
J-P-002011S	contaminated waste	5.17×10^{3}	0	0	50	50
J-P-002011T	contaminated waste	5.69×10^{4}	0	0	50	50
J-P-002012S	contaminated waste	2.33×10^{4}	0	0	50	50
J-P-002012T	contaminated waste	1.50×10^{5}	0	0	50	50
J-P-002013	contaminated waste	5.43×10^{5}	0	0	50	50
J-P-002020	contaminated waste	4.76×10^{8}	0	0	50	50
J-P-002021	contaminated waste	2.53×10^{6}	0	0	50	50
J-P-002021B	contaminated waste	4.85×10^{7}	0	0	50	50
J-P-002028	contaminated waste	2.84×10^{9}	0	0	50	50
J-P-002030	contaminated waste	6.01×10^{3}	0	0	50	50
J-P-002031	contaminated waste	2.91×10^{6}	0	0	50	50
J-P-002032	contaminated waste	1.68×10^{4}	0	0	50	50
J-P-002034	contaminated waste	1.25×10^{4}	0	0	50	50
J-P-002035	contaminated waste	1.89×10^{4}	0	0	50	50
J-P-002040	contaminated waste	1.11×10^{2}	0	0	50	50
J-P-002041	contaminated waste	5.25×10^{1}	0	0	50	50
J-P-002042	contaminated waste	1.98	0	0	50	50
J-P-002054	contaminated waste	7.53×10^{4}	0	0	50	50
J-P-002060	contaminated waste	8.92×10^{4}	0	0	50	50
J-P-002061	contaminated waste	2.16×10^{6}	0	0	50	50
J-P-002062S	contaminated waste	1.25×10^{4}	0	0	50	50
J-P-002062T	contaminated waste	1.55×10^{5}	0	0	50	50
J-P-002070	contaminated waste	2.57×10^{3}	0	0	50	50
J-P-002080	contaminated waste	2.76×10^{2}	0	0	50	50

Waste package type	^{14}C associated materials*	^{14}C activity (Bq)**	CRF***		IRF***	
			organics	inorganics	organics	inorganics
J-P-002081	contaminated waste	1.17×10^{2}	0	0	50	50
J-P-002100	vitrified L/ILW	4.36×10^{5}	0	100	0	0
J-P-003000	contaminated waste	4.51×10^{9}	0	0	50	50
J-P-003010	contaminated waste	2.55×10^{10}	0	0	50	50
J-P-003100	activated graphite	7.79×10^{11}	2.5	2.5	0.01	0.01
J-P-004000A	activated Be	1.98×10^{9}	0	0	100	0
J-P-004010	activated graphite	3.08×10^{11}	2.5	2.5	0.01	0.01
J-P-005000	contaminated waste	7.62×10^{10}	0	0	50	50
J-P-005100	contaminated waste	3.20×10^{4}	0	0	50	50
J-P-005110	contaminated waste	4.17×10^{9}	0	0	50	50
J-P-005200	contaminated waste	8.69×10^{9}	0	0	50	50
J-P-005300	contaminated waste	4.77×10^{4}	0	0	50	50
J-P-010001	activated steel	4.66×10^{7}	99.99	0	0.01	0
J-P-010003	other activated metals	6.55×10^{7}	50	0	50	0
J-P-010004	other activated metals	6.31×10^{8}	50	0	50	0
J-P-010005	other activated metals	1.98×10^{8}	50	0	50	0
J-P-010008	other activated metals	3.06×10^{9}	50	0	50	0
J-P-010010	other activated metals	4.56×10^{5}	50	0	50	0
J-P-010013S	other activated metals	2.16×10^{9}	50	0	50	0
J-P-010013T	other activated metals	9.72×10^{9}	50	0	50	0
J-P-010020	activated steel	1.70×10^{7}	99.99	0	0.01	0
J-P-010021	activated steel	4.49×10^{6}	99.99	0	0.01	0
J-P-012000	activated Pb	3.99×10^{6}	50	0	50	0
J-P-920001	activated Pb	2.00×10^{7}	50	0	50	0
J-P-920002	other activated metals	5.97×10^{11}	50	0	50	0
J-P-920003	activated heavy elements	1.32×10^{7}	0	0	100	0
J-P-960201	contaminated waste	3.81×10^{7}	0	0	50	50
J-P-960202	contaminated waste	3.95×10^{7}	0	0	50	50

Waste package type	^{14}C associated materials*	^{14}C activity (Bq)**	CRF***		IRF***	
			organics	inorganics	organics	inorganics
J-P-960203	contaminated waste	5.79×10^{7}	0	0	50	50
J-P-960211	contaminated waste	1.94×10^{4}	0	0	50	50
J-P-960221	contaminated waste	3.55×10^{3}	0	0	50	50
J-P-970001	activated concrete	5.93×10^{9}	0	0	25	25
J-P-970011	other activated metals	1.14×10^{6}	50	0	50	0
J-P-970101	activated steel	2.31×10^{9}	99.99	0	0.01	0
J-P-970111	activated steel	8.04×10^{4}	99.99	0	0.01	0
J-P-970200	activated Al	1.09×10^{9}	0	0	100	0
J-P-970301	activated steel	6.27×10^{10}	99.99	0	0.01	0
J-P-970311	activated steel	2.63×10^{6}	99.99	0	0.01	0
J-P-970400	activated steel	4.03×10^{9}	99.99	0	0.01	0
J-P-970500	activated Pb	2.02×10^{10}	50	0	50	0
J-P-970601	activated steel and activated concrete	8.33×10^{9}	49.995	0	12.505	12.5
J-P-970611	activated steel and activated concrete	2.26×10^{6}	49.995	0	12.505	12.5
J-P-970711	activated concrete	4.75×10^{7}	0	0	25	25
J-P-980001	contaminated waste	4.18×10^{9}	0	0	50	50
J-P-980002	activated steel	4.18×10^{9}	99.99	0	0.01	0
J-Z-000104	products from incineration/plasma furnace	2.69×10^{6}	0	0	0	100
J-Z-000301	contaminated waste	1.00×10^{5}	0	0	50	50
J-Z-000402	contaminated waste	2.52×10^{3}	0	0	50	50
J-Z-000403	contaminated waste	1.49×10^{1}	0	0	50	50
J-Z-000404	contaminated waste	1.57×10^{3}	0	0	50	50
J-Z-000501	contaminated waste	3.99×10^{3}	0	0	50	50
J-Z-000901	activated steel	2.04×10^{9}	99.99	0	0.01	0
J-Z-003000	activated Zr	8.57×10^{11}	99.99	0	0.01	0
J-Z-003003	vitrified L/ILW	1.51×10^{9}	0	100	0	0
J-Z-900004	contaminated waste	3.17×10^{5}	0	0	50	50
J-Z-932100	contaminated waste	8.07×10^{4}	0	0	50	50
J-Z-932101	contaminated waste	3.18×10^{6}	0	0	50	50
J-Z-932102	contaminated waste	1.50×10^{6}	0	0	50	50

Waste package type	^{14}C associated materials*	^{14}C activity (Bq)**	CRF***		IRF***	
			organics	inorganics	organics	inorganics
J-Z-932120	contaminated waste	9.53×10^{5}	0	0	50	50
J-Z-932130	contaminated waste	1.09×10^{5}	0	0	50	50
J-Z-932133	contaminated waste	5.56×10^{5}	0	0	50	50
J-Z-932200	products from incineration/plasma furnace	1.23×10^{4}	0	0	0	100
J-Z-932201	contaminated waste	2.14×10^{5}	0	0	50	50
J-Z-932202	contaminated waste	2.03×10^{7}	0	0	50	50
J-Z-970001B	contaminated waste	3.21×10^{8}	0	0	50	50
J-Z-970002B	contaminated waste	8.16×10^{7}	0	0	50	50

* Materials where ^{14}C is expected to be associated. Based on Nagra (2023) and expert judgements.

** Average ^{14}C activity predicted for each AGTs in 2075 based on Nagra (2023).

*** Only reference scenario considered here.

The inventory of these specific MIR waste has been especially characterised by experts, as they initially contributed to a non-negligeable part of the total ^{14}C inventory for L/ILW.

App. B ^{14}C activity, speciation and rate of release from individual HLW waste package types

Waste type packages	^{14}C associated materials	^{14}C activity** (Bq)	CRF***		IRF***	
			organics	inorganics	organics	inorganics
J-B-950601	SF pellets	1.64×10^{13}	97	0	1.5	1.5
	activated Zr	1.83×10^{13}	99.99	0	0.01	0
	activated steel	3.63×10^{12}	99.99	0	0.01	0
J-B-950602	SF pellets	1.07×10^{12}	97	0	1.5	1.5
	activated Zr	2.28×10^{12}	99.99	0	0.01	0
	activated steel	4.98×10^{11}	99.99	0	0.01	0
J-G-950601	SF pellets	2.39×10^{13}	97	0	1.5	1.5
	activated Zr	2.82×10^{13}	99.99	0	0.01	0
	activated steel	7.03×10^{11}	99.99	0	0.01	0
J-G-950602	SF pellets	1.12×10^{12}	97	0	1.5	1.5
	activated Zr	2.57×10^{12}	99.99	0	0.01	0
	activated steel	6.01×10^{10}	99.99	0	0.01	0
J-L-950601	SF pellets	4.51×10^{13}	97	0	1.5	1.5
	activated Zr	8.95×10^{13}	99.99	0	0.01	0
	activated steel	1.30×10^{13}	99.99	0	0.01	0
J-M-950601	SF pellets	7.56×10^{12}	97	0	1.5	1.5
	activated Zr	3.54×10^{12}	99.99	0	0.01	0
	activated steel	7.36×10^{11}	99.99	0	0.01	0
J-P-002024	contaminated waste	6.67×10^{9}	0	0	50	50
J-P-950001	SF pellets	2.23×10^{8}	97	0	1.5	1.5
	activated Zr		99.99	0	0.01	0
	activated steel		99.99	0	0.01	0
J-P-950001	SF pellets, activated Zr and steel	2.23×10^{8}	no information available			
J-Z-005000	RP-HLW	1.26×10^{10}	0	100	0	0
J-Z-005002	RP-HLW	1.00×10^{10}	0	100	0	0

* Materials where ^{14}C is expected to be associated. Based on Nagra (2023) and expert judgements.

** Average ^{14}C activity predicted for each AGT in 2075, based on Nagra (2023).

*** Only reference scenario considered here.